EXPLORING THERAPEUTIC APPROACHES FOR TREATMENT OF MEDIUM-CHAIN ACYL-COA DEHYDROGENASE (MCAD) DEFICIENCY

by

Heejung Kang

BS, Sungkyunkwan University, South Korea, 2003

MS, Sungkyunkwan University, South Korea, 2005

MS, University of Minnesota, 2008

Submitted to the Graduate Faculty of

Graduate School of Public Health in partial fulfillment

of the requirements for the degree of

Doctor of Philosophy

University of Pittsburgh

2014

UNIVERSITY OF PITTSBURGH

GRADUATE SCHOOL OF PUBLIC HEALTH

This dissertation was presented

by

Heejung Kang

It was defended on

April 15, 2014

and approved by

Dissertation Advisor: Jerry Vockley, M.D. Ph.D., Professor,
Pediatrics, School of Medicine, University of Pittsburgh

Committee Chair: Robert Ferrell, Ph.D., Professor, Human Genetics,
Graduate School of Public Health, University of Pittsburgh

David Finegold, Ph.D., Professor, Pediatrics,
School of Medicine, University of Pittsburgh

Al-Walid A. Mohsen, Ph.D., Research Associate Professor of Pediatrics
School of Medicine, University of Pittsburgh

Zsolt Urban, Ph.D., Associate Professor, Human Genetics,
Graduate School of Public Health, University of Pittsburgh

Jerry Vockley, MD, PhD

EXPLORING THERAPEUTIC APPROACHES FOR TREATMENT OF MEDIUM-CHAIN ACYL-COA DEHYDROGENASE (MCAD) DEFICIENCY

Heejung Kang, PhD

University of Pittsburgh, 2014

ABSTRACT

Medium chain acyl-CoA dehydrogenase deficiency (MCADD) is a common biochemical genetic disorder in the US. Nearly 90% of alleles from MCADD patients contain a common mutation in the *ACADM* (c.985A>G). The change replaces a lysine with a glutamate (K304E), causing improper folding. The K304E protein can fold to a mature form and is then stable and active when expressed in a prokaryotic system with molecular chaperonins. The goal of this project was to identify chemical chaperones capable of stabilizing the K304E MCAD protein. Since even a small amount of MCAD activity restores metabolic flux, inducing intra-mitochondrial folding of K304E MCAD has the potential to be protective for patients. To demonstrate proof of principle, dimethylsulfoxide, glycerol, betaine, trimethylamine *N*-oxide (TMAO), and $_{L}$-proline were tested for the ability to increase MCAD activity in lymphoblasts having c.985G>A alleles. TMAO and glycerol significantly increased MCAD activity in these cells. Phenylbutyrate is converted to its CoA ester form and metabolized to phenylacetyl-CoA through β-oxidation initiated by MCAD. As a substrate analogue for MCAD, phenylbutyryl-CoA is expected to improve protein stability. Experiments in HEK293 cells containing inducible wild type or K304E MCAD alleles, phenylbutyrate increased wild type MCAD activity by 30% and K304E MCAD activity by 154%. A clinical trial testing the efficacy of phenylbutyrate in MCAD patients is underway. Drug targeting sites were also investigated using molecular modeling. The docking site for electron

transfer flavoprotein (ETF) was hypothesized to be a viable site. Twelve amino acid peptides with variable sequences were synthesized based on ETF βArg191-βLys202. One of the peptides significantly increased thermal stability of K304E MCAD. Circular dichroism spectroscopy confirmed binding of the synthetic peptide, inducing a shift in the T_m of the enzymes. The ETF docking peptide analogue also protected K304E MCAD protein against limited proteolysis by *Staphylococcus aureus* V8. These results confirm that ETF docking site is a viable target for MCADD.

PUBLIC HEALTH SIGNIFICANCE: Even though newborn screening has reduced the mortality of the MCADD, patients still require frequent hospital visits during metabolic decompensation. New treatments for MCADD will significantly reduce the burden of disease on these patients.

TABLE OF CONTENTS

LIST OF TABLES

LIST OF FIGURES

ABBREVIATIONS

ACADs: Acyl-CoA dehydrogenases

AMP: Adenosine 3′,5′-cyclic monophosphate sodium salt monohydrate

CD: Circular dichroism

DCIP: 2,6 Dichlorphenol-Indophenol

ETF: Electron transfer flavoprotein

FAD: Flavin adenine dinucleotide

FAO: Fatty acid oxidation

IM: Inner membrane

IMS: Intermembrane space

HTS: High-throughput screening

LCAD: Long-chain acyl-CoA dehydrogenase

NBS: Newborn screening

MCAD: Medium-chain acyl-CoA dehydrogenase

MCADD: Medium-chain acyl-CoA dehydrogenases deficiency

MS: Mass spectrometry

OM: Outermembrane

PBA: Phenylbutyric acid

SCAD: Short-chain acyl-CoA dehydrogenase

TIM: Translocase of the inner membrane

TMAO: Trimethylamine *N*-oxide

TOM: Translocase of the outer membrane

VLCAD: Very long-chain acyl-CoA dehydrogenase

PREFACE

First, I would like to give thanks to my advisor, Dr. Vockley. I could not have completed this long journey to toward a PhD without his guidance and encouragement in research. He always inspired me with his passion for science. Whenever I had questions or difficulties in research, he always showed me the way to solve these problems. I felt very lucky to have him as my advisor. I would also like to thank Dr. Mohsen, who taught me so much about biochemistry. I tend to look at my data as a molecular biologist would, but he always corrected me on the right way to interpret data in the world of biochemistry. I would like to show sincere gratitude to my committee members, Dr. Robert Ferrell, Dr. David Finegold, and Dr. Zsolt Urban. I still remember the first day at university. I had so many questions about what my future would be like during my doctoral training. At that time, Dr. Ferrell answered my questions and guided me in finding a focus. I really appreciate his warm advice throughout my doctoral studies. I also experienced periods of self-doubt and disappointment throughout my doctoral studies. Thank you, Dr. Finegold, for your cheerful and loving encouragement. He dragged me from my gloomy outlook to reality. Furthermore, I would like to thank Dr. Urban. His critical questions and guidance made me nervous sometimes, but they were invaluable in helping me think about my research from a different angle and solve the limitations of my studies. Next, I would like to thank my colleagues in Dr. Vockley and Dr. Goetzman's lab members for their warm friendship and support. They offered me encouragement and inspiration in the lab. And finally, I would like

to thank my parents and my husband for their endless support and love. I would not have been able to complete my degree without their support. Thank you all.

1.0 INTRODUCTION

1.1 BIOGENESIS OF MITOCHONDRIAL PROTEINS

1.1.1 General characteristics of mitochondrial proteins

Mitochondria are unique double membrane-bound (the outer membrane and the inner membrane) organelles that are involved in several major cellular functions such as energy generation, amino acid metabolism, apoptosis, etc. Most of the mitochondrial proteins are encoded in the nucleus. About 15% of the nuclear genes are encoding mitochondrial proteins (Neupert and Herrmann, 2007). These genes are transcribed in the nucleus, the proteins are synthesized in the cytosol as precursor forms, and transported into mitochondria by different protein translocases in the outermembrane. Receptors on the surface of mitochondria can recognize mitochondrial targeting signals from the proteins and then import these proteins. There are different targeting signals that can determine the final localization of each protein. Some inner membrane proteins have N-terminus cleavable sequences and others have internal sequences. Using different prediction programs, these targeting sequences can easily be identified (Table 1). Molecular chaperones in mitochondria are known to help the proper folding of these proteins. Quality control proteases degrade the unfolded proteins in the mitochondria.

Table 1. Prediction for matrix-targeting sequences

Name	Internet address	Organization
TargetP 1.1 Server	http://www.cbs.dtu.dk/services/TargetP/	Technical University of Denmark
PSORT WWW server	http://psort.hgc.jp/	University of Tokyo, Japan
MITOPROT	http://ihg.gsf.de/ihg/mitoprot.html	Helmholtz Center Munich
INRA	https://urgi.versailles.inra.fr/predotar/predotar.html	Unité de Recherche en Génomique Végétale

There are different classes of mitochondrial membrane proteins that are located in outer membrane or inner membrane of mitochondria. Figure 1 shows the different mitochondrial membrane proteins. Proteins with β-barrel trans membrane domains are typical forms of mitochondrial outer membrane proteins such as Tom40, Sam50, or Porin (Figure 1a). Other proteins with a single or multiple α-helical transmembrane segments are also known to be involved in the outer membrane of mitochondria. Mitochondrial inner membrane proteins can be classified by the type and position of the signal sequences (Figure 1b). Many mitochondrial inner membrane proteins have presequences that will be cleaved after getting into the mitochondrial matrix.

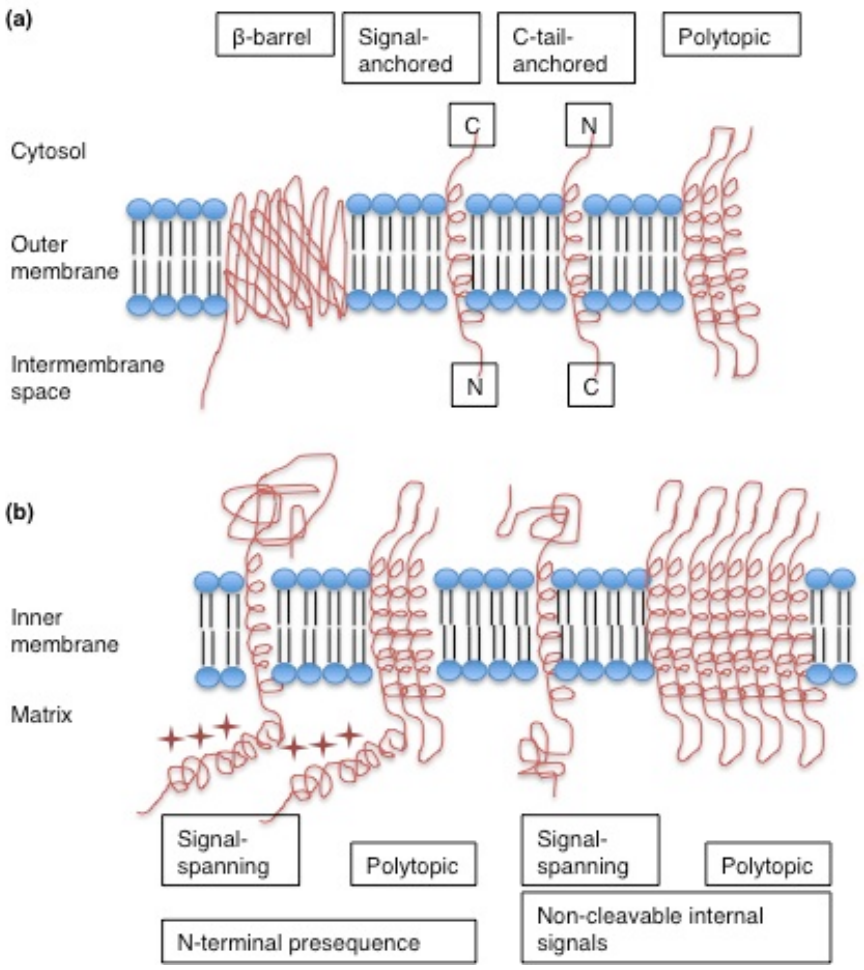

Figure 1. Major classes of mitochondrial membrane proteins

(a) Mitochondrial outer membrane proteins. Typical forms of mitochondrial outer membrane proteins have a β-barrel transmembrane domain. Some proteins have a single α-helical transmembrane segment and others have multiple α-helical transmembrane segments (polytopic membrane proteins). (b) Mitochondrial inner membrane proteins. Mitochondrial inner membrane proteins are classified based on the presence of N-terminal presequences and the number of α-helical transmembrane segments.

1.1.2 The protein import machinery of mitochondria

There are three main translocation complexes in mitochondria, TOM (translocase of the outer membrane), TIM23 (translocase of the inner membrane 23) and TIM22 (translocase of the inner membrane 22). The TOM complex is localized in the outer membrane and regulates the

import of all the proteins into mitochondria. The TOM complex is composed of two main groups of subunits: receptor subunits (Tom70, Tom22 and Tom20) and membrane-embedded subunits (Tom40, Tom7, Tom6, and Tom5). The receptor subunits have binding sites for precursor proteins in the cytosol and membrane-embedded subunits form the translocation pore that proteins in the cytosol can be transported into mitochondria inner membrane space (Figure 2). The TOM complex is also known to act as a molecular chaperone.

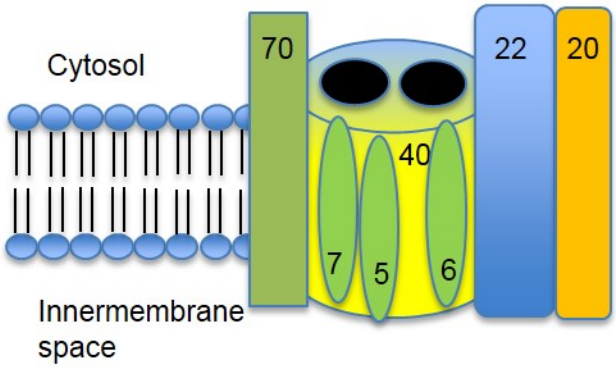

Figure 2. The TOM complex

The Tom (translocase of the outer membrane) complex is composed of surface receptors (Tom70, Tom22, and Tom20) and translocation pore (Tom40, Tom7, Tom6, and Tom5).

The TIM 23 and TIM22 complexes are located in the inner membrane. TIM23 complex can import the presequence containing preproteins and TIM22 complex can import the precursor proteins having internal targeting signals. Presequences are positively charged amphipathic α-helical segments and usually composed of about 15 to 55 amino acids (Vogtle et al., 2009).

Two major complexes, TIM23 and TIM22, are known to be involved in the transport of the proteins from the intermembrane space into mitochondrial matrix (Figure 3 and 4). In both cases, the electrical membrane potential changes are the key driving force for transporting

proteins into the matrix. TIM23 complex is composed of different proteins that are related to the interaction of the proteins in the intermembrane space and the import motor.

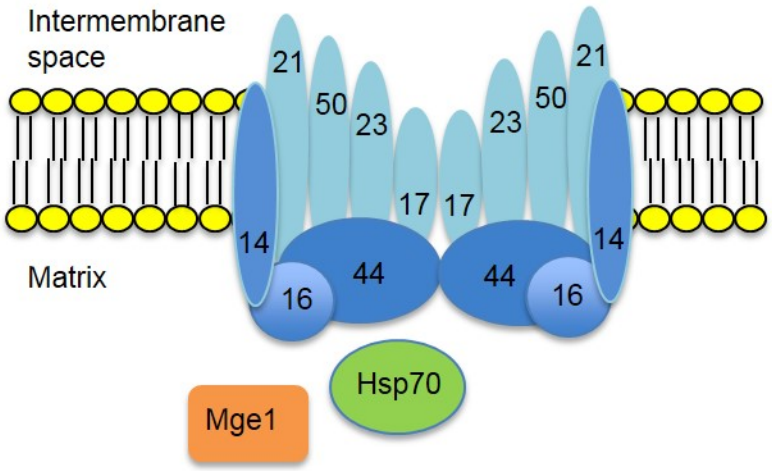

Figure 3. The TIM23 complex

The TIM23 complex is composed of membrane sectors (Tim50, Tim23, Tim21, and Tim17) and import motors (Tim44, Tim16/Pam16, Tim14/Pam18, mtHsp70, and Mge1). Membrane sectors are exposed to the intermembrane space. Especially, Tim17 and Tim23 form the translocation channel. The import motors are exposed to matrix.

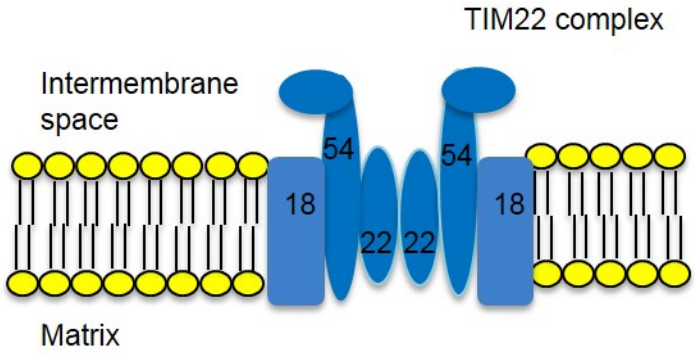

Figure 4. The TIM22 complex

TIM22 complex is composed of Tim54, Tim22, and Tim18. TIM22 translocase transports the substrate proteins by electrical membrane potential changes.

1.2 MITOCHONDRIAL B-OXIDATION

1.2.1 Mitochondrial fatty acid β-oxidation

Mitochondrial fatty acyl-CoA β-oxidation (FAO) is a major source of energy-generating reducing equivalents during stress and fasting and provides ~80% of energy for the heart even under non-stress conditions (Rinaldo et al., 2002; Shekhawat et al., 2005). FAO is comprised of two main steps: 1) import of activated fatty acids into mitochondria and 2) β-oxidation of the acyl-CoA substrates by sequential removal of two carbon acetyl-CoA units (Bartlett and Eaton, 2004).

Energy is harvested from this process in two ways. First, reducing equivalents from the FAO enzymatic reactions can enter the mitochondrial respiratory chain directly. Second, acetyl-CoA can enter the tricarboxylic acid cycle (TCA, also known as the Kreb cycle), which in turn generates additional reducing equivalents for oxidative phosphorylation. Acetyl-CoA can also lead to the generation of ketone bodies, an important alternative energy source for the brain during fasting. Figure 5 shows the overall process of the import of fatty acids into the mitochondria.

First, carnitine transporters transport carnitines from the extracellular space into the cytosol. Carnitine (β-hydroxy-ϒ-trimethylaminobutyric acid) transports long chain fatty acids into the mitochondria. When the intracellular concentrations of malonyl-CoA is reduced due to

fasting, carnitine palmitoyl transferase I (CPT I) is upregulated. Fatty acids are converted into acyl-CoA and to acyl carnitines, which are transported across the inner mitochondrial membrane by carnitine:acylcarnitine translocases (CACT). Once these acylcarnitines reach the inner mitochondrial matrix, they are converted again into acyl-CoA esters by carnitine palmitoyl transferase II (CPT II). Free carnitines are recycled and returned to the cytoplasm.

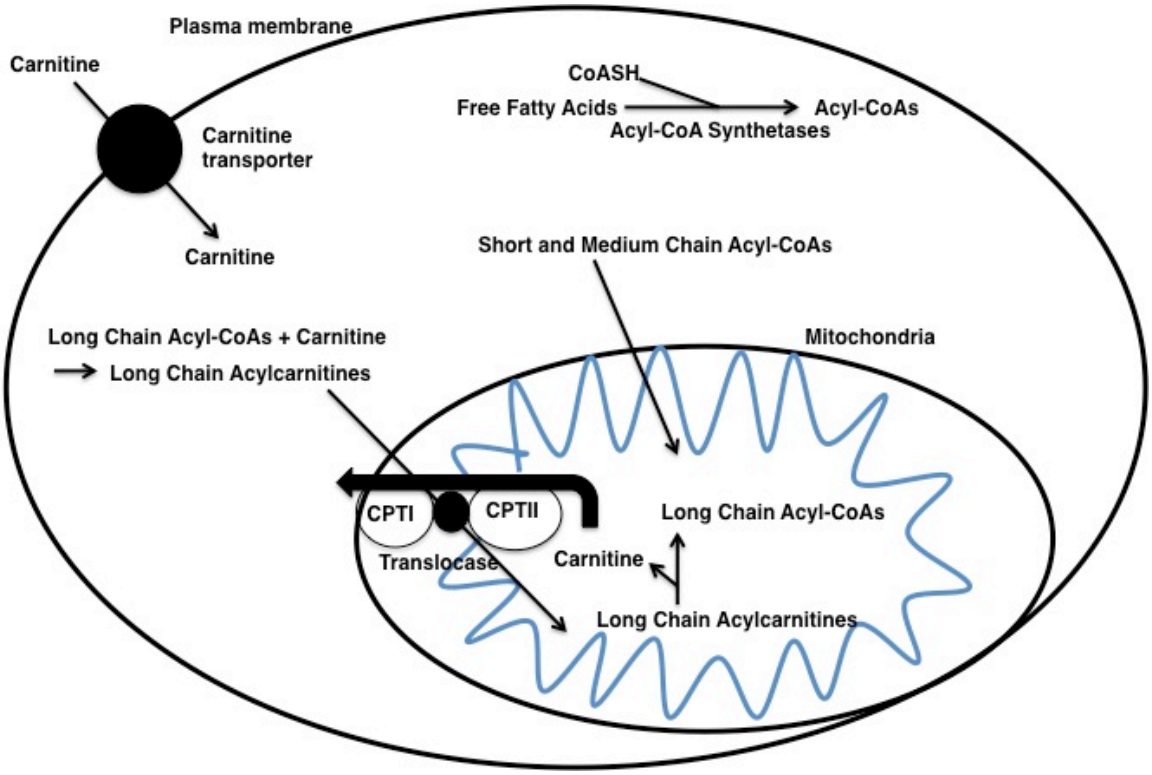

Figure 5. Transport of fatty acids into mitochondria

Detailed explanations in text.

Once the fatty acids get into the mitochondrial matrix, β-oxidation will occur. Figure 6 shows the mitochondrial β-oxidation spiral. In each step, two carbons are removed. The first step of this process is by acyl-CoA dehydrogenases (ACDs). ACDs move pro-R-α-hydrogen and the pro-R-β-hydrogen from the acyl-CoA to the N-5 position of flavin. As a final product of FAO,

acetyl-CoA will be generated. In liver, acetyl-CoA will be a source of ketone bodies. Since ketone bodies are important energy source for brain, generation of ketone bodies is critical for the body when body has high-energy demands. And in heart and skeletal muscle, acetyl-CoA esters will enter TCA cycle and be used in energy generation. Especially in mitochondria, FAO can generate ketone bodies that are a useful alternative energy source for the brain.

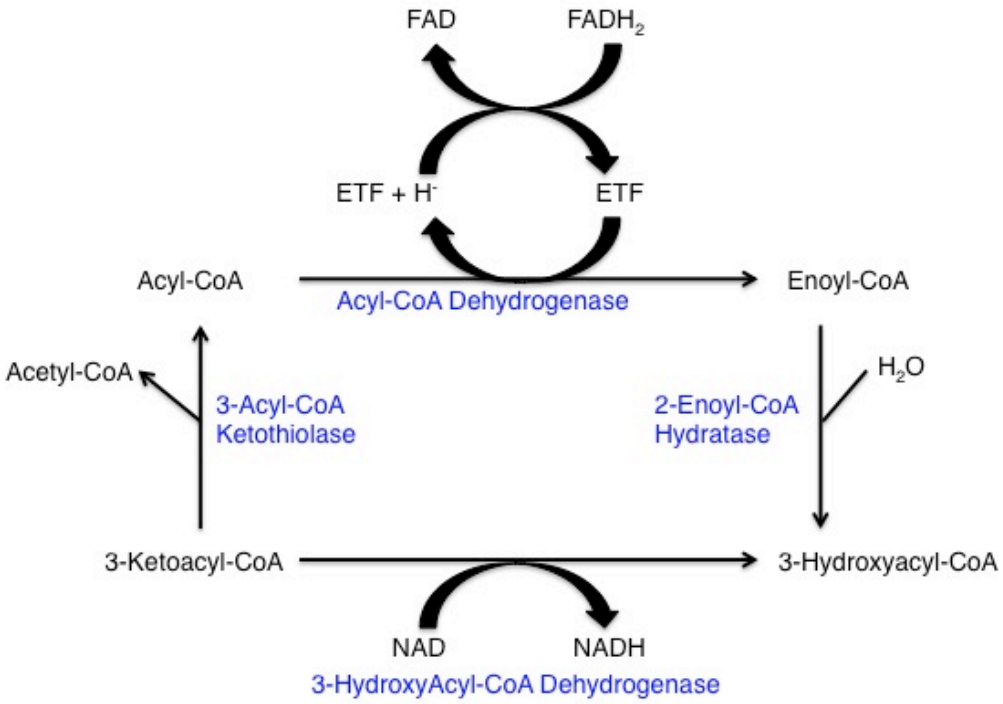

Figure 6. Mitochondrial matrix β-spirals

Detailed explanations in text.

1.2.2 Mitochondrial FAO disorders

Most of the FAO disorders (FAOD) are inherited as autosomal recessive traits. Mutations in genes related to fatty acid transport and fatty acids oxidation cause FAOD. Depending on the function of the mutant gene, intermediate forms of fatty acids or abnormal proteins can

accumulate and downstream products that can be the major sources of energy generation in the body can be depleted. Therefore, the clinical symptoms of mitochondrial FAOD are related to the loss of function of enzyme activity, accumulation of abnormal enzymes, or accumulation of upstream fatty acids, etc. Ketone bodies, products of the mitochondrial FAO, are major energy sources especially for cardiac muscle, kidneys, and the brain. Thus, FAOD can sometimes lead into serious conditions such as sudden death. The clinical symptoms of these diseases vary from mild to severe such as severe metabolic acidosis, hypoglycemia, lethargy, hyperammonemia, cardiomyopathy, liver failure, comma or even sudden death (Shekhawat et al., 2005). In case of late onset FAOD, the symptoms are episodic myopathy, neuropathy, or retinopathy. Prolonged fasting, viral infection, acute illness, strenuous physical activity, or any physiological stresses can trigger the clinical symptoms of these disorders. The clinical phenotype of each FAO disorders and the biochemical characteristics are shown in table 2.

Table 2. Mitochondrial fatty acid oxidation disorders

Enzyme deficiency	Gene	Clinical phenotype	Laboratory findings
Carnitine transporter	OCTN2	Cardiomyopahty, skeletal myopathy, sudden death	Decreased total and free carnitines
Long-chain fatty acid transporter	FATP1-6	Acute liver failure in childhood requiring liver transplantation	Reduced intracellular C_{14}-C_{18} fatty acids, reduced fatty acid oxidation
Carnitine palmitoyl transferase-I	CPT-I	Liver failure, skeletal myopathy, and sudden death	Normal or increased free carnitine
Carnitine translocase	CACT	Chronic progressive liver failure	Normal or decreased free carnitine,

Table 2 Continued

			abnormal acylcarnitine profile
Carnitine palmitoyl transferase-II	CPT-II	Liver failure, cardiomyopathy	Normal or decreased free carnitine, abnormal acylcarnitine profile
Short-chain acyl CoA dehydrogenase	SCAD	Benign to a severe presentation including encephalopathic disease to progressive myopathy	Normal or decreased free carnitine, Inconsistently abnormal acylcarnitine profile
Medium-chain acyl CoA dehydrogenase	MCAD	Hypoglycemia, sudden death	Increased plasma C_6-C_{10} free fatty acid, in creased C_8-C_{10} acyl-carnitine
Very long-chain acyl CoA dehydrogenase	VLCAD	Dilated cardiomyopathy, hypoglycemia	Increased $C_{14:1}$ and C_{14} acylcarnitine, Increased plasma C_{10}-C_{16} free fatty acids
ETF dehydrogenase	ETF-DH	Nonketotic fasting hypoglycemia	Increased acyl-carnitine
Electron transport flavoprotein-α	α-ETF	Nonketotic fasting hypoglycemia	Increased acyl-carnitine
Electron transport flavoprotein-β	β-ETF	Fasting hypoglycemia	Increased acyl-carnitine
Short-chain L-3-hydroxyacyl CoA dehydrogenase	SCHAD	Hypoglycemia	Decreased free carnitine, elevated free fatty acids, abnormal urine organic acid and plasma acylcarnitines
Long-chain L-3-hydroxyacyl CoA dehydrogenase	LCHAD	HELLP syndrome	Decreased free fatty acids, increased C_{16}-OH and C_{18}-OH carnitines
Mitochondrial trifunctional protein	MTP	Severe cardiac and skeletal myopathy, hypoglycemia	Decreased free carnitine, increased C_{16}-OH and C_{18}-OH carnitines

Table 2 Continued

Long-chain 3-ketoacyl-CoA thiolase	LKAT	Severe neonatal presentation, hypoglycemia	Increased 2-trans, 4-cis decadienoylcarnitine
2,4-Dienoyl-CoA reductase	DECR1	Hypotonia in the newborn	Increased acyl to free carnitine ratio
HMG-CoA synthetase	HMGCS2	Hypoketosis	Elevated total plasma fatty acids
HMG-CoA lyase	HMGCL	Hypoketosis	Increased C_5-OH, and methylglutaryl-carnitine

1.2.3 The use of mouse models in mitochondrial fatty acid oxidation disorders

Mouse models are useful tools to study FAOD. Mice with mutations in FAOD genes may present similar clinical symptoms to human patients, and are used to investigate the mechanisms and pathophysiology of the FAOD. The major phenotypes of these mouse models are carnitine depletion, lethality in early gestation or neonatal deaths, cold intolerance, etc. However, since currently available mouse models have null alleles, it is difficult to study the effect of certain missense mutations, or therapies specifically targeting common mutations for FAOD due to the complete lack of ACD expression. Also, some mutations show lethality in early gestation in homozygous animals. Therefore, those models also have some difficulties related to further studies in heterozygotic models. Table 3 shows the enzyme deficiencies and phenotypes of currently available mouse models.

Table 3. Mouse models of mitochondrial β-oxidation of fatty acid disorders

Enzyme deficiency	Mouse phenotype
Carnitine palmitoyl-CoA transferase-1a (liver isoform)	Normal phenotype Homozygous lethal in early gestation
Carnitine palmitoyl-CoA transferase-1b (muscle isoform)	Normal phenotype Homozygous lethal in early gestation
Very-long-chain acyl-CoA dehydrogenase deficiency: two independent mouse models	Cardiac phenotype Hepatic and myopathic phenotypes after stress
Long-chain acyl-CoA dehydrogenase deficiency	Sudden death Fatty change of liver and heart
Medium-chain acyl-CoA dehydrogenase deficiency	Neonatal death Fasting and cold intolerance
Mitochondrial trifunctional protein (TFP α-subunit) deficiency	Neonatal hypoglycemia Fatty change of liver
Mitochondrial trifunctional protein (TFP β-subunit) deficiency	Viable
Medium/short-chain 3-hydroxyacyl-CoA dehydrogenase deficiency	Fasting and cold intolerance with development of fatty liver and kidney
Short-chain acyl-CoA dehydrogenase deficiency	Fasting and cold intolerance with development of fatty liver and kidney

1.3 ACYL-COA DEHYDROGENASES

1.3.1 Acyl-CoA dehydrogenase gene family

The acyl-CoA dehydrogenases (ACADs) are a family of evolutionarily conserved nuclear encoded flavoenzymes active in mitochondrial β-oxidation and branched chain amino acid

metabolism (Ghisla and Thorpe, 2004; Kim and Miura, 2004; Swigonova et al., 2009). Unlike most cellular dehydrogenases, the ACADs use a protein as their electron acceptor, the electron transfer flavoprotein (ETF), which then transfers its electrons to the electron transfer chain through ETF dehydrogenase (ETFDH, also known as ETF:ubiquinone oxidoreductase). Five ACADs (VLCAD, LCAD, ACAD9, MCAD, and SCAD) are involved in the first step of mitochondrial fatty acid β-oxidation. These enzymes are structurally homologous, but each enzyme has a characteristic pattern of substrate utilization. Mutations in all but LCAD have been identified in patients, and each deficiency can present with large spectrum of symptoms. MCAD deficiency is the most common of these disorders with a frequency of 1:10,000-1:20,000 births in the US, with the highest incidence in Caucasians of Western European origin.

Each of these proteins are encoded in the nucleus and are located in mitochondria or peroxisome. The ACAD family has 11 known members, namely, SCAD, MCAD, LCAD, VLCAD, ACAD9, ACAD10, ACAD11, i2VD, i3VD, iBD, and GCDH. Five members (SCAD, MCAD, LCAD, VLCAD, and ACAD9) are involved in fatty acid β-oxidation. And four members (i2VD, i3VD, iBD, and GCD) are involved in amino acid metabolism. Table 4 summarizes the characteristics of each ACD (Kim and Miura, 2004).

Table 4. Acyl-CoA dehydrogenases

Abbreviations	Full name	Pathway	Location	Target fatty acids/ amino acids	Active form
SCAD	Short-chain acyl-CoA dehydrogenase	Fatty acid β-oxidation	12q24.31	C4 and C6	Homotetramer
MCAD	Medium-chain acyl-CoA dehydrogenase	Fatty acid β-oxidation	1p31	C4 to C12	Homotetramer
LCAD	Short-chain acyl-CoA	Fatty acid	2q34	C8 to C20	Homotetramer

Table 4 Continued

	dehydrogenase	β-oxidation			
VLCAD	Very long-chain acyl-CoA dehydrogenase	Fatty acid β-oxidation	17q13.1	C12 to C24	Homodimer
ACAD9	Acyl-CoA dehydrogenase 9	Fatty acid β-oxidation	3q21.3	C12 to C24	Homodimer
ACAD10	Acyl-CoA dehydrogenase 10	Unknown	12q24.12	Unknown	Unknown
ACAD11	Acyl-CoA dehydrogenase 11	Unknown	3q22.1	Unknown	Unknown
I2VD (SBCAD)	iso(2)valery-CoA dehydrogenase short/branched-chain acyl-CoA dehydrogenase	Amino acid oxidation	10q26.13	Isoleucine	Homotetramer
I3VD (IVD)	iso(3)valery-CoA dehydrogenase isovaleryl-CoA dehydrogenase	Amino acid oxidation	15q14-15q	Leucine	Homotetramer
IBD	Isobutyryl-CoA dehydrogenase	Amino acid oxidation	11q25	Valine	Homotetramer
GCDH	Glutaryl-CoA dehydrogenase	Amino acid oxidation	19p13.2	Lysine and tryptophan	Homotetramer

ACADs share 35-45% amino acid sequence homology. As expected from the amino acid sequence homologies, the overall ACAD structures are similar to each other (Kim and Miura, 2004). Also the substrate binding site of the ACADs are conserved. However, each enzyme has different substrate specificity and tissue expression profiles. Evolutionary study of ACADs enzymes showed that ACADs share the common ancestors and this implies to have important role in metabolism (Swigonova et al., 2009). Figure 7 shows the optimal substrates of ACADs. Also, there are some proteins that share a more limited homology with ACAD. The functions of these proteins include acyl-CoA oxidation, antibiotic biosynthesis, and even stress responses (Ghisla and Thorpe, 2004). Thus, ACDs and their homologs are important in a range of cellular functions.

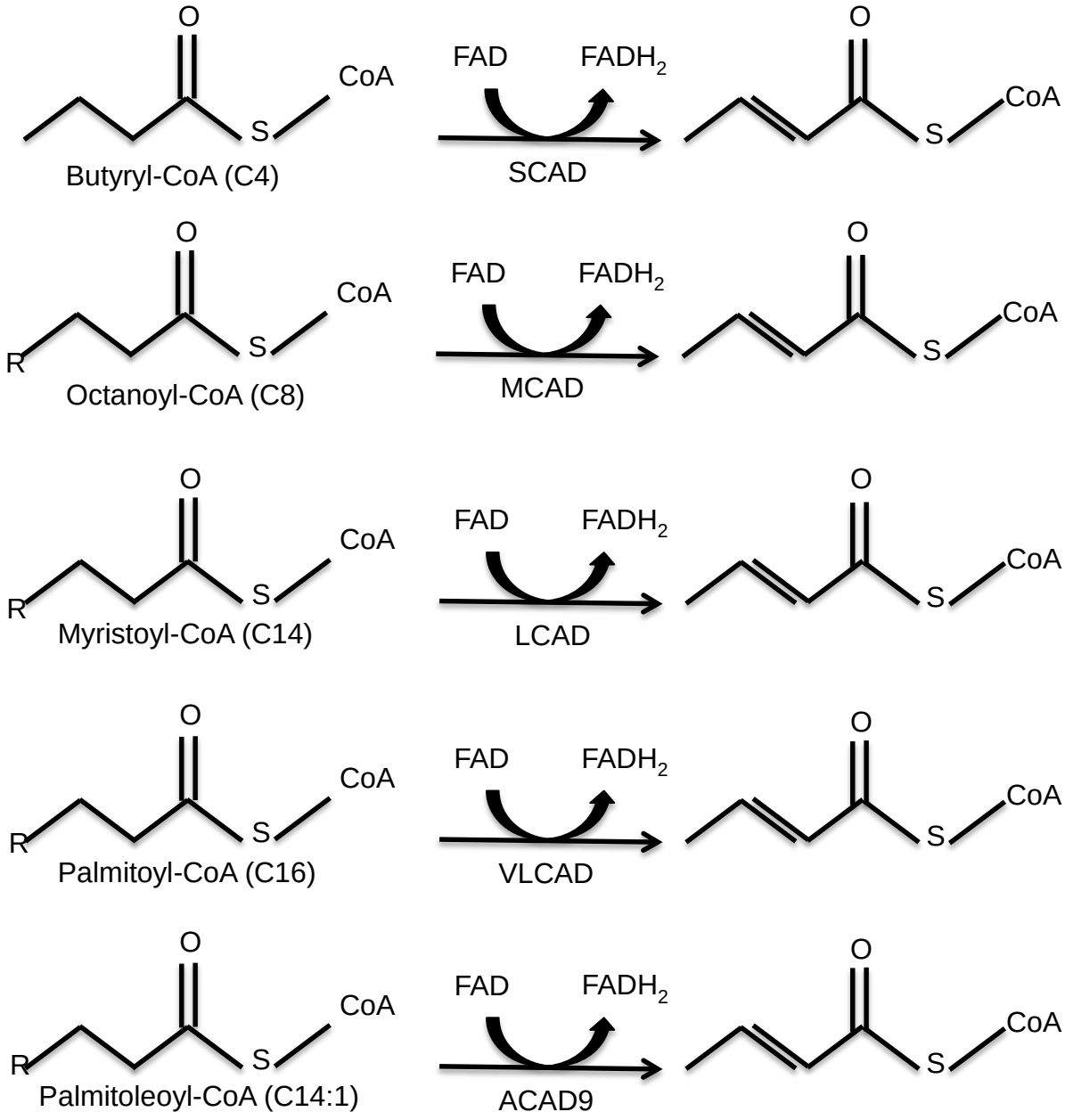

Figure 7. Optimal substrates of each ACD

CX: Each number indicates the length of the acyl-CoA chain. C14:1 indicates the unsaturated fatty acid with one double bond. R indicates straight alkyl chain. SCAD, MCAD, LCAD, VLCAD, and ACD9 are involved in fatty acid β-oxidation.

The main function of ACADs is to transfer electrons from CoA esters to the electron transfer flavoprotein (ETF). ETF dehydrogenase will transfer these electrons to the respiratory chain to finally generate energy through ETF dehydrogenase, a CoQ. Mutations in these enzyme cause fatty acid oxidation deficiencies with different spectrum of phenotypes. Out of all these enzymes, MCAD is the most intensively investigated, but the functions of ACAD10 and ACAD11 are still unknown.

1.3.2 Mechanism of ACDs

The ACDs use ETF as an electron acceptor in α,β-dehydrogenation. After accepting electrons from ACDs, ETF transfers the electrons to ETF dehydrogenase (ETFDH), and then the electrons will be delivered to respiratory chain (Figure 8).

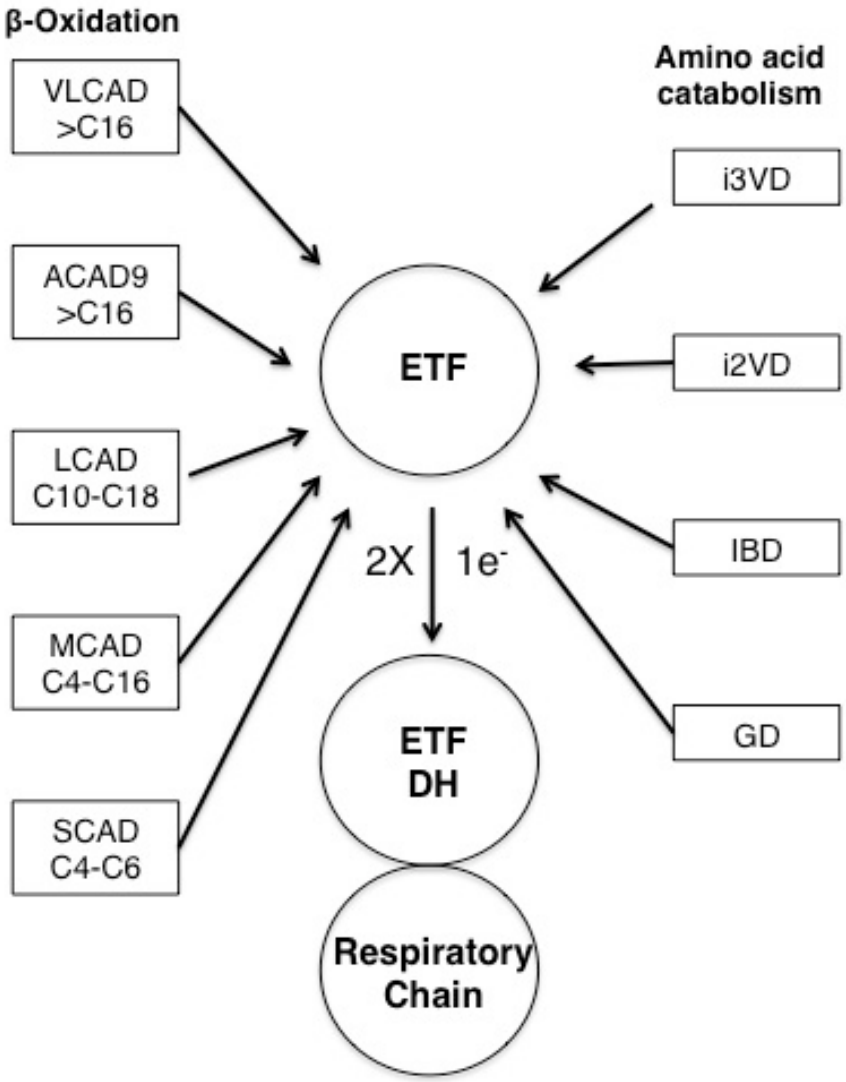

Figure 8. Acyl-CoA dehhydrogenases and their interaction with ETF in the α,β-dehydrogenation of acyl-thioesters

The enzymes involved in fatty acid β-oxidation are removing even numbered straight chains. ETF works as an electron acceptor of these dehydrogenases and then ETF dehydrogenase (ETFDH) delivers the electron to the respiratory chain.

Figure 9 shows the α,β-dehydrogenation by MCAD protein and an active catalytic site at Glu 376. Glu 376, catalytic residue, plays an important role in the initial step of dehydrogenation (Bross et al., 1999). The α-proton from the acyl-CoA substrate is abstracted by Glu 376 and Glu

376-COO^-, catalytic residue, interacts with FAD-2'OH and forming hydrogen bonds. The reduced flavin ($FADH_2$) is reoxidized through electron transfer flavoprotein (ETF).

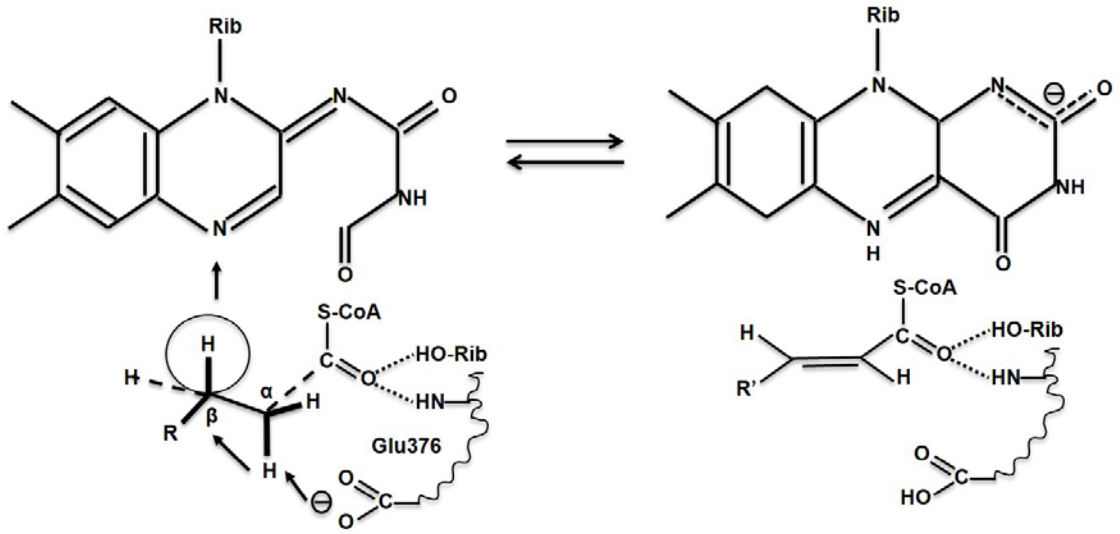

Figure 9. Reaction mechanism of the α,β-dehydrogenation by MCAD

A schematic presentation of dehydrogenation by MCAD. The active site Glu376 forms hydrogen bond with FAD and the substrate thioester carbonyl group. Rib indicates the ribityl side chain of the isoalloxazine.

1.4 MEDIUM CHAIN ACYL-COA DEHYDROGENASE DEFICIENCY IN HUMANS

1.4.1 General characteristics of MCADD

MCADD (OMIM 201450) is one of the most common inborn errors of metabolism in humans, and the most common FAOD. Prior to the advent of expanded newborn screening by

tandem mass spectrometry (MS:MS), the clinical presentation was extremely variable with onset of symptoms from neonates to adulthood. Some individuals have even remained asymptomatic lifelong. Most frequently MCADD presented between 18-36 months of life with fasting, or illness induced vomiting, hypoketotic hypoglycemia, and lethargy progressing to coma and seizures (Iafolla et al., 1994; Vockley and Whiteman, 2002; Wanders et al., 1999). Acutely ill individuals showed elevated blood concentrations of C8 (octanoyl)-carnitine together with lesser elevations of the C6 (hexanoyl)-, C10 (decanoyl)-, and C10:1 (decenoyl)- acylcarnitines (Duran et al., 1988). Approximately half of patients were not diagnosed during their initial presentation and half were diagnosed after having died. Fortunately, today diagnosis through clinical symptoms is rare as the disorder is readily identified through newborn screening by MS:MS. Patients thus identified are typically well, though at risk for hypoglycemia with recurrent illness and may require hospitalization for intravenous glucose administration. Current treatment for MCADD is simply to avoid fasting, and to reduce the dietary fat intake. The utility of carnitine supplementation is controversial.

1.4.2 Molecular genetics of MCADD

The *ACADM* gene, acyl-CoA dehydrogenase, C-4 to C-12 straight chain, is located on chromosome 1p31 and has 12 exons (Zhang et al., 1992). This gene encodes a 421-amino acid protein, the MCAD protein, with mitochondrial leader sequence. The MCAD mRNA is translated in the cytoplasm, and then the precursor protein is targeted to mitochondria, imported, folded to the mature subunit configuration, and assembled into a final homotetrameric active enzyme. Mutations in the *ACADM* gene can affect any of these steps, and lead to reduced

enzyme activity. Figure 10 shows the *ACADM* gene mutations identified in patients and screened newborns (Gregersen et al., 2008). The introduction of NBS led to the discovery of different kinds of mutations in the *ACADM* gene. Greater than 80 variants have been identified, and one mutation 985A>G (K304E MCAD protein) represents almost 90% of alleles in MCADD patients, especially predominating in Northern European populations (Blois et al., 2005; Matern and Rinaldo, 1993; Smith et al., 2010). A recent study confirmed that the frequency of the K304E mutation is significantly higher in individuals of Northern European descent (Leal et al., 2013). Expanded newborn screening (NBS) has led to the identification of additional novel mutations, but 985A>G remains the most prevalent disease causing mutation (Ensenauer et al., 2005b; Rhead, 2006; Smith et al., 2010).

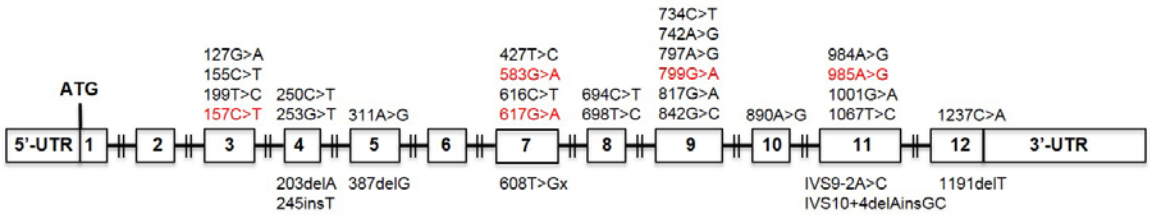

Figure 10. Spectrum of gene variations in the *ACADM* gene

The mutations found in screened newborns as MCADD.

1.4.3 MCAD structure and interaction with ETF

All ACADs except VLCAD and ACAD9 are active as homotetramers in the mitochondria matrix. VLCAD and ACAD9 are dimers with an extra C-terminus domain that occupies the space of the missing dimer in the other ACADs. The molecular mass of the precursor MCAD subunit is 44kDa. The N-terminal mitochondrial signal peptide is 25 amino

acid residues in length. After translation in the cytoplasm, it is imported into the mitochondria and the mitochondrial signal peptide is cleaved. The mature homotetramer includes FAD as a cofactor, catalyzes the first step in β-oxidation, and utilizes ETF as an electron acceptor (Matern and Rinaldo, 1993; Matsubara et al., 1992). X-ray crystallography studies have shown that the N-terminal and C-terminal regions of the MCAD protein consists of densely packed α-helices that shape the core of the tetramer (Kim et al., 1993; Kim and Wu, 1988). The middle domain has two orthogonal β-sheets located at the surface of the molecule. The MCAD tetramers are composed of a dimer of dimers. Figure 11 shows ribbon diagrams of the MCAD monomer and tetramer (Kim and Miura, 2004). Substrate binding to MCAD protein does not make significant conformational changes. However, there are significant changes at the residues that are located in the active site cavity, especially at Glu 376, a catalytic residue, Tyr 375 and Glu 99. When substrates are not bound, water molecules can fill the active site cavity and when the medium chain fatty acids approaches, the water molecules are displaced.

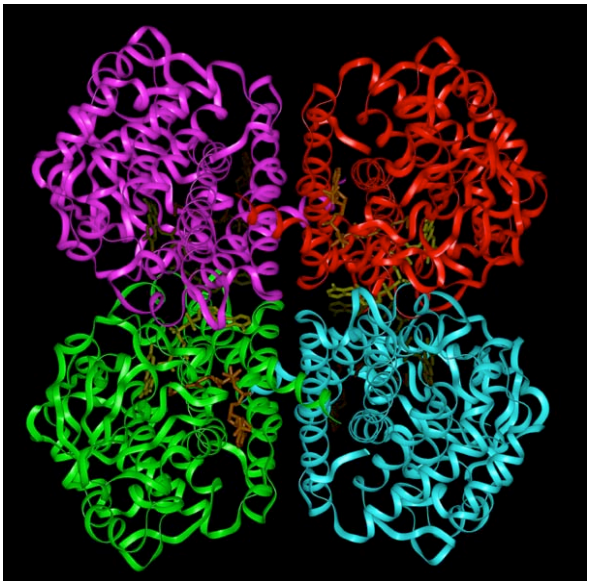

Figure 11. Ribbon structures of the MCAD protein

This represents the ribbon structures of the MCAD protein. Each color (magenta, red, green, and cobalt) indicates the monomer of the MCAD protein.

1.4.4 The common MCAD mutation leads to protein misfolding

MCAD mRNA is translated in the cytoplasm, and then the precursor protein is targeted to mitochondria, imported, folded to the mature subunit configuration, and assembled into a final homotetrameric active flavoenzyme. The K304E MCAD mutation has been shown to impair folding and assembly of the MCAD protein (Bross et al., 1995; Yokota et al., 1992). The positively charged lysine at position 304 is located in the middle of the α-helix H. Two negatively charged aspartates at positions 300 and 346 are close to position 304 and are known to interact with each other. Therefore, the positively charged lysine at position 304 replaced with a negatively charged glutamic acid presumably affects the balance of charges in the supersecondary and tertiary structure of the MCAD monomer. In patient fibroblasts, upon import into mitochondria, the K304E MCAD protein remains associated with the protein folding HSP60/10 complex, and then it is degraded. In a prokaryotic expression system, the K304E MCAD protein aggregates and leads to cellular death unless the bacterial chaperonin proteins, GroEL/ES (HSP 60/10 homologues) are co-expressed (Bross et al., 1993). In the latter case, the K304E MCAD protein is stabilized, correctly folded, and most importantly, is active. These results suggest that stabilization of the K304E MCAD protein could allow formation of sufficiently active enzyme to significantly impact disease phenotype.

1.4.5 The interaction between ETF and MCAD protein

Human electron transfer flavoprotein (ETF), the physiological electron acceptor that reoxidizes reduced MCAD, is a heterodimer, composed of α and β subunits, where the α subunit contains one FAD (Bross et al., 1999; Chohan et al., 2001; Parker, 2003a, b; Roberts et al., 1996).

The ETF has two main binding pocket areas; the recognition loop, an anchor site for the ETF:MCAD interaction, and FAD domain, a site for FAD binding. Unlike other electron carriers, ETF has a recognition peptide that the MCAD protein can dock to. The crystal structure of an ETF:MCAD complex has been solved (Figure 12) (Roberts et al., 1996; Toogood et al., 2004; Toogood et al., 2005). Also, Parker suggested that a single arginine residue is required for the interaction of ETF and MCAD protein (Parker, 2003a, b).

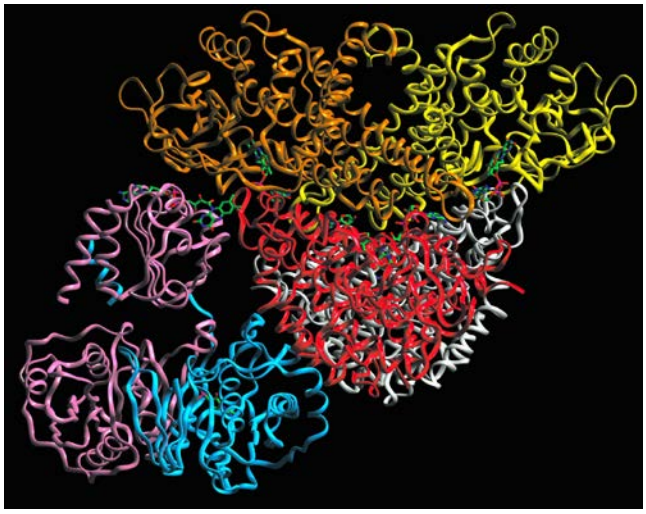

Figure 12. Ribbon representation of MCAD:ETF complex (PDB:2A1T)

MCAD monomers are shown in different colors (a in white, b in yellow, c in orange, and d in red).
The α-subunit of ETF is shown in magenta and β-subunit is shown in blue.

1.4.6 MCADD mouse model

An MCAD deficient mouse model was generated by Tolwani *et al*. By using gene targeting, the authors deleted 1.3 kb region of exon 10 and flanking sequences. After generating gene-targeted embryonic stem cell clones, these clones were injected into B6 blastocysts and then backcrossed to both 129P2 and B6. Finally MCADD mice were generated on a B6/129 mixed background. Clinical phenotypes of MCADD mice are similar to human MCADD.

MCADD mice show organic aciduria, fatty liver, and significant cold intolerance at 4°C in fasting conditions. Also they have high neonatal mortality rates. This model helps to understand the pathogenesis of MCADD.

1.4.7 MCAD activity assays

The MCAD activity can be measured from different cell types including fibroblasts and lymphoblasts or different tissues such as liver, heart, and skeletal muscle. There are different methods to detect the MCAD activity. In 1985, Frerman and Goodman developed the ETF assay to detect ACD activity (Frerman and Goodman, 1985). Since ETF is an electron acceptor of MCAD protein, ETF assay can directly detect the MCAD activity by measuring the stoichiometric reduction of ETF to $ETFH_2$ using fluorometry. This is the most sensitive test method to detect MCAD activity. However, since ETF protein is not commercially available, the ETF should be purified from pig liver which process is cumbersome. And this assay requires anaerobic condition that is another limitation of this method to be applied in different settings. Dye reduction assays are different ways to measure the MCAD activity. Since ETF is a limiting factor, dye reduction assays are using artificial electron acceptors such as dichlorophenol indophenol (DCIP) or ferricenium ions. In case of DCIP assay, phenazine methosulphate (PMS) will be a primary electron acceptor and then DCIP will accept the secondary electrons. The changes of the electrons will be measured by spectrophotometer at 600nm. In case of ferricenium assay, ferricenium hexafluorophosphate will be used as an electron acceptor (Lehman et al., 1990). However, these dye reduction assays are not as sensitive as ETF assay.

1.5 THERAPEUTIC APPROACHES FOR MCADD BY USING SMALL CHEMICAL CHAPERONES

1.5.1 Use of small chemicals and/or pharmacological chaperones as drugs in human protein misfolding diseases

Protein misfolding has been demonstrated as a common outcome of amino acids substitutions occurring at positions important for structure. Misfolding of protein promotes premature degradation of the protein (loss of function), the formation of toxic aggregates, and/or incorporation of toxic conformations into structures (gain of function) (Gregersen et al., 2005). Parkinson's disease, α-1-antitrypsin deficiency, familial neurohypophyseal diabetes insipidus are examples of the latter mechanism, while mutations in many inborn errors of metabolism have demonstrated the former (Barral et al., 2004; Gregersen et al., 2005; Gregersen et al., 2006). In case of mutations leading to degradation of protein and loss-of-function, an increase of mutant protein can have two effects. The first, an increase in at least partially active protein and rescue of function, is the desired outcome. Unfortunately, the second possibility is stabilization of a mutant protein that then aggregates and generates unintended gain of function toxicity. For the common K304E MCAD mutation, overexpression in a prokaryotic system in conjunction with the bacterial chaperonin proteins GroEL/ES leads to improved folding and rescue of activity. While the use of molecular chaperones such as the eukaryotic GroEL/ES homologous, HSP60/10 as therapeutic molecules would be challenging, development of small molecule chemicals as chaperones would be appear to be ideal potential drugs for this disease. The attractiveness of this approach is enhanced by the recognition from newborn screening studies that MCAD mutations

leaving very low levels of activity are sufficient to prevent the development of symptoms (Smith et al., 2010).

Chemical chaperones are small molecular weight compounds that promote the folding of proteins by altering the local chemical environment or stabilize their favorable conformation (i.e., without direct binding). They are used extensively *in vitro* to enhance stability of proteins in storage (glycerol), and more recently, have been explored as possible agents to correct protein misfolding in cells and rescue the protein function. Some small chemical chaperones work as osmoylates, which are compounds affecting osmosis in solution. These compounds increase the hydration of the proteins. In turn, there will be free-energy differences between a partially folded protein and its native structure. Even though the underlying specific mechanism of the function of small chemical chaperones is not clearly understood, these non-specific and/or indirect functions do change protein folding and activity. Another group of chaperones are known as pharmacological chaperones. These typically are designed or found to bind to a structural motif that helps stabilize the folded protein and increase productive folding. A number of medications are now on the market based on this mechanism of action. Table 5 shows different diseases and the rescue of each condition with different chemical and/or pharmacological chaperones (Leandro and Gomes, 2008). Identifying novel compounds that might ultimately make successful drugs is a laborious and time-consuming process. Ideally, a high-throughput assay is available to monitor an effect on a specific target protein molecule or molecular phenotype would be valuable.

Table 5. Human proteins involved in misfolded disorders rescued by chemical and pharmacological chaperones

Disease	Protein involved	Functional Localization	Mechanism of Pathogenesis	Chemical / Pharmacological chaperone
Gaucher	GC	Lysosome	Mistrafficking	Deoxynojirimycin derivatives
Fabry	GLA	Lysosome	Mistrafficking	Galatose, 1-deoxy-galactonojirimycin
Pompe	GAA	Lysosome	Mistrafficking	Deoxynojirimycine derivatives
Tay-Sachs	HEXA	Lysosome	Mistrafficking	PYR; NGT
Familial hypercholesterolemia	LDL receptor	Membrane	Mistrafficking	4-PB
Cystic fibrosis	CFTR	Membrane	Mistrafficking	Glycerol, DMSO, TMAO, 4-PB, TS3, VRT325; corr-2b; corr-4a
Nephrogenic diabetes insipidus X-linked	V2R	Membrane	Mistrafficking	SR121463B
Nephrogenic diabetes insipidus type II	AQP2	Membrane	Mistrafficking	Glycerol; TMAO; DMSO
α1-antitripsin deficiency	1-AT	Extracellular	Mistrafficking	Glycerol, 4-PB
Retinitis pigmentosa	CA IV	Membrane	Mistrafficking	Acetazolamide; ethoxzolamide (enzyme inhibitors)
Primary carnitine deficiency	OCTN2	Membrane	Mistrafficking	4-PB, quinidine, verapamil
Albinism	Tyrosinase	Membrane	Mistrafficking	DOPA, Tyr
Huntington	Huntingtin	Cytoplasm	Aggregation	Trehalose
Hypogonadotroic hypogonadism	GnRH receptor	Membrane	Mistrafficking	Indol and Quinolone derivatives
Machado-Joseph	Ataxin-3	Nucleous/ cytoplasm	Aggregation	Glycerol, TMAO, DMSO
Parkinson	α-synuclein	Cytoplasm	Misfolding/	TMAO

Table 5 Continued

			aggregation	
Creutzfeldt-Jakob	Prion	Several cellular locali	Aggregation	Acridine-based analogue
Alzheimer	β-amyloid		Misfolding/ aggregation	TMAO, glycerol
Homocystinuria	CBS	Cytoplasm	Misfolding	TMAO, glycerol, sorbitol, L-proline; DMSO
Phenylketonuria	PAH	Cytoplasm	Misfolding	Glycerol, BH_4
Maple syrup urine disease	BCKD	Mitochondria	Misfolding	TMAO
Cancer	P53	Nucleus	Misfolding	Glycerol, TMAO, D_2O, CP249175, CP31398

In recent study, Zhang *et al*. found that small molecule compounds can recover the PEX1-Gly843Asp proteins causing Zellweger spectrum disorder (ZSD). ZSD is a disorder in peroxisome biogenesis leading to the failure to assemble normal peroxisomes. It is genetically heterogeneous and is caused by mutation in one of nearly 20 genes. No effective therapy is available. PEX1-Gly843Asp can cause the misfolding of the PEX1 protein and lower the stability of the protein and degrade the protein. In patients' fibroblasts having homozygous PEX1-Gly843Asp, only 5-15% of the PEX1 proteins were present compared to the wild type. The authors treated small molecule compounds for 48 hours and found the recovery of the proteins by confirming the recovery of the peroxisome structure using immunostaining (Zhang et al., 2010). All these studies related to protein misfolding disorder using small chemical compounds as therapy support that small chemical chaperones can stabilize the K304E MCAD protein.

1.5.2 Small recovery of the MCAD activity is sufficient for MCADD therapy

To investigate effective therapeutic approaches for MCADD, it is important to know the level of MCAD activity necessary to prevent the development of symptoms. In a recent study, Smith *et. al.* reported that minimal residual enzyme activity is sufficient to prevent MCADD (Smith et al., 2010). Therefore, potential MCADD therapies need not reproduce wild type MCAD activity levels. Rather even small increases in deficient patients will likely be sufficient to prevent the manifestations of MCADD.

1.5.3 Small chemical chaperones therapy for MCADD

Previously, many studies have shown that co-expression of the bacterial chaperonin GroEL/ES significantly stabilize the K304E MCAD protein (Bross et al., 1993). Also in eukaryotic system, down regulation of molecular chaperone, Hsp60, by RNAi impairs folding of wild type and mutant (K304E and R28C) MCAD proteins (Corydon et al., 2005). These support that molecular chaperones help the proper folding of the MCAD protein and by using small chemical chaperones we can rescue the MCAD protein folding and activity.

1.5.4 Metabolism of Sodium Phenylbutyrate

4-phenylbutyrate (PBA) is an aromatic fatty acid that composed of an aromatic ring with a butyric acid side chain (structure in table 7). It was originally used clinically as an ammonia conjugation agent, but has also been investigated as an inhibitor of the histone deacetylase HDACI, and as a non-specific chemical chaperone (Iannitti and Palmieri, 2011). *In vivo*, PBA

has been proposed to be activated to its CoA intermediate, then undergoes one round of mitochondrial fatty acid oxidation to its active form phenylacety-CoA (PAA). PAA can then be conjugated with one molecule of glutamine to form phenacetylglutamine (PGG), which can be excreted through urine. Thus, PBA provides an alternative source of ammonia excretion through PGG for patients with genetic defects of the urea cycle. PBA has also been shown to act as a histone deacetylase inhibitor (HDACI). Histone deacetylation can repress the transcriptional activation of genes and lead to gene silencing. Gene expression is a key process for cancer due to its function in cell growth and differentiations, and PBA has been proposed as a therapeutic option to control important cellular functions, including cell cycle arrest, induction of apoptosis, and activation of tumor suppressor genes, etc. Lastly, PBA has been studied as a chemical chaperone in protein misfolding disorders including cystic fibrosis, ischemia, Huntington disease, etc. (Iannitti and Palmieri, 2011).

1.5.5 High-throughput screening (HTS) as a tool for investigating possible drug for MCADD

HTS method is a well-established screening tool for drug discovery. It was first introduced in the mid-1990s to identify drugs for the treatment of human diseases (Mayr and Bojanic, 2009). HTS uses miniaturized assay systems, automation of the procedures, and large-scale data analysis. Therefore, by using this method, the overall cost of the assays and time can be reduced significantly. This method has been used generally for investigating small-molecule lead compounds (Zhu and Cuozzo, 2009). Since small chemical libraries containing FDA approved drugs are commercially available, the development of HTS method for MCADD will be useful to save time and cost for MCADD drug discovery. Changes in either MCAD protein

expression or MCAD activity in the presence of drug can be measured to find the positive hits from these libraries. Miniaturization and optimization of the detection methods will be the first step for HTS in MCADD drug discovery.

1.6 HYPOTHESES AND SPECIFIC AIMS OF THIS STUDY

The overall hypothesis of this study is that even a small increase in MCAD activity will prevent clinical manifestations, and that protein stabilizing agents can increase MCAD enzyme activity *in vivo* and *in vitro*. My project has two main specific aims. Specific aim 1 is to study the effect of small chemical chaperones such as dimethylsulfoxide (DMSO), glycerol, trimethylamine *N*-oxide (TMAO), betaine, and L-proline on K304E mutant protein folding and activity. I hypothesize that incubation of these agents with MCAD deficient lymphoblasts will improve folding of the K304E MCAD protein and partially restore enzyme activity. Specific aim 2 is to identify specific drug-targeting sites on the K304E MCAD protein *in silico*, as targets for therapeutic intervention. I hypothesize that synthetic peptides modeled on the K304E MCAD protein structure will promote stable folding of K304E MCAD protein and thus serve as a new class of molecules for chaperone therapy.

2.0 MATERIALS AND METHODS

2.1 CELL CULTURE

The cell lines used in this study and their sources are summarized in table 6.

Table 6. Summary of cell types and source

Cell name	Cell Type	Source
FB 554	Wild type human diploid fibroblasts	Vockley lab
GM13275	MCAD (K304E) patient diploid fibroblasts	NIGMS Human Mutant Cell Repository, Coriell Institute, Camden NJ
GM07844	MCAD (K304E) patient diploid fibroblasts	NIGMS Human Mutant Cell Repository, Coriell Institute, Camden NJ
TL 596	Wild type lymphoblasts (EBV transformed)	Vockley lab
TL 598	Wild type lymphoblasts (EBV transformed)	Vockley lab
TL 671	MCAD (K304E) patient lymphoblasts (EBV transformed)	NIGMS Human Mutant Cell Repository, Coriell Institute, Camden NJ
TL 672	MCAD (K304E) patient lymphoblasts (EBV transformed)	NIGMS Human Mutant Cell Repository, Coriell Institute, Camden NJ
pcDNA	HEK 293 T-REX Flp-In pcDNA; a transformed epithelial cell line with an empty (control) pcDNA vector integrated	Dr. Thomas Corydon, Aarhus University, Aarhus, Denmark
MCAD	HEK 293 T-REX Flp-In *MCAD* (wild type); a transformed epithelial cell line with an integrated pcDNA vector containing a wild type *MCAD* cDNA insert	Dr. Thomas Corydon, Aarhus University, Aarhus, Denmark

Table 6 Continued

K304E	HEK 293 T-REX Flp-In *MCAD* (K304E); a transformed epithelial cell line with an integrated pcDNA vector containing a *MCAD* K304E cDNA insert	Dr. Thomas Corydon, Aarhus University, Aarhus, Denmark
R28C	HEK 293 T-REX Flp-In *MCAD* (R28C); a transformed epithelial cell line with an integrated pcDNA vector containing a *MCAD* R28C cDNA insert	Dr. Thomas Corydon, Aarhus University, Aarhus, Denmark

2.1.1 Human diploid fibroblasts

Wild type and MCADD patients' fibroblasts were cultured in Dulbecco's Modified Eagle Medium (DMEM) supplemented with 1% $_{L}$-glutamine, 1% penicillin streptomycin and 15% fetal bovine serum (FBS) at 37°C, 5% CO_2, and humid incubator.

2.1.2 HEK 293 T-REX Flp-In inducible cell line

All HEK 293 T-REX Flp-In inducible cell lines were cultured in Dulbecco's Modified Eagle Medium (DMEM) supplemented with 1% L-glutamine, 1% penicillin streptomycin and 15% fetal bovine serum (FBS) at 37°C, 5% CO_2, with humidity. 100µg/ml of hygromycin and 15µg/ml blasticidin were also added to ensure continued integration of the vectors. 1µg/ml of tetracyclin was added to induce the vector insert.

2.1.3 Human lymphoblasts

Both wild type and MCADD patients' lymphoblasts were cultured in Roswell Park Memorial Institute (RPMI) medium supplemented with 1% $_{L}$-glutamine, 1% penicillin streptomycin and 15% fetal bovine serum (FBS) at 37°C, 5% CO_2, with humidity.

2.2 HIGH-THROUGHPUT IMMUNOASSAY FOR MCAD STABILITY

To facilitate screening of a chemical library for compounds with chaperonin activity for mutant MCAD, a high-throughput immunoassay was developed. Wild type and MCADD mutant human diploid fibroblasts were seeded at 3,000 cells per well in collagen coated 384-well black-walled clear-bottom plates and cultured overnight at 37°C, 5% CO_2, with humidity. The next day, cells were washed once with Dulbecco's phosphate buffered saline (PBS) without Ca^{2+} or Mg^{2+} and fixed with 3.7% formaldehyde containing Hoechest dye for 10 minutes at room temperature. Cells were permeabilized with 0.5% Triton X-100 in PBS for 90 seconds at room temperature then washed with PBS. Either polyclonal or monoclonal primary MCAD antibody (1:62.5 dilution in TBST) was incubated for 1 hour at room temperature. Then, cells were washed with PBS and secondary Alexa Fluor® AF488 anti-rabbit antibody (1:500 dilution in TBST) was added and incubated for 1 hour at room temperature. After secondary antibody incubation, cells were washed with PBS and the cell plates were sealed and imaged by the ArrayScan VTI imaging platform.

2.3 SMALL CHEMICAL CHAPERONES

DMSO, TMAO, L-proline, betaine, glycerol, and 4-phenylbutrate were purchased from Sigma (St. Louis, MO). DMSO, glycerol, TMAO, and 4-phenylbutyrate were dissolved in tissue culture media and filter sterilized. L-proline and betaine were dissolved in distilled water and filter sterilized. Table 7 shows the structure of each chemical (http://pubchem.ncbi.nlm.nih.gov/).

Table 7. Structures of small chemical chaperone

Name	Molecular formula	Molecular weight	Structure
DMSO	C_2H_6OS	78.13344	
TMAO	C_3H_9NO	75.10966	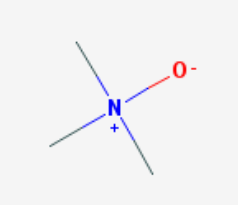
Betaine	$C_5H_{11}NO_2$	117.14634	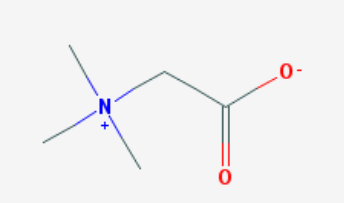
Glycerol	$C_3H_8O_3$	92.09382	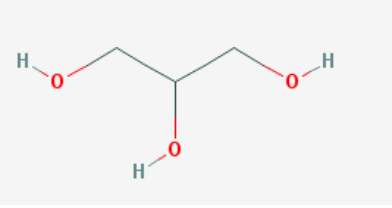

Table 7 Continued

L-proline	$C_5H_9NO_2$	115.13046	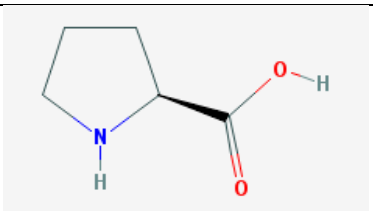
4-phenylbutrate	$C_{10}H_{12}O_2$	164.20108	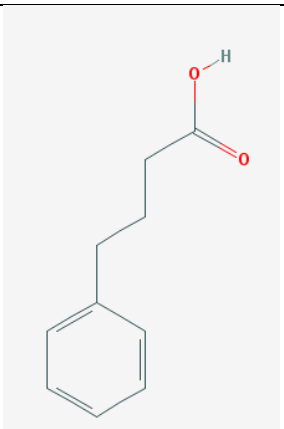

2.4 PROTEIN QUANTIFICATION

Proteins from cell free extracts or bacterially purified proteins were quantified by DC Protein Assay Kit from BioRad (Hercules, CA).

2.5 PROTEIN PURIFICATION

2.5.1 MCAD purification

Expression of recombinant human MCAD protein expression plasmids was as described (Matsubara et al., 1989). Briefly, pKe-*MCAD* and pKe-*MCAD* K304E, were co-transformed with pGroEL/GroES (encoding the bacterial chaperonin *GroEL* and *GroES* genes) in *E. coli* JM105

cells (Amersham Biosciences Crop; Piscataway, NJ). Cells were grown overnight with antibodies, ampicillin (100μg/ml) and chloramphenicol (50μg/ml) at 37°C with shaking, and the vectors were induced by the addition of 0.5mM isopropyl β-D-1-thiogalactopyranoside (IPTG) for three hours at 30°C. Cells were harvested by centrifugation, lysed by sonication on ice and subjected to centrifugation at 250,000 x g for 30 minutes. Cell free extracts were fractionated sequentially with 30% and 50% ammonium sulfate. The final ammonium sulfate pellet was dissolved in 50mM potassium phosphate buffer (KP, pH 8.0) and 25μM FAD dialyzed for 4 hours in the same buffer, then subjected to centrifugation for 20 minutes at 19,000 rpm at 4°C. Supernatant was loaded onto a DEAE (diethylaminoethyl) Sepharose^{TM} fast flow (GE Health care Life sciences; Piscataway, NJ) column by using an ÄKTA UPC-900 pump FPLC system (Amersham Biosciences Corp; Piscataway, NJ) and eluted with a gradient of 50mM KP to 400 mM KP, pH8.0. Fractions were tested for the presence of MCAD protein by SDS-PAGE and Coomassie blue staining. Those containing the highest amount of protein were pooled, buffer exchanged in a Centriprep 30K (Merk Millipore LtD; Darmstadt, Germany) to a 10 mM KP (pH 8.0) loaded onto a CHT^{TM} ceramic hydroxyapatite type I (BioRad; Hercules, CA) column, and eluted with a linear gradient to 300 mM KP, pH 8.0. Peak fractions containing MCAD protein were identified by spectrophotometer at 447nm.

2.5.2 ETF purification

ETF isolation method was performed as described (Vockley et al., 2000). Briefly, fresh pig liver was cut into small pieces and washed with PBS to remove the blood. The tissue was homogenized by blending in 50 mM KPO_4 (pH 8.0), 1 mM EDTA, 2.5% glycerol and 250 mM sucrose, filtered through cheese clothes. Cellular debris was removed by low speed

centrifugation, 2,500 rpm in a Beckman J6-HC, followed by a higher speed centrifugation, 9,000 rpm in Sorval RC 5B Plus, to pellet mitochondria. The pellet was washed at least 3 times in homogenization buffer. The final pellet was stored at -80°C. For ETF purification, pellets weighing 400-500 mg were mixed 0.3:1 (volume: weight) with 10 mM EDTA, 3 mM K_2HPO_4 (pH8.0), 0.12 mM FAD, and 0.541 mM AMP, sonicated on ice, then subjected to centrifugation at 250,000 X g. The supernatant was fractionated by ammonium sulfate (40% then 60%). The 60% fraction pellet was dissolved in sonication buffer and dialyzed extensively in three changes of 15 mM K_2HPO_4 (unbuffered) and 5% glycerol overnight, and the dialysate was loaded onto a DEAE-sepharose column (GE Health care Life sciences; Piscataway, NJ) and eluted with 15 mM K_2HPO_4 (unbuffered) and 5% glycerol. Fractions containing significant fluorescence under UV light were pooled and applied to a carboxymethyl (CM) Sepharose column (GE Health care Life sciences; Piscataway, NJ) and eluted with a gradient of 10 mM Tris, pH 8.5 to 10 mM Tris, 100 mM NaCl, pH8.5. Fractions with an A_{270}/A_{436} ratio below 8 were pooled and used for regular test assays, or further applied to a ceramic hydroxyapatite column (BioRad, Hercules, CA). Fractions with an A_{270}/A_{436} ratio below 6.5 were pooled for kinetic studies.

2.6 SDS-PAGE

For visualization of fractionated proteins samples, aliquots were separated on 4-12 %T Tris gels or 16.5 %T Tricine gels and stained with either Coomassie blue (0.025% Coomassie blue R-250 in 40% methanol, and 7% acetic acid) or a with ProteoSilver™ Plus Silver Stain Kit from Sigma (St. Louis, MO).

2.7 ETF FLUORESENCE REDUCTION ASSAY

Anaerobic ETF fluorescence reduction assay using a rubber sealed cuvette with sample deaerated with argon and vacuum was performed using a Jasco FP-6300 fluorescence spectrofluorometer (Easton, MD) to measure the MCAD and VLCAD activity as described (Frerman and Goodman, 1985). Samples were mixed with reaction buffer containing 50 mM Tris, pH8.0, 0.5% glucose and 30μM octanoyl-CoA as a substrate for MCAD activity. Palmitoyl-CoA was used in the same concentration as control in cellular extracts. Octanoyl-CoA and palmitoyl-CoA were purchased from Sigma (St. Louis, MO). Background fluorescence was measured in the absence of ETF. Then, ETF was added to a 2μM final concentration and baseline fluorescence of the reaction mixture was determined. The reduction in fluorescence over 30 sec was monitored and the rate was calculated. One mU of activity is defined as the amount of enzyme necessary to completely reduce on μ mole of ETF in 1 minute (Frerman and Goodman, 1985). To test for thermal stability, MCAD protein at 130nM and the MCAD:ETF at 10 mM of docking site peptide, wild type sequence or mutant, were incubated on ice for 10 minutes, 10μL final volume in 50 mM Tris (pH 8.0) buffer. Each sample was incubated at temperature ranging from 30ºC to 62.5ºC with increments of 2.5ºC for 5 minutes, then assayed for residual MCAD activity.

2.8 SAMPLE PREPARATION FOR ETF ASSAY

2.8.1 Treatment of cells with chemical chaperones

Wild type and patient lymphoblasts were incubated for 48 hours in 0.5% glycerol, 3% DMSO, 100 mM betaine, 200mM TMAO, or 300 mM L-proline were treated with both wild type and patients', having homozygous K304E mutant lymphoblasts. The lymphoblasts were harvested by centrifugation, lysed in a water bath sonicator, Misonix S-4000 (Misonix, Farmingdale, NY). The protein concentration of the supernatant was measured using the DC the protein assay kit from BioRad (Hercules, CA) and ACAD activity was measured with the ETF reduction assay. Wild type and K304E MCAD mutant lymphoblasts and diploid fibroblasts were incubated with sodium phenylbutyrate (0.5 mM or 1 mM) and cultures for 48 hours at 37ºC. Cells were harvested by centrifugation and assayed for protein and ACAD activity as above.

2.8.2 ETF and peptide experiment

130 nM of MCAD protein and 10 mM of selected peptide targeting ETF docking were incubated on ice for 10 minutes. Then whole reaction mixture was used for ETF assay.

2.8.3 ETF assay sample preparation for peptide thermal stability experiment

The sample preparation was done like previously in peptide experiment. 130nM of MCAD protein and 10 mM of selected peptide were incubated on ice for 10 minutes. Then, each sample

was incubated at the assigned temperature for 5 minutes. Assigned temperatures ranged from 30ºC to 62.5ºC with data acquired every 2.5°C.

2.9 DCIP ASSAY

2,6 Dichlorophenol-Indophenol (DCIP) dye reduction assay was performed to investigate the MCAD activity independent of ETF interaction. Phenazine methosulfate (PMS) was used as an intermediate electron acceptor with DCIP was used as the final electron acceptor and reaction indicator. The reaction mixture contained 100mM potassium phosphate (pH 8.0), 3mM PMS, 100µM FAD, and 60µM substrate, and was started with octanoyl-CoA added to a final concentration of 50µM. The reduction of absorbance was measured at 600nm using a Jasco V-650 spectrophotometer. MCAD activity was calculated as follows: Activity/ml = $O.D._{600}$ X 47.6 X 1000/ volume of enzyme used. One mU of activity is defined as the amount necessary to completely reduce one µM of DCIP.

2.10 QUANTITATIVE REVERSE TRANSCRIPTION PCR

Total RNA was isolated from cells treated with chemical chaperones using the RNeasy Mini Kit (Qiagen). One microgram of RNA was reverse transcribed (SuperScript III, Invitrogen) with random hexamer or oligo (dT) primers in a 20µl reaction. *ACADM* sequences were quantitated in triplicate by qPCR in an Applied Biosystems 7300 Real Time PCR system with SYBR green (Power SYBR® Green PCR Master Mix, Applied Biosystems) as the fluorescent

label, *GAPDH* primers were used as for normalization. Threshold cycle (CT) was reported. Table 8 shows the primers for qPCR.

Table 8. Primers

Primer name	Nucleotide Sequence
Human GAPDH 5’	5' ATG GAA ATC CCA TCA CCA TCT T 3'
Human GAPDH 3’	5' CGC CCC ACT TGA TTT TGG 3'
hMCAD 164-188 5’	5’ TTG CCA GAG AGG AAA TCA TCC CAG T 3’
hMCAD 478-452 3’	5’ CAC AAT AAG CAC ACA TCA ATG GCT CG 3’

2.11 STRUCTURAL ANALYSIS OF MCAD PROTEIN

To analyze the MCAD K304E structure, published crystal structures of MCAD from different species were compared. Table 9 shows the sources of crystal structure of MCADs.

Table 9. Description of analyzed crystal structure of MCAD protein

PDB ID	Description	Reference
3MDE	The pig MCAD structure with octanoyl-CoA	(Kim et al., 1993)
3MDD	The pig MCAD structure	(Kim et al., 1993)
2A1T	The human MCAD:ETF βE165A complex	(Toogood et al., 2005)
1UKW	The crystal structure of MCAD from *Thermus thermophilus* HB8	Atomic coordinates only deposited under the code 1UKW

2.12 GENERATION OF ETF DOCKING SITE BINDING SYNTHETIC PEPTIDES

A crystal structure of an MCAD:ETF complex has been reported (Toogood et al., 2004). Based on this model, 12-mer peptides were designed for enhanced binding to the MCAD ETF-docking site, ETF amino acid residues Arg191 to Lys202, using *Insight*II (Accelrys) Molecular Modeling software package. Figure 13 shows a ribbon representation of MCAD monomer and the ETF docking peptide. The various peptides were synthesized at the University of Pittsburgh Genomics and Proteomics Core Laboratories. Table 10 shows the amino acid sequence of various synthetic peptides.

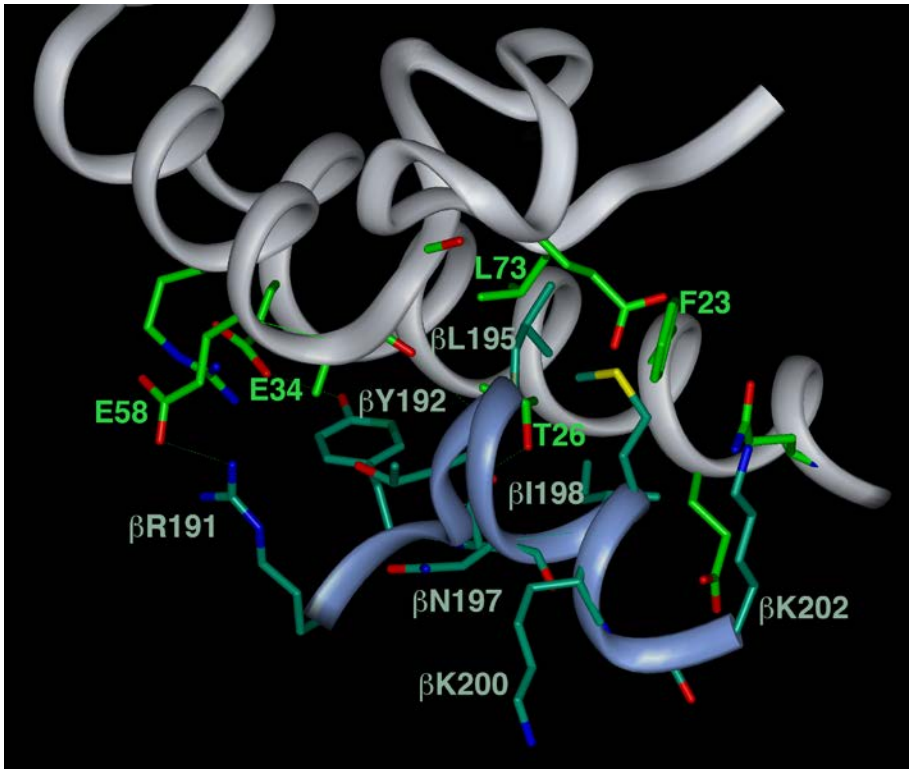

Figure 13. Ribbon representation of the MCAD ETF docking site (gray ribbons) and the ETF docking peptide

ETF βR191-βK202 (blue ribbon). (The rest of the MCAD tetramer and ETF dimer are hidden)

Table 10. Amino acid sequences of the synthetic ETF docking site peptide sequences

YAT 191 (Wild type)	RYATLPNIMKAK
YAT 2	YATLPNIMKAK
YAT 193	YAT193*
YAN	YANLPNIMKAK
YANF	YANLPNIFKAK
YRQF	YRQLPNIFSN
YRQR	YRQLPNIRSN
YAT 194	RYANMPNIFKAK
YAT 195	RYATLPNIFKAK
YAT 196	RYANLPNIFKAK

*Sequence not revealed for patent rights

2.13 CIRCULAR DICHROISM (CD)

Purified recombinant wild type or K304E MCAD protein at 5μM concentration was mixed with an MCAD:ETF docking peptides to give 1mM final concentration in 25mM KP buffer, pH8.0. CD and US-visible spectral changes were measured with a Jasco J-810 Spectropolarimeter at 445nm with 1ºC increase from 33ºC to 73ºC. At each temperature, the machine equilibrated for 1 minute, then the CD spectrum was acquired as the difference in fluorescence intensities for left and right circularly polarized excitation.

2.14 LIMITED PROTEOLYSIS

Ten micrograms of purified recombinant wild type and K304E mutant MCAD protein were co-incubated with an MCAD:ETF docking peptide with or without *Staphylococcus aureus* V8 protease in 50mM NH_4 bicarbonate buffer, pH8.0, a buffer favoring Glu-C hydrolysis. The reaction was initiated by adding the protease at a MCAD:protease ratio of 20:1 (w/w) and then incubating at 37°C. Samples were collected at 0, 2.5, 5, 7.5, 10, 15, and 30 minutes. A no protease control was incubated for 30 minutes in the same buffer. Reactions were stopped by adding Laemmli SDS-PAGE sample buffer and boiling the collected samples for 5 minutes. Peptide patterns were visualized by separation on 16.5% Tris-Tricine gels, followed by silver staining with ProteoSilver™ Plus Silver Stain Kit from Sigma (St. Louis, MO). Peptide bands were identified by excising them from the gel and subjected to mass spectrometry by the University of Pittsburgh Genomic and Proteomic Core Laboratory. To test the protease sensitive enzyme activity, 35nM of MCAD protein and 3mM of a peptide targeting MCAD:ETF docking were incubated on ice for 30 minutes, 6.7 μL total volume in 50mM NH_4 bicarbonate buffer, pH8.0, with or without *Staphylococcus aureus* V8 protease at 750 units. Then entire reaction mixture was used as sample for the ETF reduction assay.

2.15 DENSITOMETRIC ANALYSIS OF PROTEIN BANDS

Determination of the rates of generation of the MCAD proteolytic peptides after SDS PAGE with silver or Coomassie Blue staining, and western blot bands were carried out using Alpha Imager 2200, and AlphaEaseFCTM software following scanning with a computer driven

Epson, Inc scanner. Distinct protein bands were quantitated and normalized by its background. Calculated protein density numbers were then compared to each other.

2.16 MS/MS ANALYSIS

After limited proteolysis, Coomassie stained gels were washed with water and band of interest was excised and analyzed by University of Pittsburgh Genomics and Proteomics Core Laboratories.

3.0 RESULTS

3.1 DEVELOPMENT OF A HIGH-THROUGHPUT SCREENING ASSAY FOR MCADD

Screening chemical libraries for compounds that are clinically active in a specific disorder is laborious and time consuming. Most drug discovery programs screen tens or hundreds of thousands of molecules to identify second tier candidates. There are two options to expedite this process. First, the development of a high-throughput screening assay system allows large numbers of compounds to be tested quickly, reserving more specific assays for follow up studies. Alternatively, a more targeted approach in selecting candidate molecules based on a prior knowledge of the system in combination with *in silico* design might allow testing of fewer candidate compounds. To explore the first possibility, a high-throughput screening assay method for MCADD based on immunostaining of MCAD protein in patient fibroblasts was tested. Wild type or one of the two different MCADD patient fibroblasts were seeded into 384 well plates and MCAD antigen was visualized in an automated ArrayScan VTI imaging platform after reacting with an MCAD specific monoclonal or polyclonal antibody (Figure 14 and 15). Unfortunately, all three cell lines stained nearly equally, and thus could not be differentiated under these conditions. Of note, publications to date have differed on the presence or absence of antigen in patient cells.

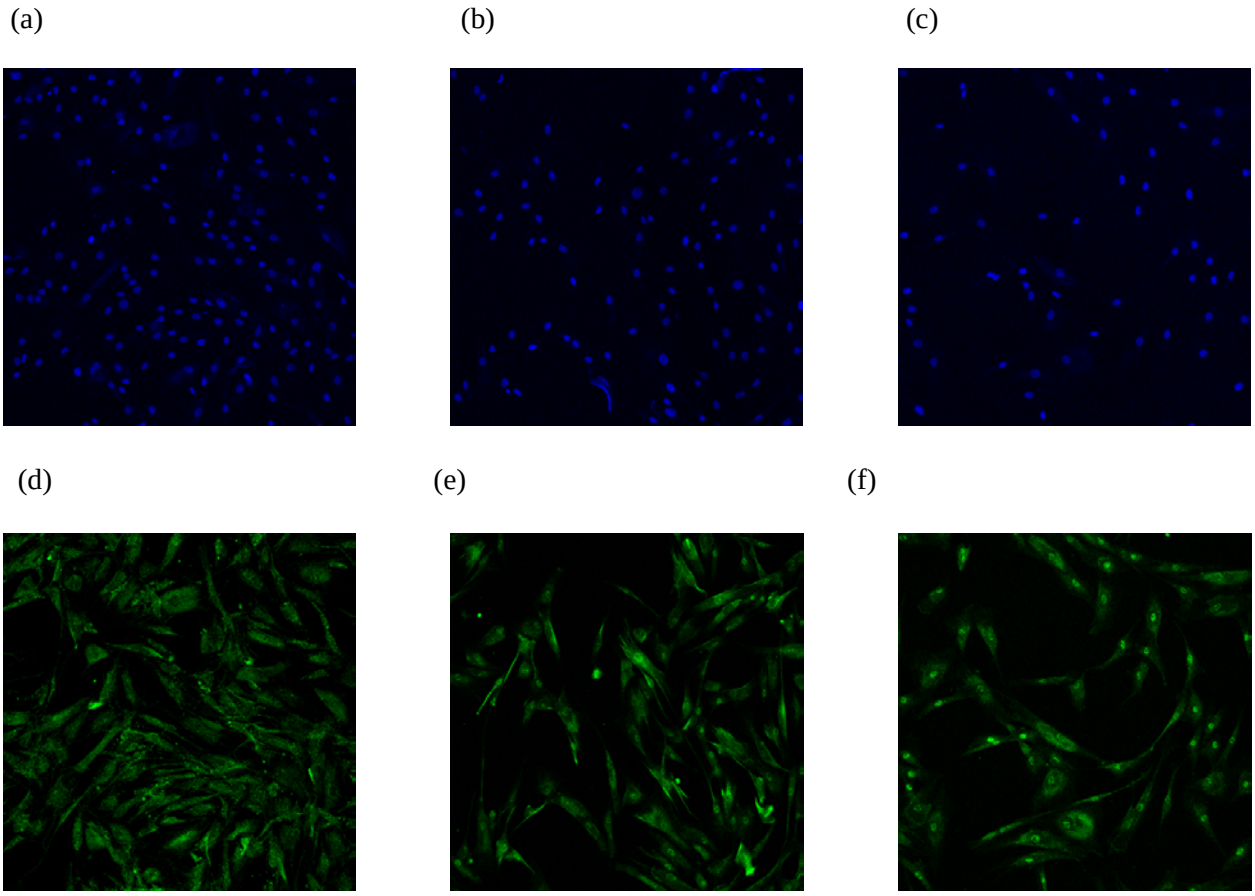

Figure 14. Immunofluorescent staining of MCAD staining in fibroblasts with polyclonal MCAD antibody

Human diploid fibroblasts from control and two different patients were seeded at 3,000 cells per well in collagen coated 384 well plates and cultured overnight at 37°C. The next day, the cells were permeabilized and incubated with a polyclonal MCAD antibody. The plates were sealed and imaged by the ArrayScan VTI imaging platform. Blue indicates the nuclear staining and green indicates MCAD protein. (a,d: Wild type fibroblasts, b,e: GM13275, c.f: GM07855)

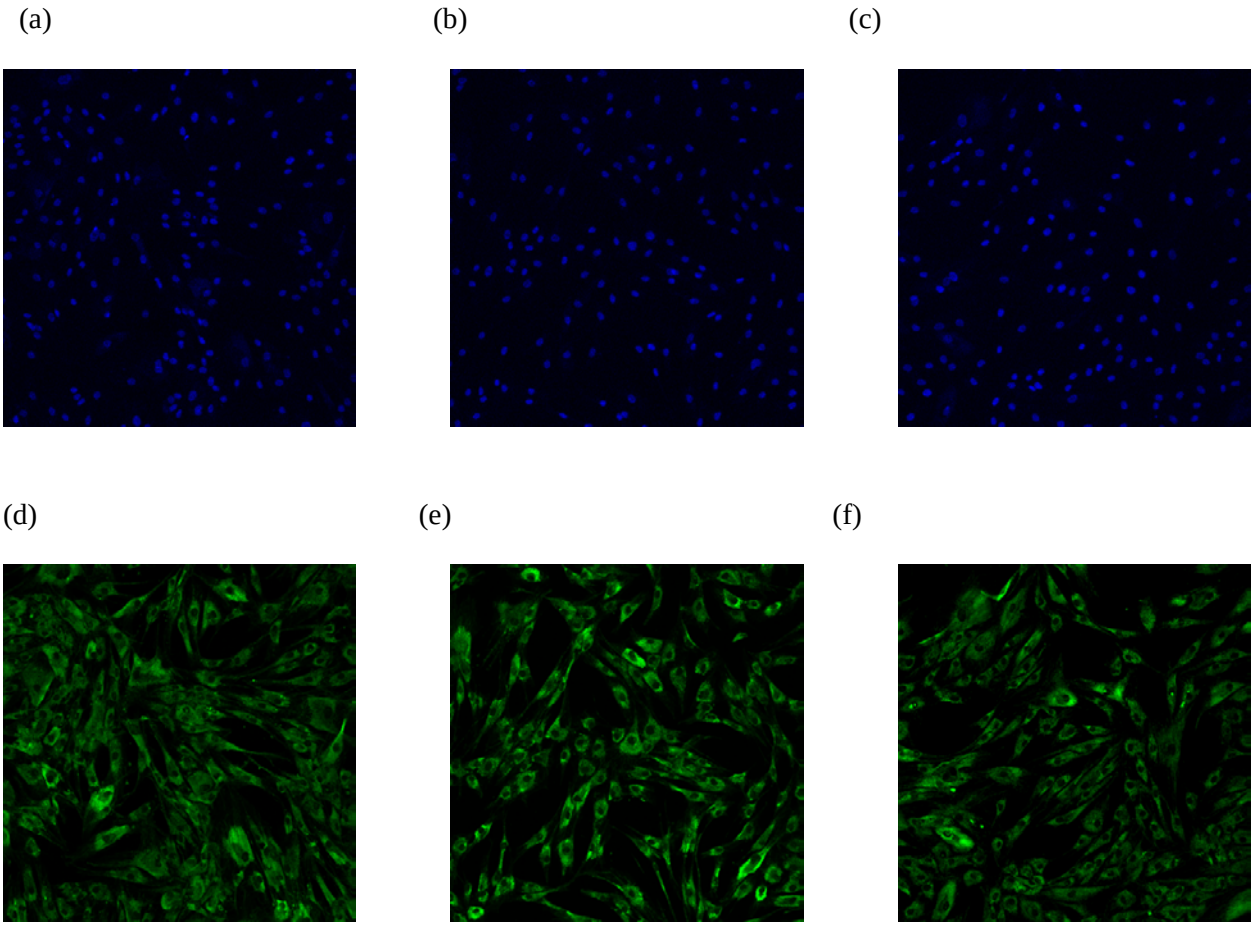

Figure 15. Immunofluorescent staining of MCAD staining in fibroblasts with monoclonal MCAD antibody

Human diploid fibroblasts from control and two different patients were seeded at 3,000 cells per well in collagen coated 384 well plates and cultured overnight at 37°C. The next day, the cells were permeabilized and incubated with a monoclonal MCAD antibody. The plates were sealed and imaged by the ArrayScan VTI imaging platform. Blue indicates the nuclear staining and green indicates MCAD protein. (a,d: Wild type fibroblasts, b,e: GM13275, c.f: GM07855)

3.2 SMALL CHEMICAL CHAPERONES STABILIZE MCAD IN MUTANT LYMPHOBLASTS

3.2.1 Basal MCAD enzyme activity and *ACADM* gene expression in lymphoblasts

As proof of principle before starting large-scale chemical screening studies, several small chemicals with known protein stabilization properties were tested for their ability to rescue activity in lymphoblasts homozygous for the K304E MCAD mutation. Basal MCAD enzyme activity in these cells was measured first (Figure 16). Lymphoblasts from a control (596) and two different MCAD patients (671 and 672), were cultured at 37°C and 30°C respectively, and enzyme activity was tested. MCAD activity was almost zero in patient lymphoblasts but was easily detectable in control cells at both temperatures.

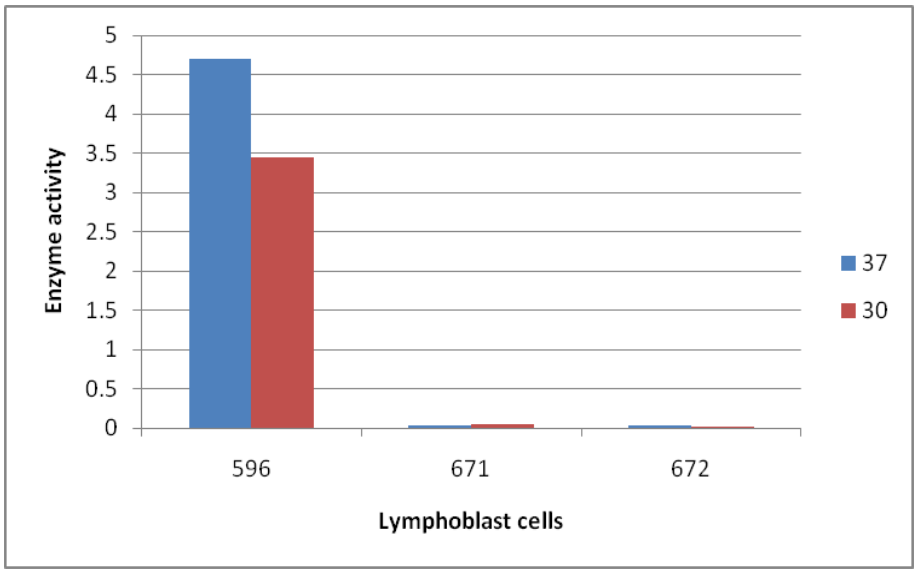

Figure 16. Basal MCAD enzyme activity in lymphoblasts

Both wild type (596) and MCADD patients' (671 and 672) lymphoblasts were grown at different temperature, 37°C and 30°C. Then cells were lysed and cell free extracts were assayed for MCAD activity using ETF fluorescence reduction assay. Assays were duplicated and average values were plotted.

The reduction in MCAD activity in K304E patient lymphoblasts was not due to changes in gene expression, which was similar in all cell lines (Figure 17).

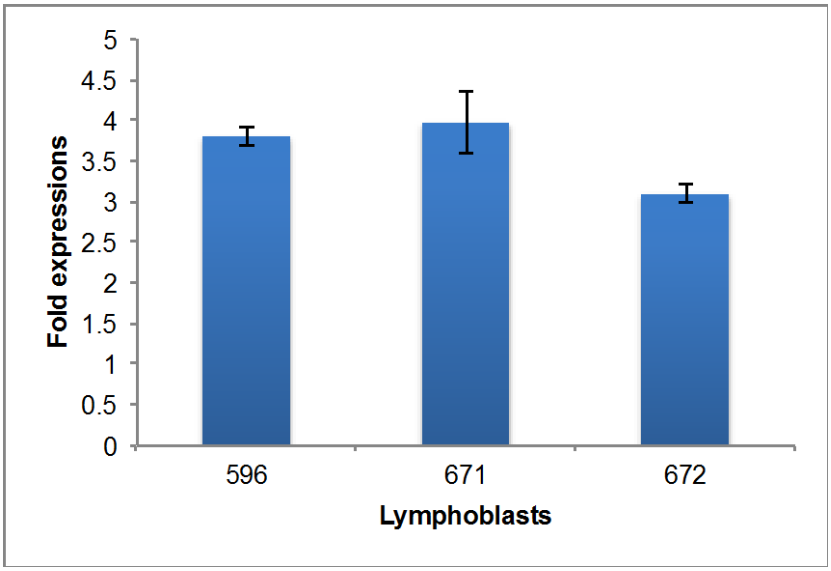

Figure 17. Quantification of the *ACADM* expression in lymphoblasts by qRT-PCR

Wild type (596) and MCADD patients' (671 and 672) lymphoblasts were cultured and the RNA from these cells was extracted and qRT-PCR was performed. Error bars represent standard deviation.

3.2.2 Small chemical chaperones increase the activity of K304E mutant MCAD in patients' lymphoblasts

To investigate the effect on enzyme stability, lymphoblasts cultures were incubated with a variety of small chemicals with protein stabilization properties, DMSO, glycerol, betaine, TMAO, and L-proline, and tested for MCAD activity. Patient cells showed a significant increase in MCAD activity with glycerol and TMAO treatment (Figure 18).

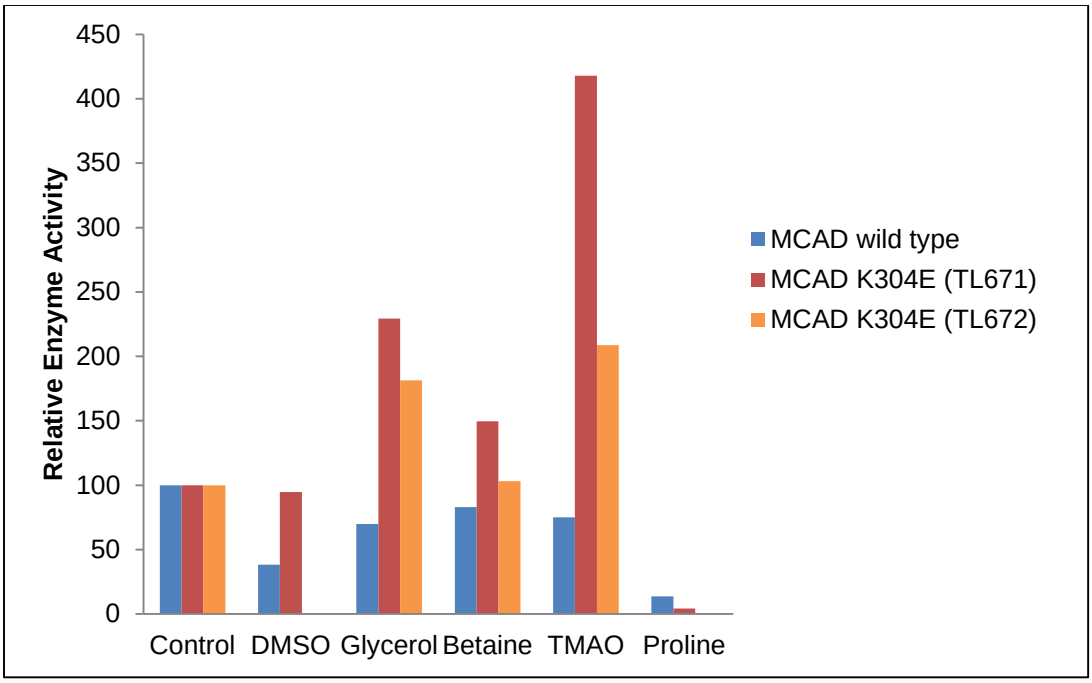

Figure 18. The MCAD activity changes in the presence of small chemical chaperones

Both wild type (596) and MCADD patients' (671 and 672) lymphoblasts were cultured for two days at 37°C with different small chemical chaperones (3% DMSO, 0.5% glycerol, 100mM betaine, 200mM TMAO, or 300mM $_{L}$-proline). Then cells were harvested and lysed. Cell free extracts were assayed for MCAD activity using ETF fluorescence reduction assay. Assays were duplicated and average values were plotted.

To test whether these small chemical chaperones can influence the activity of other ACADs, VLCAD activity was measured. While glycerol and TMAO increased the K304E MCAD activity, there was no increase in VLCAD activity with the treatment of either glycerol or TMAO (Figure 19). The VLCAD activity in both wild type and K304E MCAD expressing lymphoblasts decreased in the presence of glycerol and TMAO. This indicates that the small chemical chaperones affect the K304E mutant MCAD activity but doesn't provide similar increasing effect in VLCAD activity.

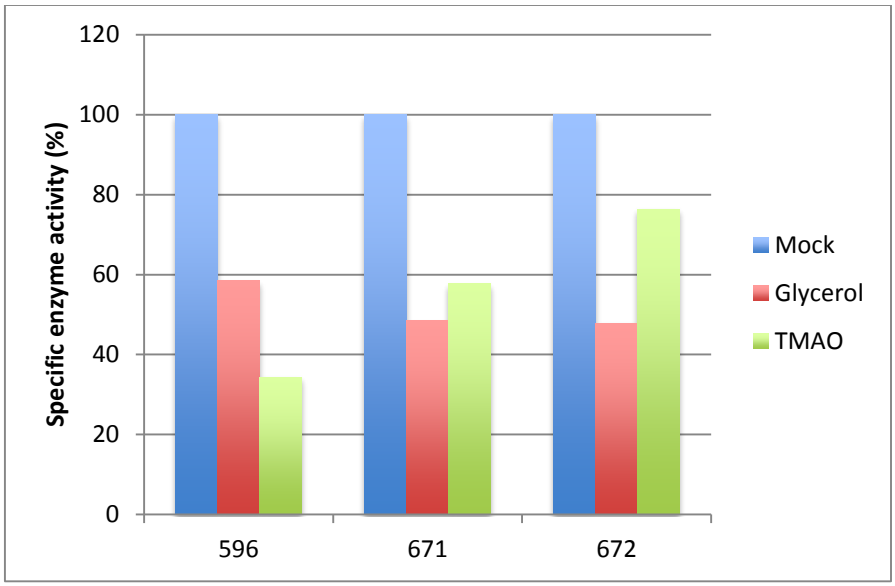

Figure 19. Relative VLCAD enzyme activity changes in lymphoblasts treated with glycerol or TMAO
Both wild type (596) and MCADD patients' (671 and 672) lymphoblasts were cultured for 2 days at 37°C with 0.5% glycerol or 200mM TMAO, and then cells were harvested and lysed. Cell free extracts were assayed for VLCAD activity using ETF fluorescence reduction assay. Assays were duplicated and average values were plotted.

To determine if these effects were due to transcriptional overexpression, qPCR was used to examine the level of MCAD mRNA sequence in cells under each condition (Figure 20). While the patient cell line 672 had a slightly higher level of MCAD message compared to 671, treatment with the small molecule chaperones did not affect the level in either cell line. The treatment of glycerol and TMAO reduced VLCAD enzyme activity both in wild type and MCAD deficient lymphoblasts. The mechanism is unclear but this can be due to the toxicity of the glycerol and TMAO.

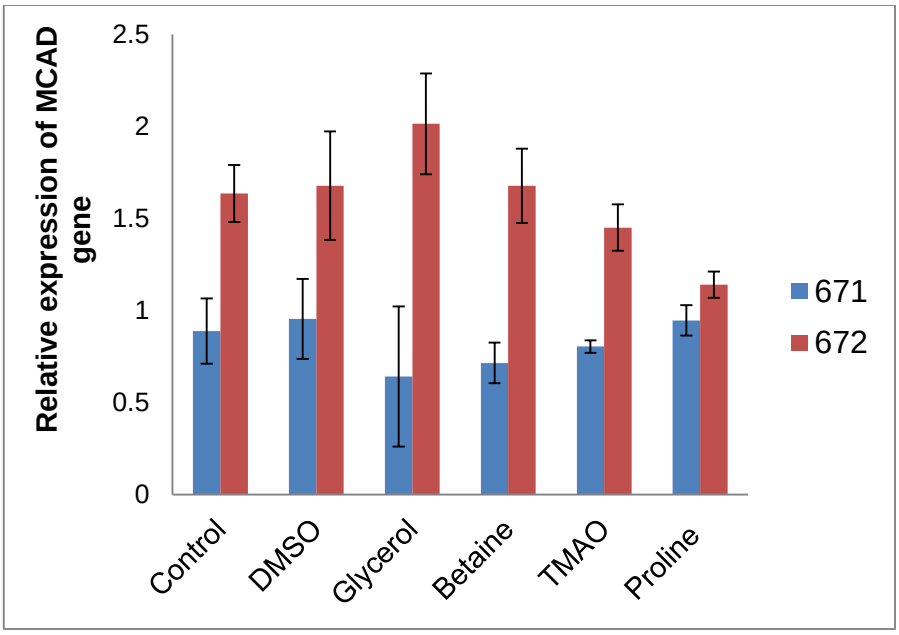

Figure 20. The *ACADM*, MCAD coding gene, expression in lymphoblasts with the treatment of different chemical chaperones by qRT-PCR

Both wild type (596) and MCADD (671 and 672) lymphoblasts were cultured with different small chemical chaperones for two days. Then, the RNA from these cells were extracted and qRT-PCR was performed. Error bars represent standard deviation.

3.3 PHENYLBUTYRATE AS A POTENTIAL TREATMENT FOR MCADD.

As demonstrated in Chapter 5 of this thesis, phenylbutyryl-CoA is a substrate for MCAD (Kormanik et al., 2012). Phenylbutyrate (PBA) is an FDA approved medication used to treat inborn errors or the urea cycle. Substrate analogues are among the most potent small molecules enhancer of protein folding, and so it has been hypothesized that phenylbutyryl-CoA could work as a chaperone for the K304E MCAD protein. To examine this possibility, phenylbutyryl-CoA or octanoyl-CoA was incubated with purified recombinant K304E MCAD protein without a secondary electron acceptor at different temperatures for 5 minutes and residual MCAD activity was measured. Under these conditions, substrate remains bound with enzyme as a stable charge-

complex intermediate. Phenylbutyryl-CoA proved to be as nearly as effective at stabilizing K304E MCAD protein as octanoyl-CoA, the optimum substrate for MCAD (Figure 21).

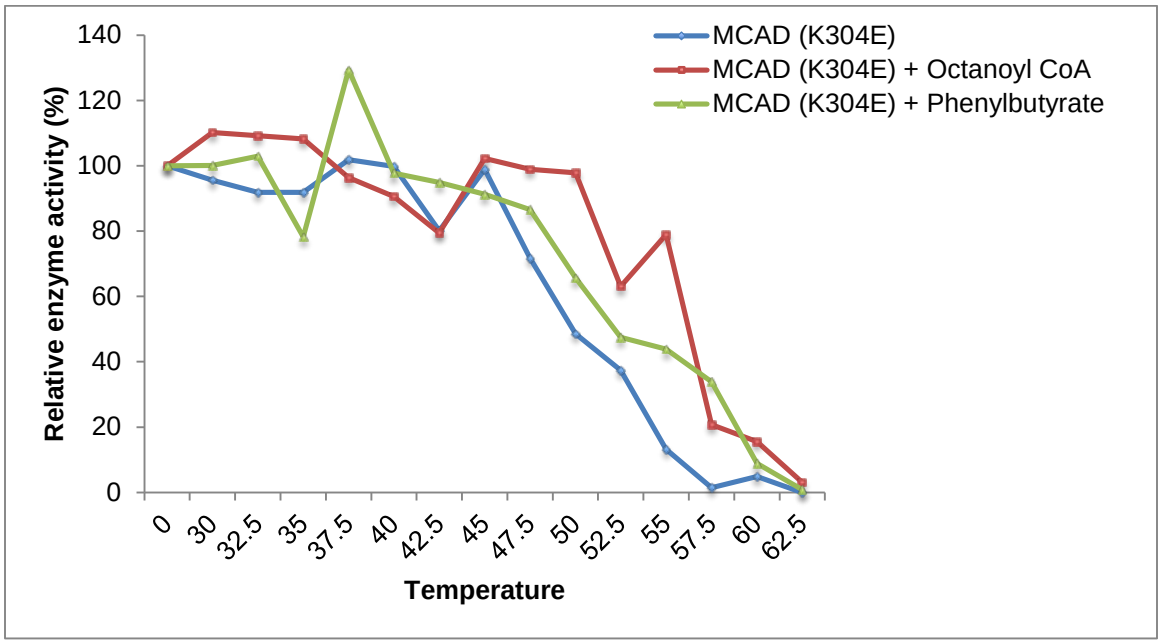

Figure 21. Thermal stability of the K304E mutant MCAD protein with and without added phenylbutyryl- CoA or octanoyl-CoA

The recombinant K304E MCAD protein was incubated at different temperatures (30°C to 62.5°C) with 2.5°C increment for 5 minutes in the presence or absence of phenylbutyryl-CoA or octanoyl-CoA. Assays were duplicated and average values were plotted.

To further test the effect of PBA on K304E MCAD activity, lymphoblasts were cultured with PBA and the MCAD activity was measured (Figure 22 and 23). Although the basal MCAD activity was difficult to measure in MCAD deficient cells (671 and 672), there was consistent pattern of increase of MCAD activity with phenylbutyrate in MCAD deficient patients' lymphoblasts.

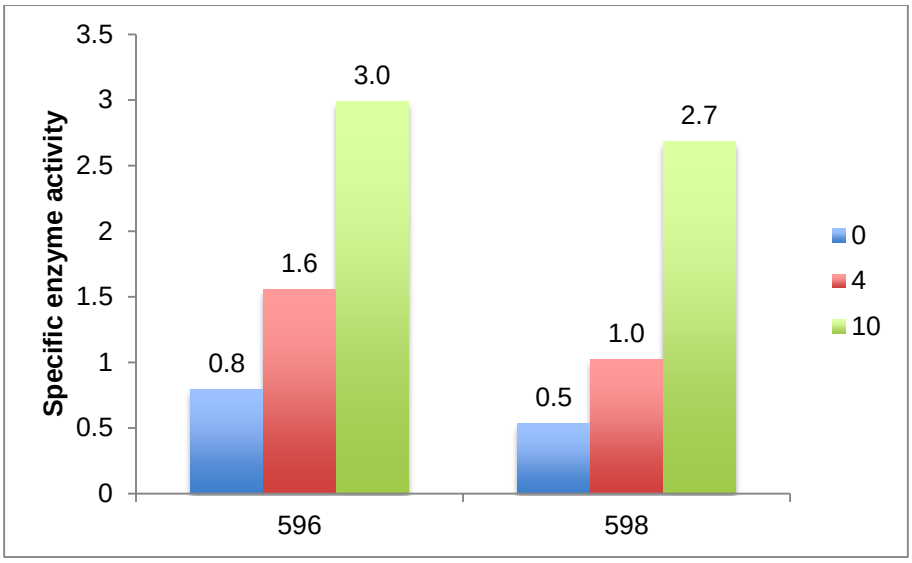

Figure 22. The effect of phenylbutyric acid on MCAD activity in wild type (596 and 598) lymphoblasts

Both wild type (596) lymphoblasts were cultured for two days at 37°C with 4mM and 10mM of phenylbutyrate. Then cells were harvested and lysed. Cell free extracts were assayed for MCAD activity using ETF fluorescence reduction assay. Assays were duplicated and average values were plotted.

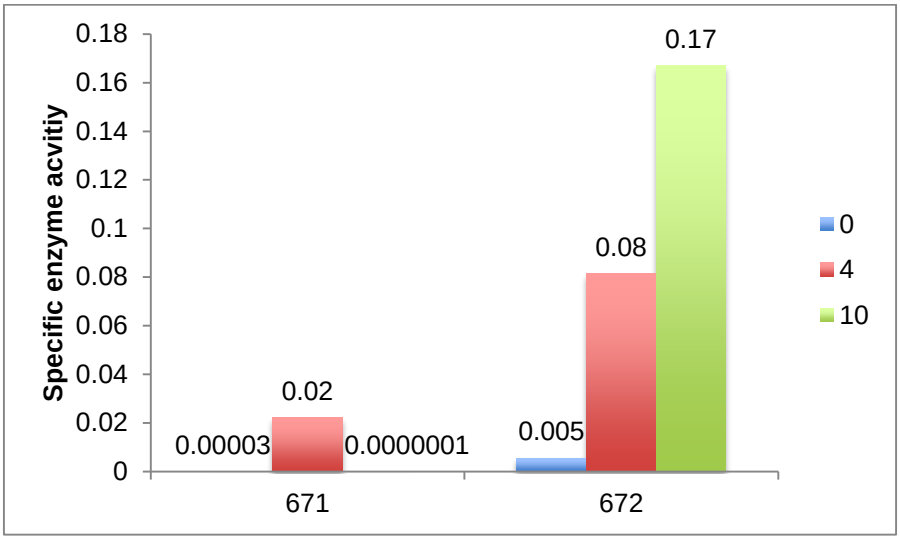

Figure 23. The effect of phenylbutyric acid on MCAD activity in MCAD deficient (671 and 672) lymphoblasts

MCAD deficient (671 and 672) lymphoblasts were cultured for two days at 37°C with 4mM and 10mM of phenylbutyrate. Then cells were harvested and lysed. Cell free extracts were assayed for MCAD activity using ETF fluorescence reduction assay. Assays were duplicated and average values were plotted.

Because the staining levels of MCAD activity in fibroblasts and lymphoblasts are low, it was difficult to quantitate changes in treated cells relative to untreated cells. To increase the MCAD signal mutant and wild type MCAD were overexpressed in HEK 293 cells using a T-REX Flp-In inducible vector. In this system, the vector insert is induced using tetracycline. Treatment of cells expressing wild type and mutant MCADs with 0.5mM phenylbutyrate increased activity in cells expressing wild type enzyme significantly compared to untreated cells, without increasing the amount of MCAD protein (Figure 24 and 25). In contrast, phenylbutyrate increased MCAD activity and protein in cells expressing mutant MCAD.

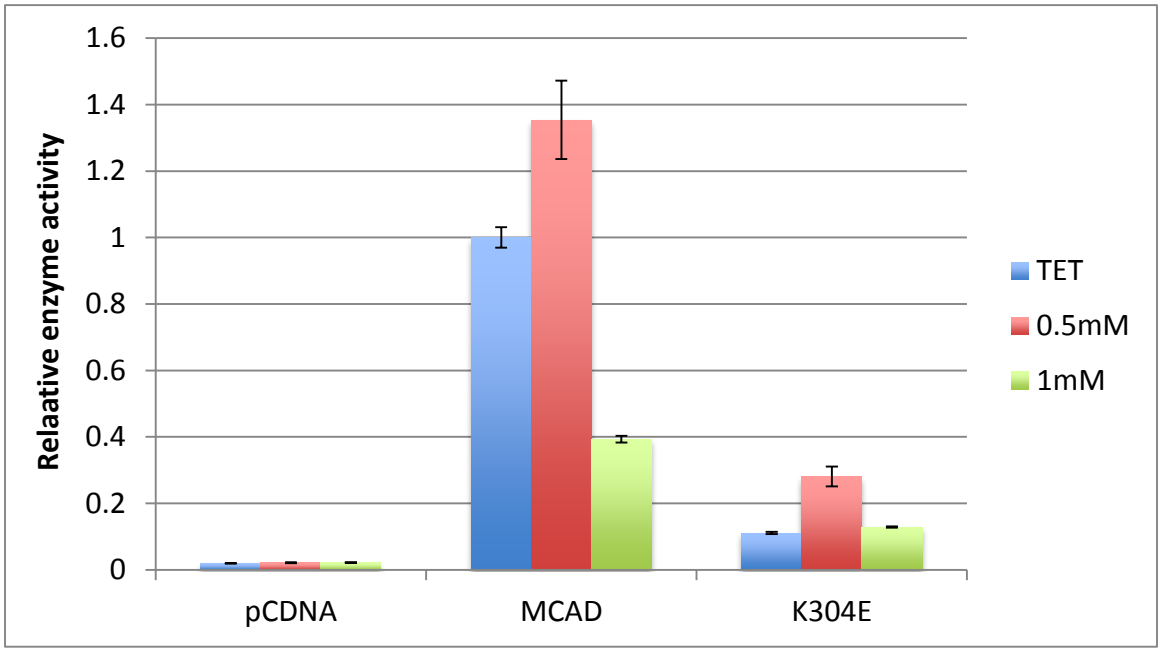

Figure 24. The effect of phenylbutyrate on MCAD activity in HEK 293 T-REX Flp-In inducible cell line

HEK 293 T-REX Flp-In pcDNA, MCAD, and K304E expressing cell lines were cultured for two days at 37°C with 0.5mM and 1mM of phenylbutyrate. Then cells were harvested and lysed. Cell free extracts were assayed for MCAD activity using ETF fluorescence reduction assay. Error bars represent standard deviation.

The MCAD expression in different cell lines was detected by western blotting and relative protein density was measured using Alpha Imager 2200 (Figure 25). The expression of K304E MCAD protein was increased in the presence of 0.5mM phenylbutyrate treatment.

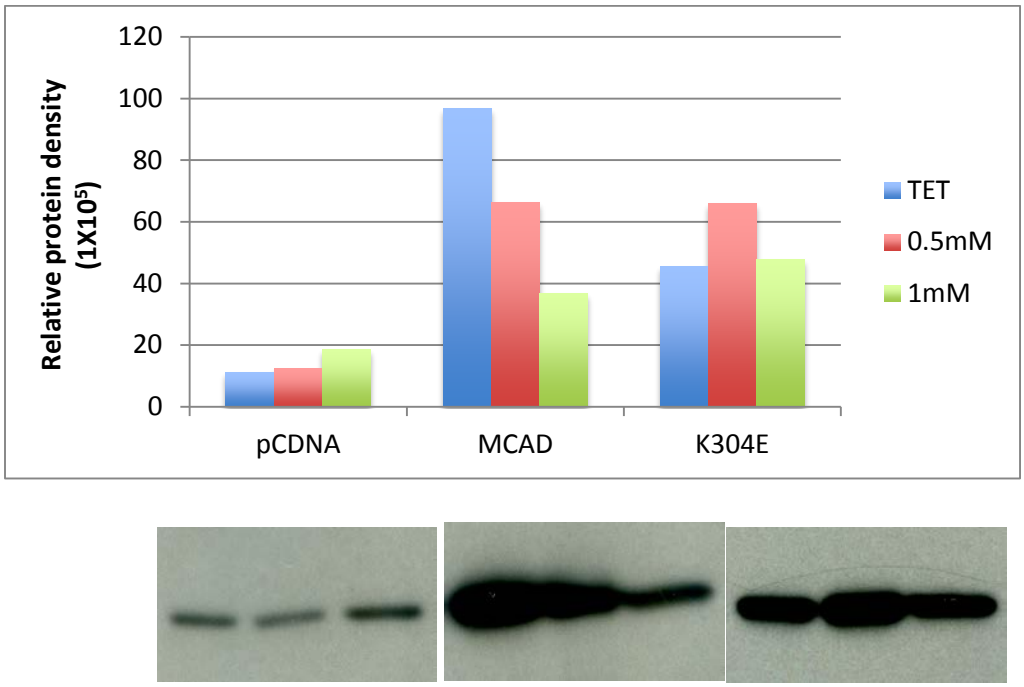

Figure 25. Relative protein densitometry of the MCAD protein in HEK 293 T-REX Flp-In inducible cell line
Anti-MCAD western blotting of phenylbutyrate treated HEK 293 T-REX Flp-In cell extracts. Twenty-five microgram total protein was loaded per lane.

3.4 INVESTIGATION OF DRUG TARGET SITE OF MCADD

The experiments with phenylbutyrate show the potential benefit of small chaperones as a therapy for MCAD deficient patients harboring at least one copy of the common mutation. However, the MCAD activity in treated cells was still far below normal levels, stressing the

importance of identifying additional binding sites on the protein with pharmacophore characteristics favorable for binding highly specific potential drugs and stabilizing the mutant MCAD. To identify such possible drug targeting site for K304E MCAD protein, recombinant K304E MCAD purified to essential homogeneity was supplied to our collaborator Dr. Kevin Battaile for crystal growth and X-ray crystallography and the K304E MCAD crystal structure was determined at to 1.73 Å resolution

3.4.1 Structural analysis of MCAD K304E protein

The MCAD K304E protein crystal structure was resolved to 1.73 Å. This structure was compared to published crystal structures of MCAD from various sources, including pig (PDB: 3MDE), (J-J Kim 1993), human MCAD complexed with ETF βE165A (PDB code: 2A1T), (Toogood et al., 2005), and bacteria (PDB: 1UKW). The crystal structure findings substantiated that the structure of the mutant MCAD enzyme was relatively unaltered and the atomic coordinates at such high resolution can be used *in silico* chemical library screening and for structure or fragment based drug design.

The MCAD Tetramer Core: While in the wild type, K304 N_ζ, located in Helix H, is shown consistently within a hydrogen bonding distance to the amide oxygen of Q342 (Helix I), in the MCAD K304E mutant the carboxylate at the 304 position induces the amide group to move away from its original position by 3.6 Å rotating the Q342 C_α-C_β bond by ~97º degrees (Figure 26). This change in conformation positions the amide group oxygen closer by one Å to D346 carboxylate oxygen OD1 and within an interacting distance <3.0 Å. In addition to these structural perturbations, the methyl group of the thiomethyl moiety of M297, Helix H, seemed to also move away from facing the D346 residue to the opposite side of the methionine sulfur.

Other subtle structural perturbations that are secondary have also been observed in this region but cannot be confirmed to be directly or indirectly induced by the mutation at the 304 position.

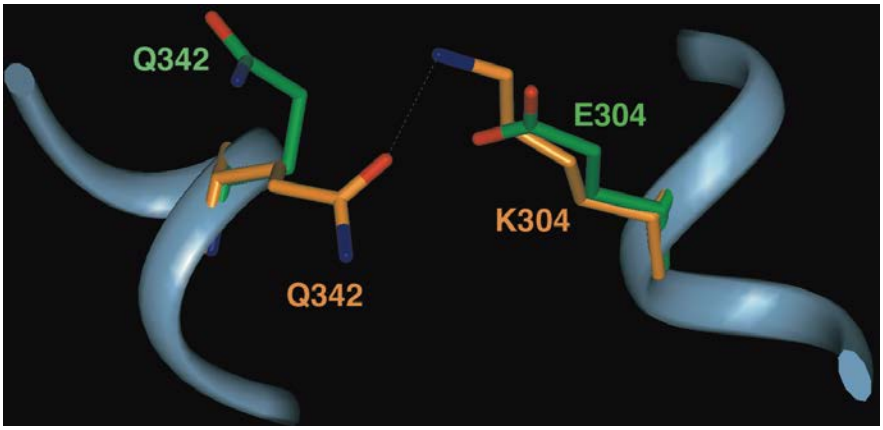

Figure 26. Ribbon and stick representation of parts of the MCAD protein at its core

The key amino acids at K304 and Q342 are shown in stick model. Original wild type residues carbons are shown in orange and the residues carbons in the mutant protein are shown in green.

The MCAD Active Site: The most important changes in the active site are apparent when comparing the conformations of residues in the absence and presence of the octanoyl-CoA ligand and relate those observed conformations in the MCAD K304E mutant and the MCAD in the presence of ETF. Octanoyl-CoA binding induces displacement of a string of water molecules, 802 to 805, occupying the active site at the octanoyl moiety binding site. While the of E376 is positioned closer to the FAD isoalloxazine ring in the structure without the substrate in the pig MCAD as in the human MCAD K304E structure, it is observed to move away by 1.9 Å in the presence of the octanoyl moiety of the CoA ester and, interestingly, to the same position as observed in the MCAD:ETF ternary complex. This implies similar conformational changes are induced by the binding of substrates, either the acyl-CoA or ETF, to MCAD and is consistent with a hypothetical induced fit mechanism. Another active site residue of interest is E99. In the MCAD K304E mutant, its γ-carboxylate is observed at a similar position to the one in the MCAD in the absence of either the octanoyl-CoA or ETF substrates. In the MCAD with

octanoyl-CoA bound, substrate binding induces a dramatic 4.1 Å movement away from its location to allow for the octanoyl binding.

The ETF Docking Site: Residues at ETF docking site of the MCAD protein were carefully examined because of the potential of the site for drug development. Human MCAD complexed with ETF βE165A was compared to MCAD K304E mutant and pig MCAD with and without substrate. The ETF docking interface includes two major areas, the docking site pocket and the docking pocket surrounding surface. The docking site pocket is essentially all hydrophobic formed by residues that are part of helices, A, C, and D and the loop connecting helices C and D. Specifically, the F23, T26, A27, L59, G60, L61, L73, L75, and I83 residues line the inside of this pocket. Among these residues G60 is the only invariant residue in all ACADs, while others are either highly conserved, *e.g*. F23, L59, and L61, or conserved, e.g., L73, L75, I83. When comparing available, published MCAD crystal structures, these residues within the docking site pocket have similar conformations. There are some minor changes in the MCAD:ETF co-structure, where conformational changes induced by ETF binding include tilting of the phenyl moiety of F23 by almost 90 degrees to allow for the protrusion of the leucine β195 residue into the docking site pocket. On the docking pocket surrounding surface there are other apparently important interactions including interactions of the ETF Yβ192 residue, which is invariant among all known ETF proteins, with residues on the MCAD including a hydrogen bond between the hydroxyl hydrogen and the carboxyl oxygen of glutamate 34, which is 2.6 Å away, and interactions of βY192 residue with L59 and R55 that are 2.9 Å and 3.1 Å away, respectively. Another residue is the ETF βA193 with it backbone oxygen at a 2.7 Å distance from MCAD T26 hydroxyl oxygen, which is not conserved in other ACAD proteins. Table 11 summarizes the key contacts between ETF and MCAD proteins.

Table 11. ETF docking peptide key interacting atoms at the ETF:MCAD interface

ETF Residue	MCAD Residue*	Distance (Å)
Tyr β192:CD2	Leu59:CD2	3.8
Tyr β192:CD1	Tys29:CD	4.0
Tyr β192:CE1	Tys29:CD	3.6
Tyr β192:CE1	Tys29:CG	3.2
Tyr β192:CE1	Tys29:CB	3.5
Tyr β192:CB	Leu59: CD2	3.9
Tyr β192:CE2	Arg55:NH2	3.1
Tyr β192:CG	Leu59:CD2	2.9
Tyr β192:OH	Glu34: OE1	2.6
Ala β193:O	Thr26:OG1	2.7
Thr β194:OG1	Glu58:O	3.9
Leu β195:CG	Gly60:O	3.9
Leu β195:CG	LeuD59:O	3.8
Ile β198:CG2	Glu22:OE1	3.5
Ile β198:CD1	Glu22:O	3.6
Ile β198:CD1	Thr26:OG1	4.0
Ile β198:CD1	Glu22:CB	3.9
Ile β198:CG2	Glu22:CB	3.7
Ile β198:CG2	Gln19:CG	3.9
Met β199:CA	Gln19:NE2	3.6
Lys β202:NZ	Gln19:CG	3.6

*Atoms' designation as they appear in the PDB atomic coordinates file.

3.4.2 Synthetic ETF docking peptide analogs compete with ETF binding to wild type and K304E mutant MCAD

If the synthetic ETF docking site peptides effectively interact with MCAD, then they should compete with native ETF for binding and reduce its ability to reoxidize the enzyme in the ETF-fluorescence reduction assay. To test this hypothesis, wild type and K304E MCAD were incubated with the synthetic peptide prior to the addition of native ETF in the enzyme assay, then the remainder of the assay was performed. One of the peptides, YAT191 was particularly effective in reducing the apparent MCAD activity, indicating that it interfered with the native ETF binding (Figure 27).

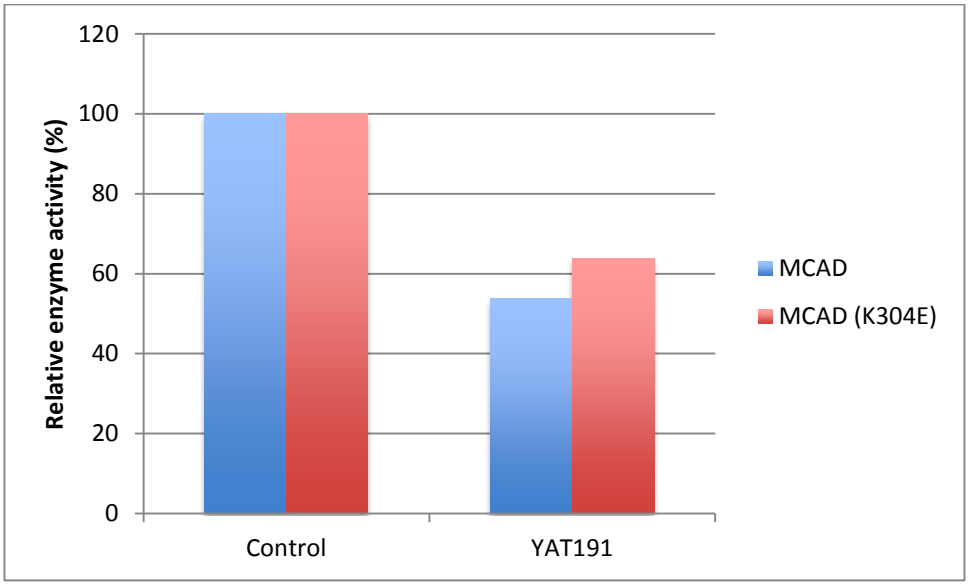

Figure 27. ETF enzyme assay of the wild type and K304E MCAD with and without the wild type ETF docking site targeting peptide, YAT191

About 130nM of purified recombinant wild type and K304E MCAD proteins were co-incubated for 5 minutes with final 2.5mM of YAT191 peptide. Then ETF reduction assay was performed to measure the MCAD activity. Assays were duplicated and average values were plotted.

A number of variations on wild type YAT191 were then synthesized and similarly tested searching for the ability to improve the inhibition of MCAD activity, which would imply stronger binding and more efficient protein stabilization. All of the peptides were able to interfere with interaction of ETF in this assay with maximum reduction to 20-30% of control activity (Figure 28).

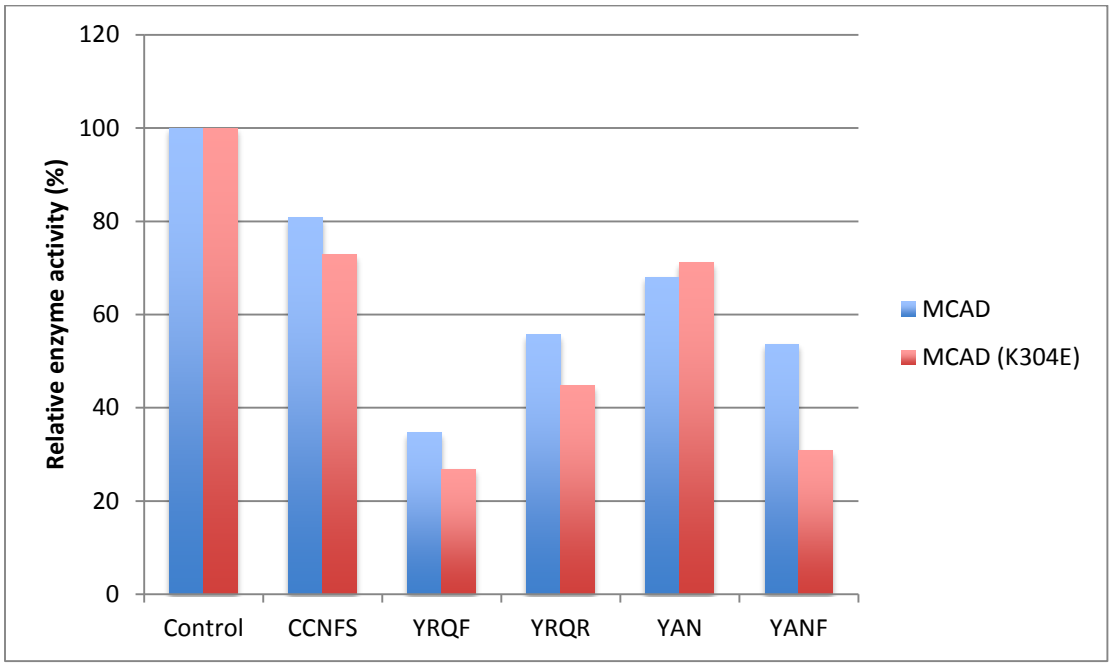

Figure 28. ETF enzyme assay of the wild type and K304E MCAD with and without ETF docking site targeting synthetic peptides (CCNFS, YRQF, YRQR, YAN, and YANF)

About 130nM of purified recombinant wild type and K304E MCAD proteins were co-incubated for 5 minutes with 2.5mM of each synthetic peptide. The ETF reduction assay was then performed to measure the MCAD activity. Assays were duplicated and average values were plotted.

To verity that these results were in fact due to interference with the binding of ETF to MCAD by the synthetic peptides, wild type and K304E MCAD activity was measured with the DCIP assay. This assay is based on colorimetric changes in the dye indicator and uses the small chemical electron acceptor PMS rather than ETF to reoxidize the enzyme in the second half

reaction. Thus, binding of a synthetic peptide to the ETF docking site would not be expected to affect the measured activity in this assay. This was in fact the case (Figure 29).

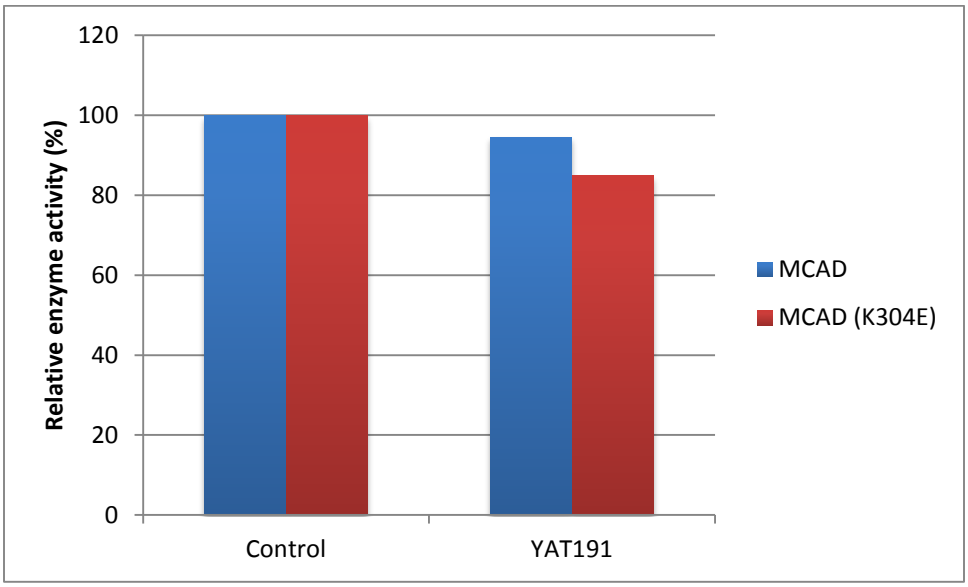

Figure 29. DCIP assay with wild type and K304E MCAD protein with and without added YAT191
About 130nM of purified recombinant wild type and K304E MCAD proteins were co-incubated for 5 minutes with final 2.5mM of each synthetic peptide. Then DCIP colormetric assay was performed to measure the MCAD activity. Assays were duplicated and average values were plotted.

3.4.3 ETF docking site targeting peptides increase the thermal stability of MCAD

Interaction of native ETF with MCAD stabilizes both proteins. Thus, binding of the ETF docking site peptides were predicted to increase the thermal stability of the MCAD protein. To examine this hypothesis, wild type and mutant MCAD was tested for activity using the ETF fluorescence reduction assay at increasing temperatures with and without pre-incubation with the synthetic peptides. As expected, the K304E MCAD was less stable to thermal stress than wild type enzyme without the addition of the peptides (Figure 30).

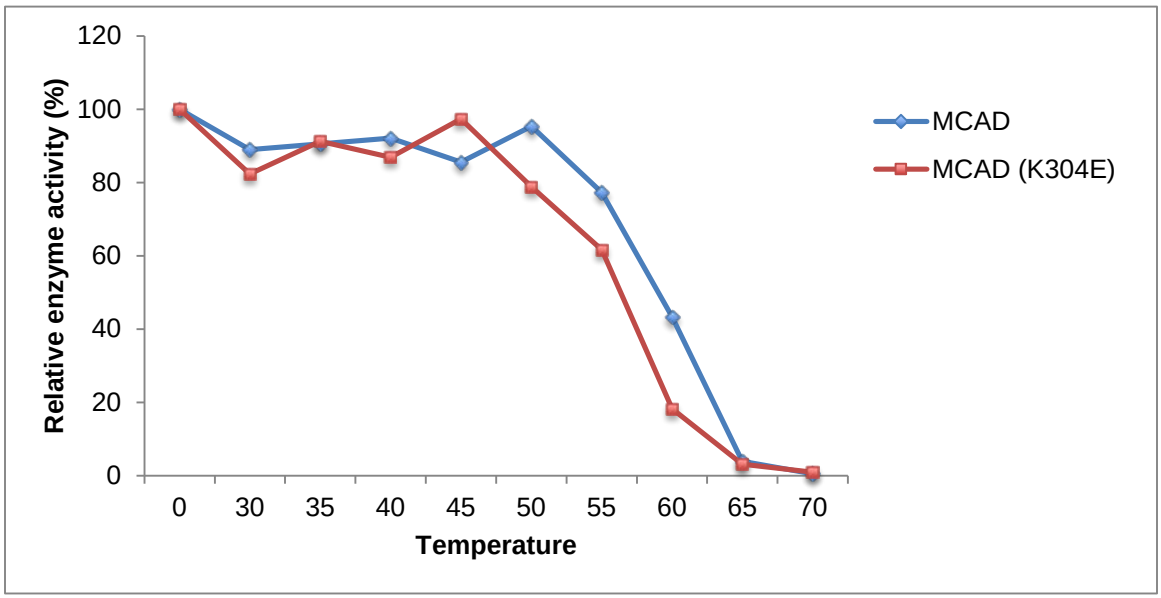

Figure 30. The thermal stability of the purified recombinant wild type and K304E MCAD protein

The recombinant wild type and mutant (K304E) were incubated at range of temperatures, at 2.5°C increments, for 5 minutes each and measured for MCAD activity. Assays were duplicated and average values were plotted.

Using the same approach, the change of MCAD activity at different temperatures in the presence of the ETF docking site targeting synthetic peptides was measured by the ETF assay. Figure 31 and figure 32 shows the changes of enzyme activity with various temperatures in the presence and absence of peptides, YATF, YRQF, YRQR, 194, 195, and 196. YRQR increased the thermal stability of the K304E MCAD. However, none of the other peptides showed significant increase in the thermal stability of the mutant MCAD, even though all of these peptides could reduce the activity of K304E MCAD in the ETF assay.

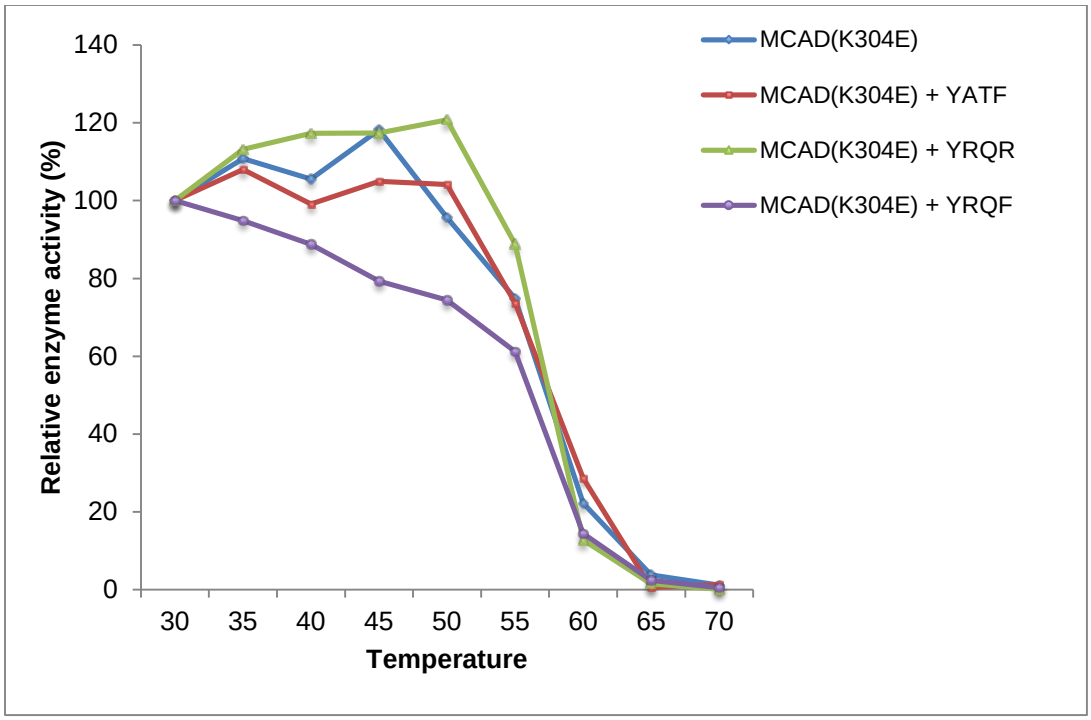

Figure 31. The thermal stability of the bacterially purified K304E MCAD protein with ETF docking site targeting peptide (YATF, YRQR, and YRQF)

The recombinant MCAD K304E was co-incubated with ETF docking site targeting peptide and then incubated at certain temperatures for 5 minutes and then MCAD K304E activity was measured. Assays were duplicated and average values were plotted.

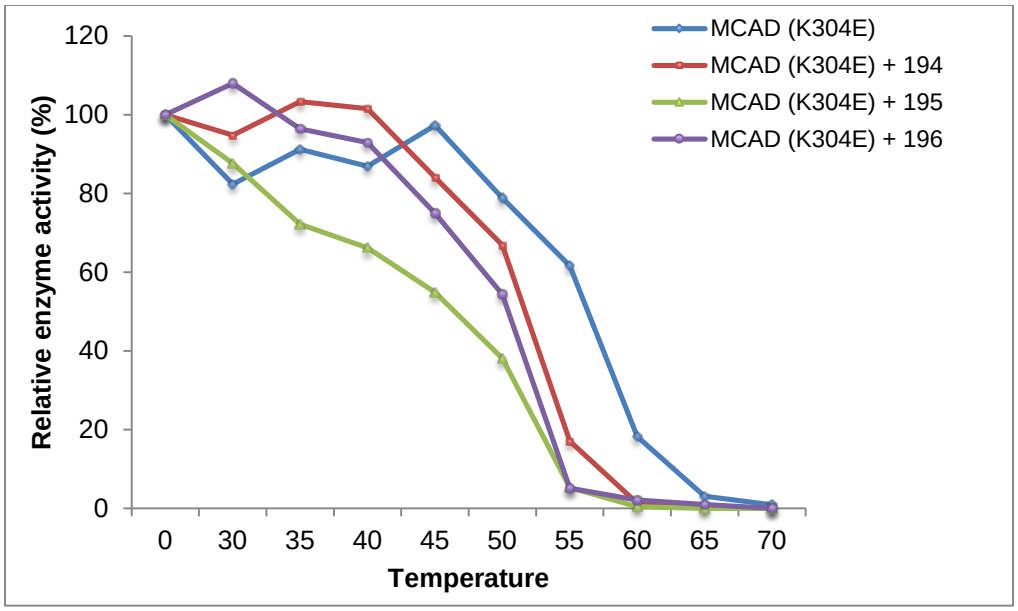

Figure 32. The thermal stability of the bacterially purified wild type and K304E MCAD protein with or without 194, 195, or 196

The recombinant MCAD K304E was co-incubated with ETF docking site targeting peptides (194, 195, and 196) and then incubated at certain temperatures for 5 minutes and then MCAD K304E activity was measured. Assays were duplicated and average values were plotted.

One of the peptides, YAT 193, with one amino acid change from the wild type peptide, significantly increased the thermal stability of the K304E MCAD activity (Figure 33).

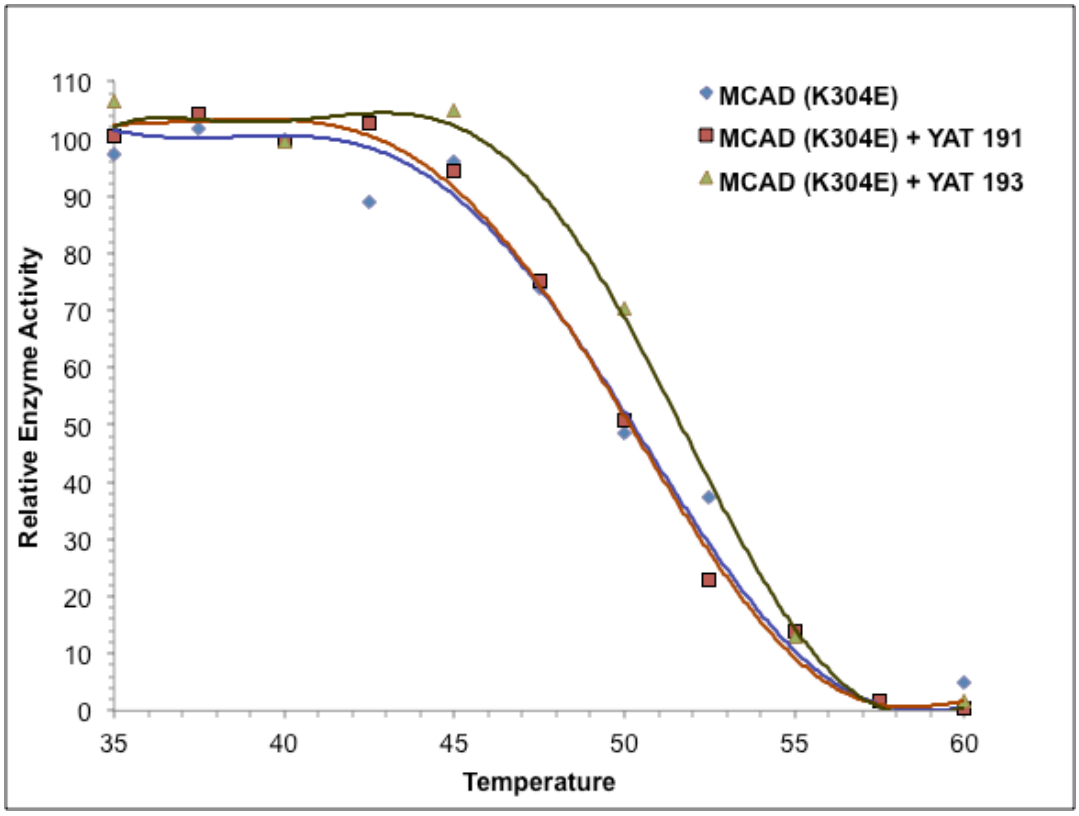

Figure 33. Relative enzyme activity of K304E mutant MCAD in the presence and absence of peptides YAT191 and YAT193 at various temperatures

The recombinant MCAD K304E was co-incubated with ETF docking site targeting peptide and then incubated at certain temperatures for 5 minutes and then MCAD K304E activity was measured. Assays were duplicated and average values were plotted.

3.4.4 Binding of the YAT193 alters the structure of K304E MCAD as measured by CD spectroscopy

To further examine the effect of the YAT 193 peptide K304E MCAD protein structure, the CD spectra of enzyme with and without peptide was determined. Co-incubation of YAT 193 with the K304E MCAD protein led to significant changes in light polarization, consistent with a secondary structural change following binding of the peptide (Figure 34). These results support the observed increase in thermal stability.

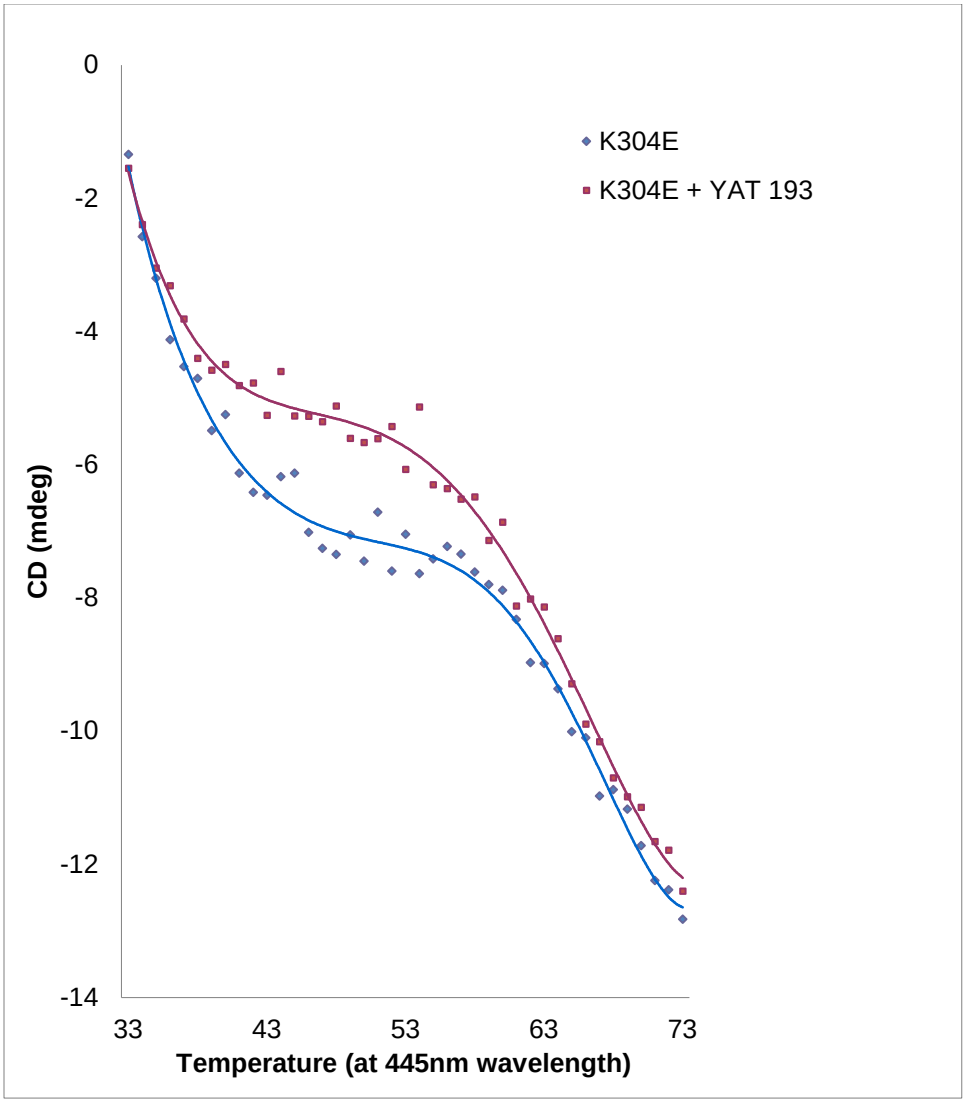

Figure 34. Effect on the recombinant K304E MCAD in the presence and absence of peptides YAT193 by CD spectrum

The recombinant K304E MCAD protein and K304E MCAD co-incubated with YAT193 were incubated at certain temperature for 5 minutes and then measured by CD spectrometry. Readings at 445nm wavelength were graphed.

3.4.5 YAT193, ETF docking site targeting synthetic peptide, showed protective effect on the K304E MCAD protein from *Staphylococcus aureus* V8

Mutant proteins often have a more open tertiary configuration compared to wild type counterparts due to subtle changes in protein folding. These changes in tertiary structure leave then more susceptible to digestion by cellular proteases, one mechanism for increased turnover rate of mutant proteins. In vitro, such changes can be demonstrated by treating mutant and wild type proteins with proteases under conditions leading to partial digestion, leading to more rapid degradation of a protein with an abnormal, more open configuration Therefore, I treated wild type and K304E MCAD for various times with endoproteinase Glu-C from *Staphylococcus aureus* V8 with and without pre-incubation with the ETF docking peptides. *Staphylococcus aureus* V8 can cut at glutamate residues, and the peptide pattern generated can be predicted from the amino acid sequence (Table 12).

Table 12. Expected sizes of MCAD fragment by *Staphylococcus aureus* V8 protease

Size	MW	pI	Enzyme	From:To	Enzyme
8	1032.11	10.99	N-terminus end	1:08	Staph-V8
8	852.9	3.62	Staph-V8	9:16	Staph-V8
3	395.4	3.62	Staph-V8	17:19	Staph-V8
4	531.52	6.13	Staph-V8	20:23	Staph-V8
11	1324.4	10.99	Staph-V8	24:34	Staph-V8
1	147.13	3.62	Staph-V8	35:35	Staph-V8
7	711.81	3.62	Staph-V8	36:42	Staph-V8
6	711.66	4.12	Staph-V8	43:48	Staph-V8
11	1399.6	9.05	Staph-V8	49:59	Staph-V8
10	1124.27	5.14	Staph-V8	60:69	Staph-V8
17	1669.78	3.32	Staph-V8	70:86	Staph-V8

Table 12 Continued

1	147.13	3.62	Staph-V8	87:87	Staph-V8
13	1325.43	3.62	Staph-V8	88:100	Staph-V8
27	2991.22	9.41	Staph-V8	101:127	Staph-V8
1	147.13	3.62	Staph-V8	128:128	Staph-V8
10	1129.31	3.62	Staph-V8	129:138	Staph-V8
15	1400.39	6.2	Staph-V8	139:153	Staph-V8
5	575.52	6.2	Staph-V8	154:158	Staph-V8
43	4844.18	9.22	Staph-V8	159:201	Staph-V8
12	1284.33	6.21	Staph-V8	202:213	Staph-V8
16	1825.99	6.21	Staph-V8	214:229	Staph-V8
7	813.84	6.2	Staph-V8	230:236	Staph-V8
38	3786.07	6.3	Staph-V8	237:274	Staph-V8
7	794.82	6.13	Staph-V8	275:281	Staph-V8
10	1190.32	9.81	Staph-V8	282:291	Staph-V8
10	1146.27	5.14	Staph-V8	292:301	Staph-V8
6	707.84	6.13	Staph-V8	302:307	Staph-V8
12	1481.63	9.05	Staph-V8	308:319	Staph-V8
41	4290.39	4.47	Staph-V8	320:360	Staph-V8
4	506.54	3.62	Staph-V8	361:364	Staph-V8
13	1670.83	8.63	Staph-V8	365:377	Staph-V8
13	1470.62	10.09	Staph-V8	378:390	Staph-V8
7	916.92	8.68	Staph-V8	391:397	COOH

To optimize the protein visualization prior to proteolysis, different concentrations of purified recombinant K304E MCAD proteins were loaded onto 16.5 %T Tricine and 4-12 %T Tris SDS gels and stained with either Coomassie blue or silver staining following electrophoresis (Figure 35). Since silver staining can visualize smaller amount of proteins, silver staining in Tricine gel was used for the limited proteolysis experiment.

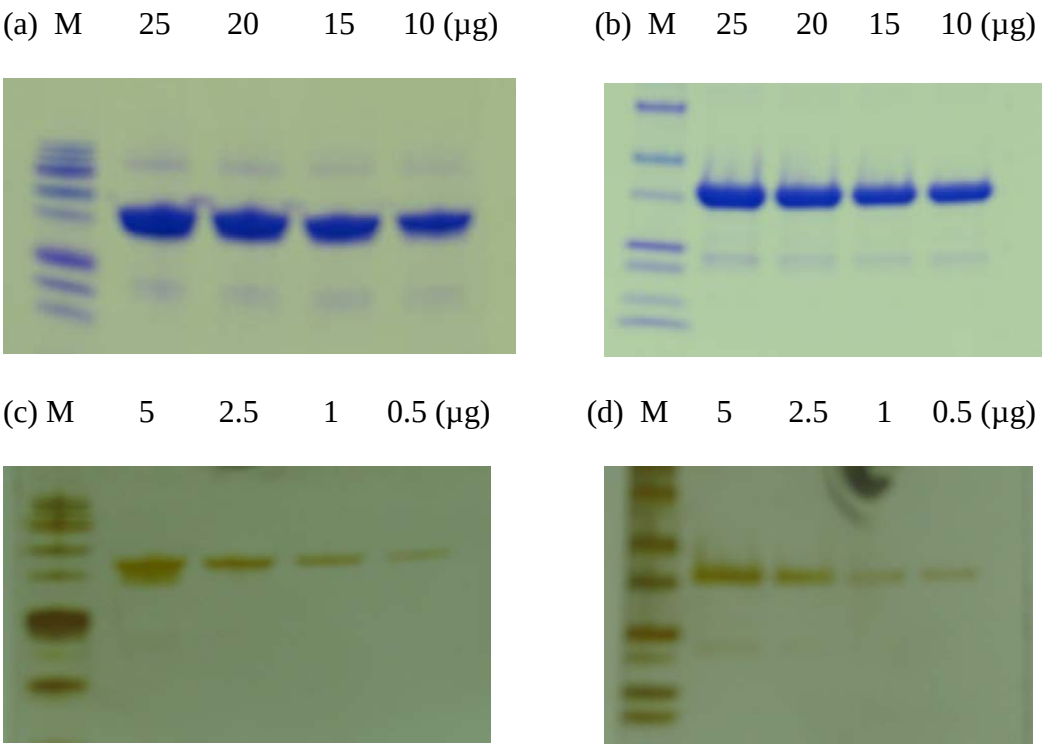

Figure 35. Staining of the recombinant K304E MCAD protein in different gel

The recombinant K304E MCAD proteins were loaded 25, 20, 15, 10 µg for Coomassie staining and 5, 2.5, 1, 0.5 µg for silver staining. (a) Coommassie staining in 16.5 %T Tricine gel, (b) Coommassie staining in gradient 4-12 %T Tris gel, (c) silver staining in 16.5 %T Tricine gel, (d) silver staining in gradient 4-12 %T Tris gel.

Figure 36 and figure 37 show results of a limited proteolysis experiment of K304E MCAD protein in the presence and absence of the YAT 191 and YAT 193 peptides, respectively. Panel (a) shows control proteolysis of the K304E MCAD protein and panel (b) shows the pattern of limited proteolysis in the presence of YAT 191 (Figure 36) and YAT 193 (Figure 37). Under the conditions used, proteolysis was rapid enough that even at the 0 time point (right after the addition of the V8 protease) digested fragments were visible. With increased protease incubation, additional cleavage bands appeared. The appearance of several of these bands was delayed following incubation with the docking peptides (most noticeable with the 12 kDa fragment labeled with the red arrow). To identify of these fragments, mass spectrometry was performed

(Figure 40), and its rate of appearance of this fragment was quantified by measuring the optical density of the fragment in proteolysis gels over several experiments (Figure 38 and 39). In the absence of YAT 191 in the digestion reaction, the appearance of the fragment plateaued at 7.5 minutes. However, in the presence of YAT 191, the concentration of the fragment was increasing even at 30 minutes digestion, indicating resistance to digestion (Figure 38). When enzyme was pre-incubated with YAT 193, the 12 kDa fragment had also not peaked by 30 minutes of digestion (Figure 39). Note, that since relative gel staining was variable form one gel to the next, each graph was generated from the internal control included on that gel.

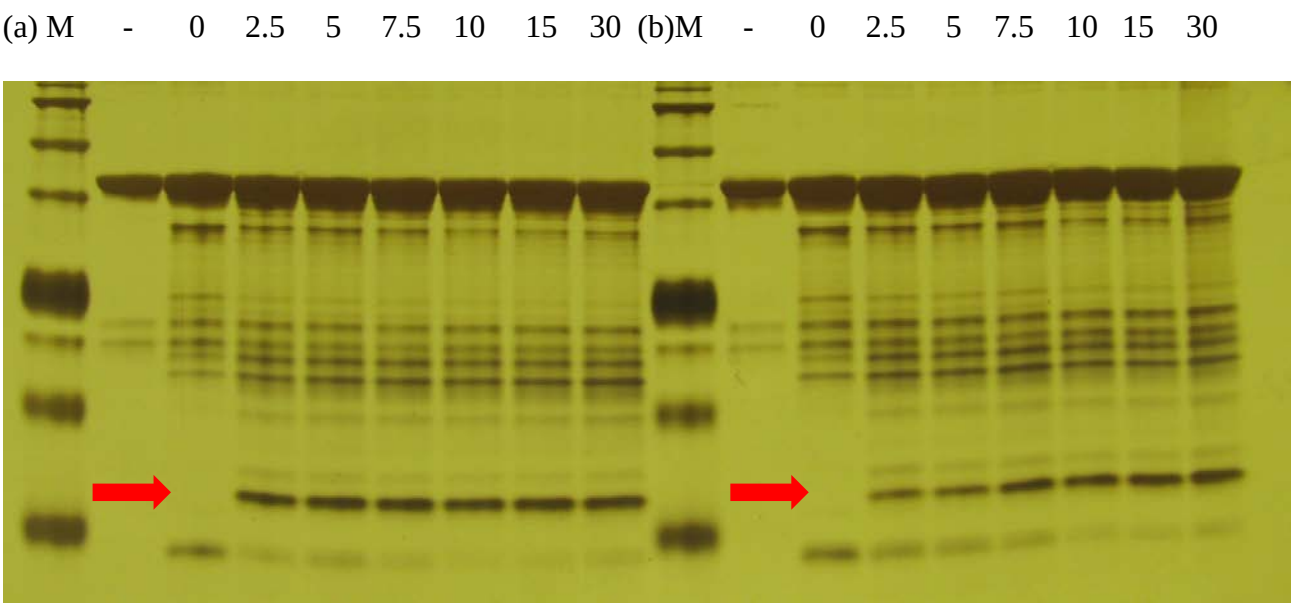

Figure 36. Limited proteolysis of the K304E MCAD protein with and without YAT191

(a) K304E MCAD protein, (b) K304E MCAD protein with YAT191. The recombinant K304E MCAD protein was digested with V8 protease in the presence or absence of YAT191 peptide at different incubation time. Total 10 μg of the protein is loaded on each lane, electrophoresed in 16.5 %T Tricine gel, and stained with silver staining kit from Sigma.

(a) M - 0 2.5 5 7.5 10 15 30 (b) M - 0 2.5 5 7.5 10 15 30

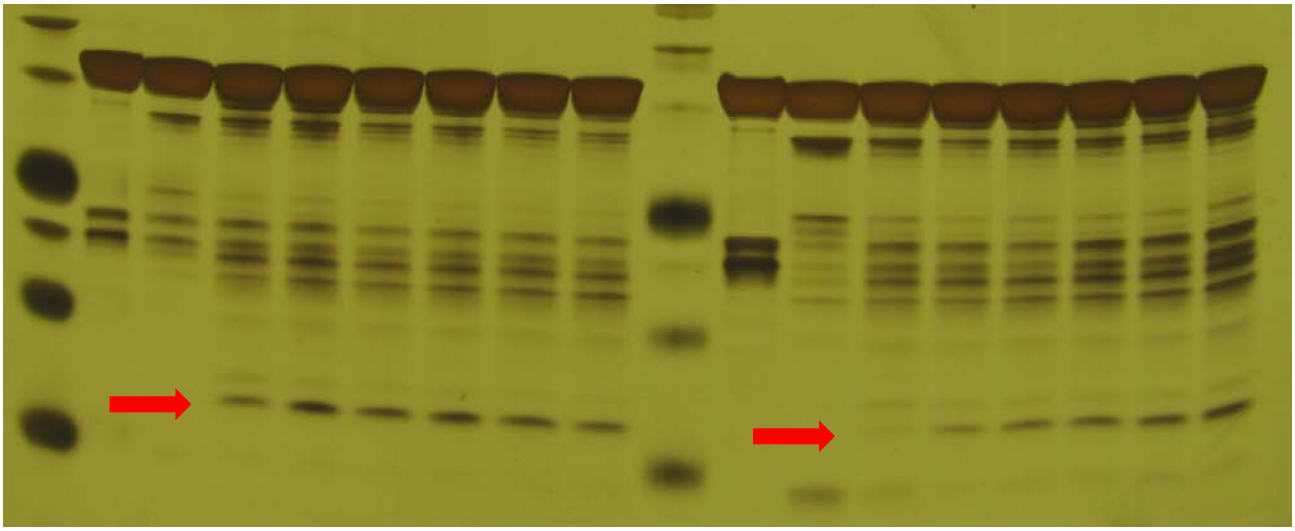

Figure 37. Limited proteolysis of the K304E MCAD protein with and without 193

(a) K304E MCAD protein, (b) K304E MCAD protein with 193. The recombinant K304E MCAD protein was digested with V8 protease in the presence or absence of YAT193 peptide at different incubation time. Total 10 μg of the protein was loaded on each lane, electrophoresed in 16.5 % T Tricine gel, and stained with silver staining kit from Sigma.

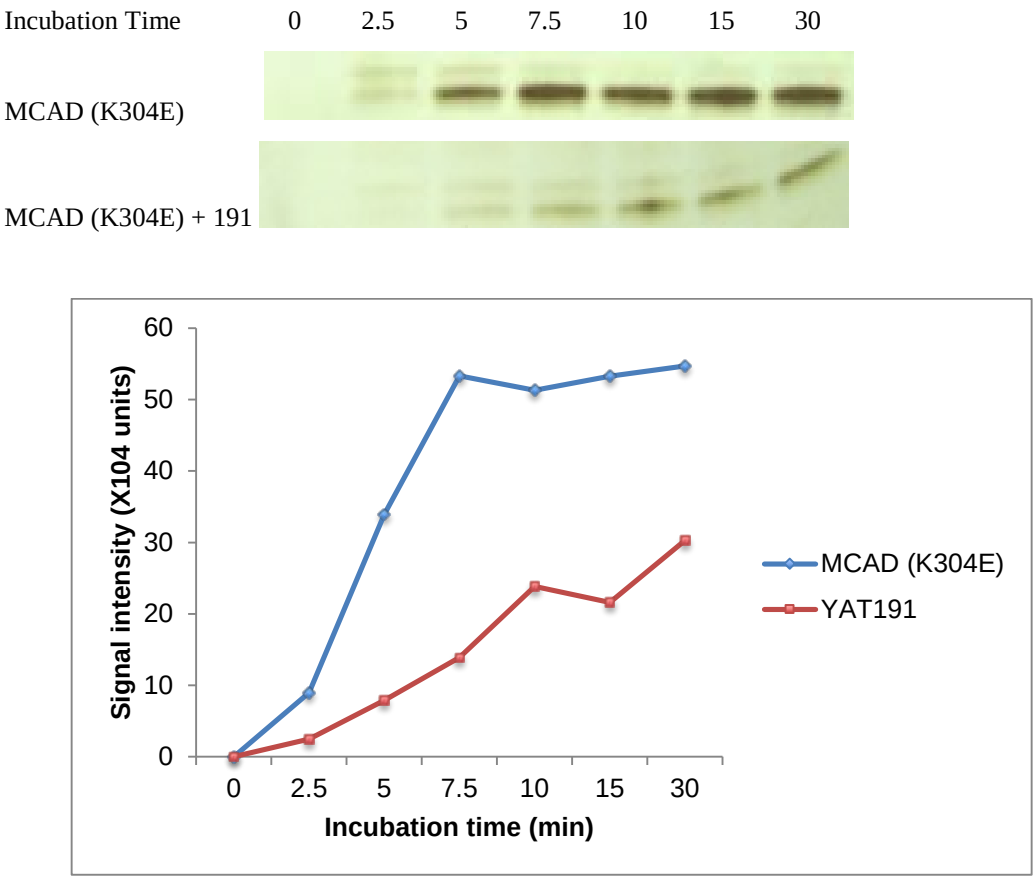

Figure 38. Limited proteolysis of K304E MCAD protein in the presence or absence of YAT191

Recombinant K304E MCAD protein was treated with V8 protease in the presence or absence of YAT191 peptide and samples were withdrawn and reaction stooped at different incubation time. A total of 10 µg protein was loaded on each lane, electrophoresed in 16.5 %T Tricine gel, and stained with silver staining kit from Sigma. One of the proteolytic fragments, 12 kDa, was analyzed to investigate the relative density of the proteolysis product in the presence and absence of the YAT191.

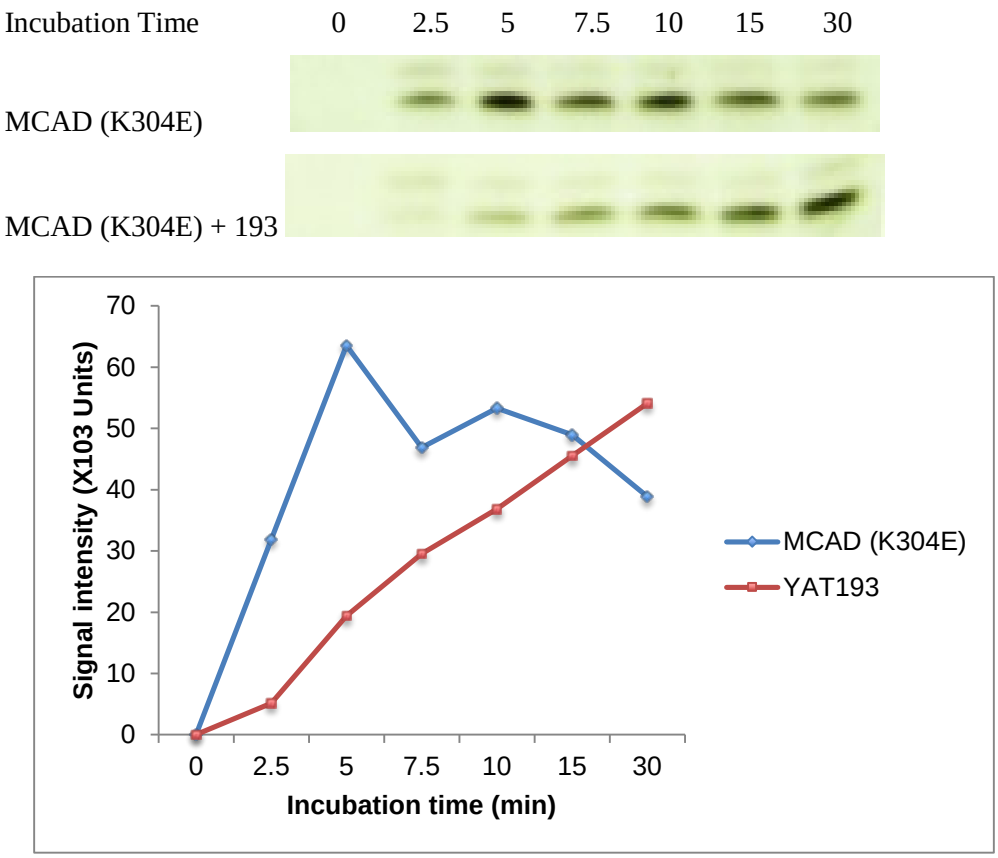

Figure 39. Limited proteolysis of K304E MCAD protein in the presence or absence of YAT193

The recombinant K304E MCAD protein was digested with V8 protease in the presence or absence of YAT193 peptide at different incubation time. A total of 10 µg protein was loaded on each lane, electrophoresed in 16.5 %T Tricine gel, and stained with silver staining kit from Sigma. One of the proteolysis fragments, 12 kDa, was analyzed to investigate the relative density of the proteolytic product in the presence or absence of YAT193.

3.4.6 MS/MS of a 12 kDa fragment of the K304E MCAD protein

To further investigate the proteolytic products, one of the smallest fragments (about 12 kDa) was analyzed by MS/MS. Figure 40 shows that the size and composition from the proteolysis fragment.

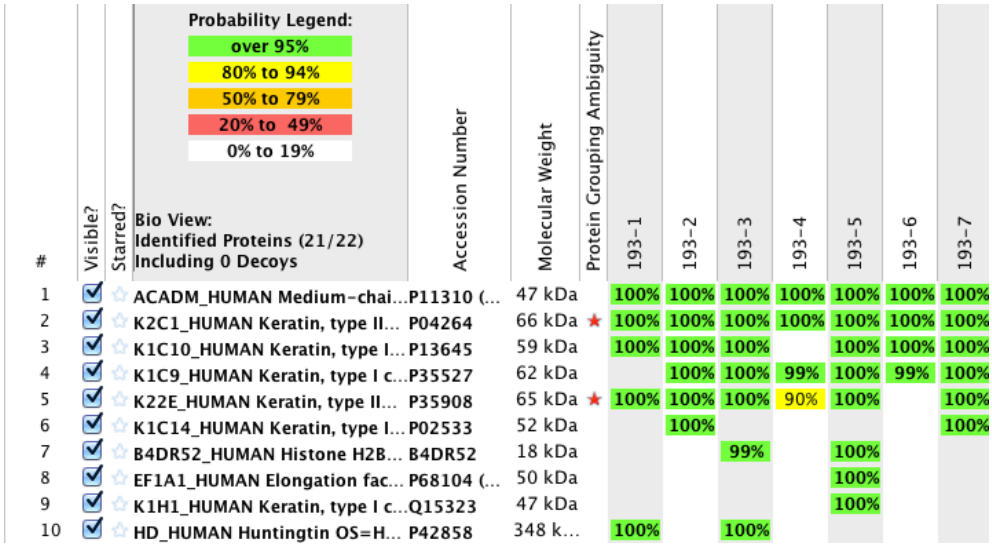

Probability Legend:
over 95%
80% to 94%
50% to 79%
20% to 49%
0% to 19%

Bio View:
Identified Proteins (21/22)
Including 0 Decoys

#	Visible?	Starred?		Accession Number	Molecular Weight	Protein Grouping Ambiguity	193-1	193-2	193-3	193-4	193-5	193-6	193-7
1	☑	☆	ACADM_HUMAN Medium-chai...	P11310 (...	47 kDa		100%	100%	100%	100%	100%	100%	100%
2	☑	☆	K2C1_HUMAN Keratin, type II...	P04264	66 kDa	★	100%	100%	100%	100%	100%	100%	100%
3	☑	☆	K1C10_HUMAN Keratin, type I...	P13645	59 kDa		100%	100%	100%		100%	100%	100%
4	☑	☆	K1C9_HUMAN Keratin, type I c...	P35527	62 kDa			100%	100%	99%	100%	99%	100%
5	☑	☆	K22E_HUMAN Keratin, type II...	P35908	65 kDa	★	100%	100%	100%	90%	100%		100%
6	☑	☆	K1C14_HUMAN Keratin, type I...	P02533	52 kDa			100%					100%
7	☑	☆	B4DR52_HUMAN Histone H2B...	B4DR52	18 kDa				99%		100%		
8	☑	☆	EF1A1_HUMAN Elongation fac...	P68104 (...	50 kDa						100%		
9	☑	☆	K1H1_HUMAN Keratin, type I c...	Q15323	47 kDa						100%		
10	☑	☆	HD_HUMAN Huntingtin OS=H...	P42858	348 k...		100%		100%				

Figure 40. MS/MS results of limited proteolysed of K304E MCAD

Selected V8 protease proteolysis K304E MCAD fragments were sent for MS/MS. 193-1 to 193-7 indicate different fragments from proteolysed K304E MCAD.

Even though MS/MS confirmed that the generated fragments were MCAD protein fragments, we could not fine map the proteolysed pattern comparing to theoretic proteolysis estimation due to trypsin digestion in the MS/MS procedure (Table 8). Since the analysis itself added additional digestion, it was difficult to compare these proteolytic fragments to estimated fragments and fine map the proteolysis pattern.

4.0 DISCUSSION

4.1 SMALL CHEMICAL CHAPERONES AS A POTENTIAL TREATMENT FOR MCADD

Previous studies with protein misfolding disorders have shown that small chemical chaperones can enhance proper folding of a mutant protein and stabilize its activity (Leandro and Gomes, 2008). As the result of a founder effect, ~90% of MCADD patients carry at least one copy of a K304E mutation that leads to the misfolding of the subunit following import into mitochondria, with subsequent degradation of the abnormal protein. The main hypothesis of this thesis was that small chemical chaperone can be used as a potential drug for MCADD by inducing proper folding of the K304E MCAD protein and/or stabilize already folded protein.

To test this hypothesis, MCAD activity was measured in lymphoblasts and fibroblasts from controls and patients homozygous for the common K304E mutation. MCAD activity in mutant cells was almost zero and was not improved by culture at low temperature as was observed in bacterial overexpression experiments (Bross et al., 1995). Of note, transcription of the mutant MCAD gene was the same as in wild type cells, and the MCAD antigen could be detected, consistent with a protein misfolding mechanism for loss of MCAD activity. Treatment of K304E MCAD mutant cells with the non-specific small chemical chaperones, TMAO and glycerol, partially rescued MCAD activity, and even increased activity in control cells, although

there was no effect on VLCAD activity in either cell line. These results provide proof-of-principle that small chemical chaperones can significantly improve the K304E MCAD activity, substantiating its potential for drug development. The increase of normal MCAD protein in control cells following chaperone treatment suggests that this protein is inefficiently folded even under normal conditions, and that chaperone therapy may be more generally applicable to MCAD deficiency. Of course, glycerol and TMAO are not practical reagents to use in patients, and thus a compound more amenable to human therapy is required.

Since about 90% MCADD patients have K304E mutation causing the failure of tetramerization, we hypothesized that small chemical chaperones can be used as a potential drug for MCADD by helping proper fold of the K304E MCAD protein.

To test the hypothesis, the basal activity of the MCAD protein from control and patients', homozygous for K304E MCAD, lymphoblasts was measured. Since K304E MCAD protein expression in bacteria showed the increased expression at low temperature and some misfolded proteins tend to be more stable at lower temperatures, lymphoblasts were also cultured at 30°C to test whether culturing at lower temperature can increase the K304E MCAD activity. The basal MCAD activity was almost zero in MCAD patients' lymphoblasts and culturing at low temperature did not increase activity. Also there was no significant transcriptional change between control and K304E lymphoblasts. Therefore, we confirmed that the loss of MCAD activity in patients' cells is not due to the mRNA expression.

Substrate binding pocket analogues are among the most effective chemical chaperones described in other enzyme systems. Since octanoate has neurotoxic effects, it is not a viable candidate for chaperone development. In contrast, sodium phenylbutyrate, an FDA approved medication for treatment for urea cycle disorders, is well tolerated at supra-physiologic

concentrations compared to octanoate. Phenylbutyrate is activated to phenylbutyryl-CoA, which undergoes one round of β-oxidation initiated by MCAD as shown in this thesis. Thus phenylbutyryl-CoA was hypothesized to accumulate in MCAD deficient cells containing at least one copy of the K304E mutation, bind to folding mutant enzyme, and promote stability of the abnormal enzyme. To examine this hypothesis, phenylbutyryl-CoA was first shown to increase the thermal stability of K304E MCAD in an *in vitro* assay. Its ability to increased MCAD activity was then tested in fibroblasts and lymphoblasts from patients homozygous for the common mutation. These experiments unequivocally confirmed that the K304E MCAD was stabilized in phenylbutyrate treated cells. However the final activity was low enough to make accurate quantitation difficult. To overcome this issue, a HEK293 cell line with inducible wild type or K304E MCAD vectors were used to boost MCAD expression for improved detection. These experiments showed a consistent increase in K304E MCAD activity following treatment with 0.5 mM PBA, while MCAD gene expression remained constant. These results are promising proof-of-principle for a clinical trial in MCAD patients since identification of mild deficiencies through newborn screening programs has led to the suggestion that even a small amount of MCAD activity is sufficient to protect against metabolic decompensation. Based on these findings, a limited clinical trial has already been started at Children's Hospital of Pittsburgh to treat patients homozygous for the K304E MCAD allele with sodium phenylbutyrate.

4.2 INVESTIGATING ALTERNATIVE SITES FOR DRUG TARGETING IN MCADD

As with substrate binding to their binding pockets, binding of ligands to other sites on a protein can serve to stabilize it. To identify additional potential "drugable" sites for K304E MCAD, the mutant was expressed it in *E. coli*, purified to essential homogeneity, and was provided it to a collaborator to determine its X-ray crystal structure. The protein structural modeling showed that there were only minor differences in the trajectory of some surface loops between wild type and K304E MCAD protein structure. The three dimensional structure now provides an opportunity to identify targets for development of pharmacologic chaperones for treatment of MCAD deficiency. One such option is the core of the MCAD tetramer where the K304E mutation lies (Figure 41).

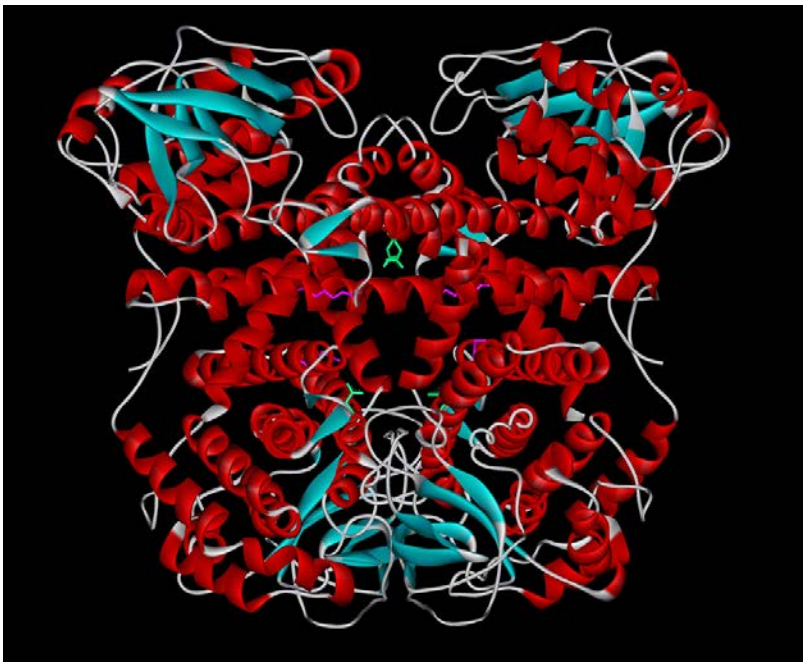

Figure 41. Ribbon representation of the crystal structure of the MCAD tetramer core

The four monomeric MCAD subunits are shown. The tetrameric core is located in the middle.

Another site for drug targeting is the interface between ETF and MCAD. The structure of this complex has previously been determined through X-ray crystallography and examination of published model allowed the design of 12 amino acid peptides predicted to bind to ETF docking site. Since the interaction of ETF and MCAD stabilizes these proteins, binding of peptides to the MCAD:ETF docking site were predicted to increase the stability of MCAD. Enzymatic analysis of MCAD incubated with ETF docking site peptides confirmed that they were bound to the enzyme and interfered with subsequent interaction of native ETF with MCAD. To examine the effect of synthetic ETF docking peptides on MCAD stability, K304E MCAD was incubated at increasing temperatures with selected synthetic peptides and the MCAD activity and circular dichroism were monitored. One of the 12-mer ETF docking site peptides, YAT193, increased the thermal stability. Limited proteolysis experiments confirmed its effect on stability, showing reduced rate of proteolysis of the K304E MCAD protein after incubation with the YAT193 peptide.

These results identify the MCAD:ETF docking site as a candidate pharmacophoric site for MCADD drug development. Generation of clinically applicable drugs will require modification of the synthetic peptide structure using structure-based drug design. This process will be greatly enhanced by the having the crystal structure of K304E MCAD now available. Co-crystalization of K304E MCAD protein and the YAT193 peptide will allow better characterization of the atomic forces driving this interaction and allow the use of YAT193 as a scaffold for more appropriate molecules for physiologic use. Also, *in silico* library screening can be used to examine other drug-like compounds to identify those with the potential to bind to the ETF docking site or use a fragment-based drug design approach.

An additional benefit of the experiment in this thesis is the potential for development of medications to treat other ACAD deficiencies. The other ACADs are highly homologous to MCAD (Figure 42), and the x-ray crystal structure of many of them has been determined. Lessons learned in this thesis thus provide a starting point for similar attempts for the other enzymes.

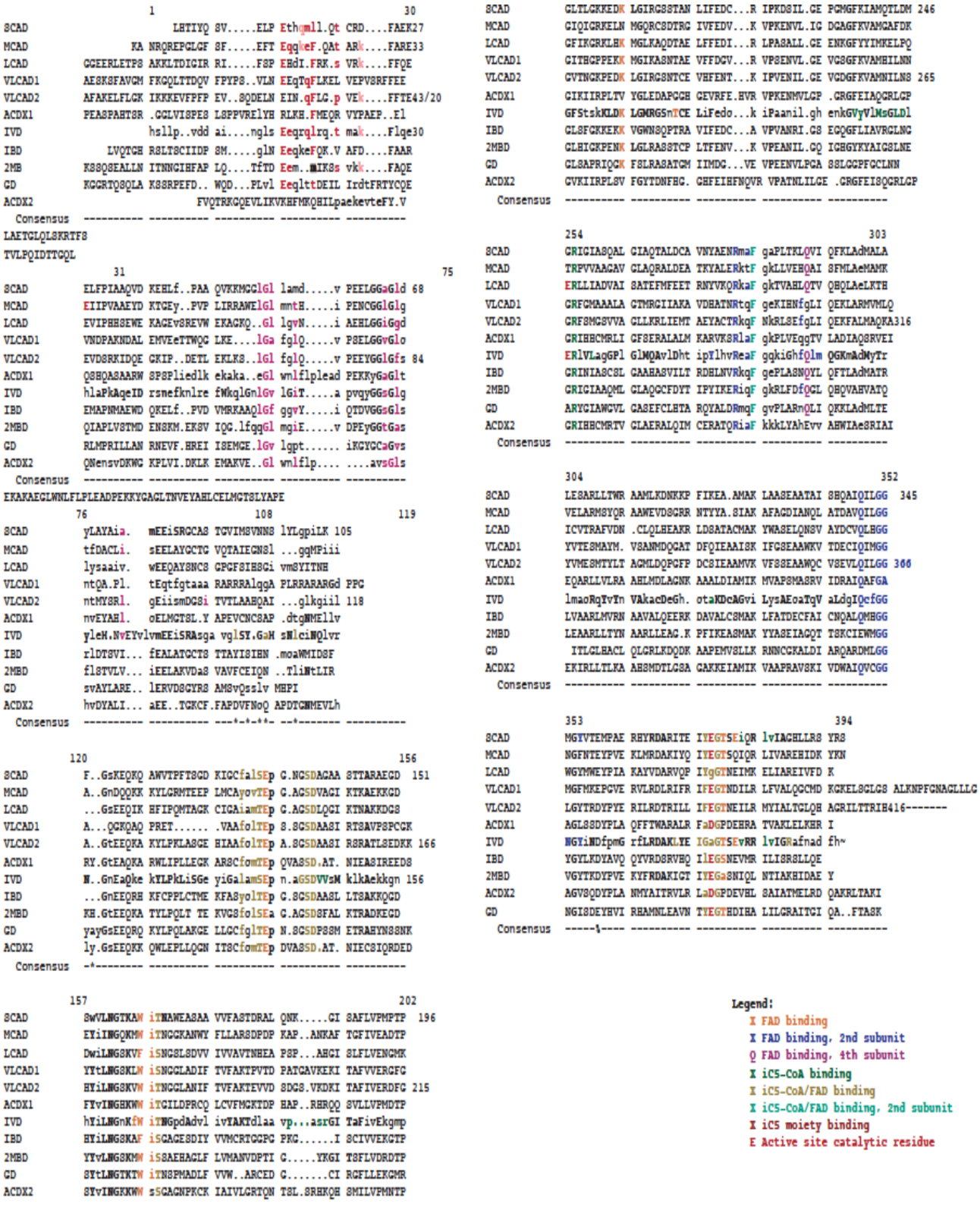

Figure 42. Amino acid sequence alignment of ACADs.

4.3 DEVELOPMENT OF HIGH-THROUGHPUT ASSAY FOR MCAD FUNCTION AND DRUG SCREENING

Experiments in this thesis were possible because only a small number of potential chaperones identified on the basis of the known enzyme structure were examined. While this is a viable alternative for potential drug-binding sites, the development of a high-throughput assay system would be beneficial to identify candidate chemical chaperones for MCAD and other ACADs in more extensive chemical libraries. To this end, a high-throughput assay for MCADD based on imaging of immunostained cells in 384 well microtiter plates using a highly automated robotic platform was attempted. After what seems to be initial success, later results were inconsistent showing no significant difference in immunologic signal between wild type and fibroblasts homozygous for the K304E mutation. Previous literature reports were conflicting as to the relative stability of MCAD antigen in such cells, with some publications showing near normal levels of the antigen in K304E mutant cells, while others report little or no mutant protein. However, the discrepancy seems to be related to cell passage number, which seems to affect mitochondrial content of wild type and patient cells. It is also possible that some undescribed variation in culture or staining conditions account for this discrepancy, and future attempts at developing an antigen-based assay will need to further explore these factors.

Another possibility for a high-throughput assay is to test directly for MCAD activity. The ETF fluorescence reduction assay used throughout this thesis is highly sensitive, reliable, and highly specific for the ACADs, and demonstrates complete lack of activity in cells homozygous

for the K304E mutation. Thus adaptation of this assay to 96 microtiter plates would allow ready screening of chemical libraries for chaperone function. Unfortunately there are some experimental limitations to the adaptation of this assay to higher throughput technology, including problems related to robotic processing of cellular extracts.

4.4 FUTURE DIRECTIONS

This study showed two approaches to investigate the development of MCADD therapy: first, the use of small chemical chaperones as drugs and second, and investigation of an MCAD drug targeting site. Since the common K304E MCAD mutation results in protein misfolding leading loss-of-function of the MCAD protein, recovery of this mutant MCAD activity is the key to overcome this condition. This study provided the proof-of-principle that the use of small chemical chaperone can increase the K304E MCAD activity. Also, by targeting ligand-binding site of the K304E MCAD protein, the stabilization and increase in activity in K304E MCAD protein are possible.

There can be other approaches to improve the mutant MCAD activity whether it is a common mutation having K304E or any other mutations. Hepatocyte transplantation (HTx) has been used as a bridging therapy for some inborn errors of metabolism disorders especially those are involved in liver. We can apply hepatocyte transplantation as a therapy for MCADD. To investigate whether HTx can be a doable therapy for MCADD, first, we can use a MCAD knock-out (KO) mice model, which is available, to test the HTx for MCADD treatment. Hepatocytes from wild type mice can be directly injected into the liver pulp of neonatal MCAD KO mice. The

utility of HTx can be evaluated by MCAD enzyme activity, composition of metabolites before and after the transplantation, and fasting and cold challenge of these mice. If this can be validated from MCAD KO mice model we can apply this method into MCADD patients. The limitations of this method can be the side effects of immune response and lack of the sources of wild type hepatocyte. The use of induced pluripotent stem (iPS) cells from the patients could overcome these limitations since the sources of wild-type hepatocytes are from the same patients but gene correction would be required before the generation of hepatocytes.

4.5 PUBLIC HEALTH IMPORTANCE OF THIS STUDY

MCADD is the most common inborn error of metabolism identified by tandem mass spectrometry in the United States, affect ~1:16,000 babies. Before the era of NBS, about 20 to 25% of the MCADD patients either died in early childhood or developed serious disabilities as a result of an acute metabolic episode (Grosse et al., 2006). With universal NBS in the United States, affected individuals are detected easily, and proper care prevents acute and severe adverse outcomes. However, multiple problems still exist relating to the proper management of MCADD (Schatz and Ensenauer, 2010). First, clinical manifestations of MCADD remain a considerable problem, especially in children age 3 to 24 months. This counters the common perception that MCADD is effectively treated by diet. Emergency care with hospitalization at clinical onset is required in as high as 95% of MCADD patients (Iafolla et al., 1994). Manifestations of MCADD occur in both children and adults even after the common adoption of NBS (Schatz and Ensenauer, 2010), and poor outcomes of MCADD in adolescence and young adults have also

been reported (Mayell et al., 2007; Wilhelm, 2006; Yusupov et al., 2010). Under the best of circumstances, careful monitoring of frequent food intake when ill is critical. Also, there are no set clinical standards for fasting tolerance even in well children. One study suggests a maximum duration of fasting in children with MCADD of 8 hours for the ages of 6 months to 1 year of age, 10 hours for the second year of life, and 12 hours, thereafter, but no global consensus exists (Derks et al., 2007). Also, many studies tried to investigate genotype-phenotype relationship for mutations in MCADD (Andresen et al., 2001; Andresen et al., 2012; Gregersen et al., 2001; Leal et al., 2013; Waddell et al., 2006). However, it remains contentious. Even though about 90% of patients have at least one 985A>G allele, other mutations or combinations with the 985A>G allele have not been carefully studied yet. Recently, Touw et al. tried to set a guideline to help the patients by comparing MCAD activity between in vitro and in vivo and data analysis from a cohort study (Touw et al., 2012; Touw et al., 2013). However, these cannot be applied clinically due to possible unexpected physiological stress or any other emergent metabolic episodes. These present difficulty when advising patients of the risk for episodes of metabolic decompensation and how to properly manage their condition. Current treatment options are frequent food intake, restriction in long-chain fatty acid intake, and cofactor supplementation (Vockley and Whiteman, 2002). IV glucose for metabolic episodes is needed. In total, these issues identify a need for a better therapy for MCADD. Development of a pharmacologic treatment for MCADD will eliminate the risk or metabolic decompensation and improve the lives for affected patients.

4.6 CONCLUSIONS

In conclusion, these results in these studies demonstrate that small chemical chaperones can increase the K304E mutant MCAD enzyme activity *in vivo*. The CoA ester substrate binding and the ETF docking sites are suitable targets for drug development. Phenylbutyrate, an FDA approved drug for treatment of the urea cycle, rescues K304E MCAD activity and thus represents a viable medication to test through clinical trials. Determination of the X-ray crystal structure of the K304E MCAD will allow identification of additional motifs to target for drug design. Development of a drug treatment for MCAD deficiency will provide significant benefits to patients with this disorder and their families.

5.0 EVIDENCE FOR INVOLVEMENT OF MEDIUM CHAIN ACYL-COA DEHYDROGENASE IN THE METABOLISM OF PHENYLBUTYRATE

This work has been previously published (Kormanik et al., 2012) and is also included in the PhD thesis of Kaitlyn Kormanik. My role in the study included expression and purification of the recombinant MCAD, participation in design and analysis of enzymatic experiments, and participating in the preparation of the manuscript for publication. Copyright permission was obtained to include the manuscript in this thesis dissertation.

Kormanik K, Kang H, Cuebas D, Vockley J, Mohsen AW. (2012) Evidence for involvement of medium chain acyl-CoA dehydrogenase in the metabolism of phenylbutyrate. *Mol. Genet. Met*. 107(4):684-9.

5.1 ABSTRACT

Sodium phenylbutyrate is used for treating urea cycle disorders, providing an alternative for ammonia excretion. Following conversion to its CoA ester, phenylbutyryl-CoA is postulated to undergo one round of β-oxidation to phenylacetyl-CoA, the active metabolite. Molecular modeling suggests that medium chain acyl-CoA dehydrogenase (MCAD; EC 1.3.99.3), a key enzyme in straight chain fatty acid β-oxidation, could utilize phenylbutyryl-CoA as substrate. Moreover, phenylpriopionyl-CoA has been shown to be a substrate for MCAD and its intermediates accumulate in patients with MCAD deficiency. We have examined the

involvement of MCAD and other acyl-CoA dehydrogenase (ACADs) in the metabolism of phenylbutyryl-CoA. Anaerobic titration of purified recombinant human MCAD with phenylbutyryl-CoA caused changes in the MCAD spectrum that are similar to those induced by octanoyl-CoA, its bona fide substrate, and unique to the development of the charge transfer ternary complex. The calculated apparent dissociationconstant (KD app) for these substrates was 2.16 μM and 0.12 μM, respectively. The MCAD reductive and oxidative half reactions were monitored using the electron transfer flavoprotein (ETF) fluorescence reduction assay. The catalytic efficiency and the Km for phenylbutyryl-CoA were 0.2 $mM^{-1}\cdot sec^{-1}$ and 5.3 μM compared to 4.0 $mM^{-1}\cdot sec^{-1}$ and 2.8 μM for octanoyl-CoA. Extracts of wild type and MCAD-deficient lymphoblast cells were tested for the ability to reduce ETF using phenylbutyryl-CoA as substrate. While ETF reduction activity was detected in extracts of wild type cells, it was undetectable in extracts of cells deficient in MCAD. The results are consistent with MCAD playing a key role in phenylbutyrate metabolism.

5.2 INTRODUCTION

Impairment of urea synthesis in humans is caused by defects in the activity of enzymes in the urea cycle including carbamylphosphate synthetase, ornithine transcarbamylase, argininosuccinic acid synthetase, argininosucinate lyase, and arginase and leads to hyperammonemia. High levels of ammonia in blood may lead to encephalopathy and death (Foundation, 2005). Sodium phenylbutyrate is the active ingredient in Buphenyl ® (Corporation, 2005-2006) and is currently used for treating primary hyperammonemia caused by certain urea cycle defects (Pharmaceutical, 2005-2006). Sodium phenylbutyrate may also be useful in

treating secondary hyperammonemia that accompanies other inborn errors. In addition, phenylbutyrate has been and is being investigated in numerous clinical settings including modulation of fetal hemoglobin gene expression in sickle cell and in thalassemia, treatment of myleodysplastic syndromes and acute myeloid leukemia, cerebral and liver ischemic injury protection, among others (Egger et al., 2007; Gore et al., 2001; Saito et al., 2009; Vilatoba et al., 2005). As of this writing >30 trials involving sodium phenylbutyrate are listed on the www.clinicaltrial.gov website. The mechanism proposed for ammonia clearance by phenylbutyrate administration involves its activation to phenylbutyryl-CoA, conversion to phenylacetyl-CoA, and conjugation with glutamine (Figure 43) for excretion by the kidneys (Qi et al., 2004).

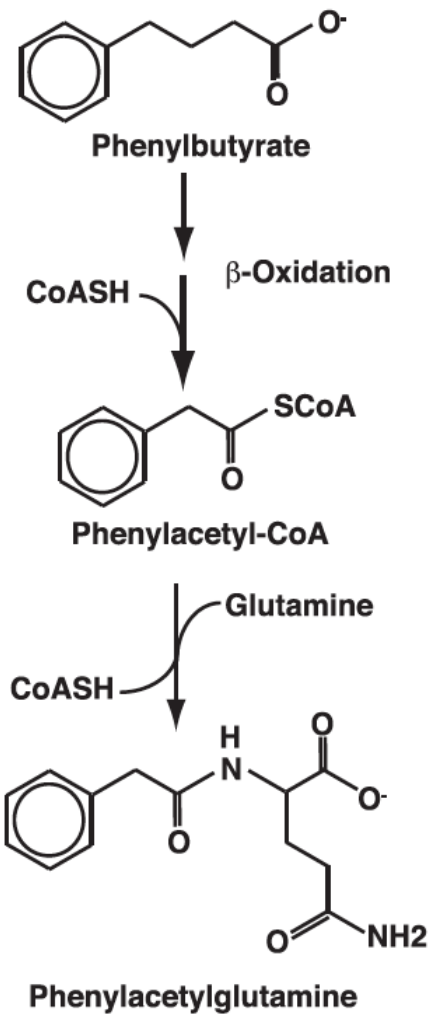

Figure 43. Metabolism of phenylbutyrate to its final metabolite

The conversion of phenylbutyryl-CoA to phenylacetyl-CoA is presumed to occur through one cycle of β-oxidation in mitochondria. The first step in the β-oxidation cycle is the α,β-dehydrogenation of fatty acid CoA esters catalyzed by members of the acyl-CoA dehydrogenase (ACAD) family of enzymes. Nine members of this enzyme family have been identified, each with characteristic substrate specificity profile (Ikeda et al., 1983; Ikeda et al., 1985b; Ikeda and Tanaka, 1983; Izai et al., 1992; Nguyen et al., 2002; Rozen et al., 1994; Willard et al., 1996; Zhang et al., 2002). Short, medium, long, saturated very long, unsaturated very long chain acyl-

CoA dehydrogenases (SCAD, MCAD, LCAD, VLCAD and ACAD9) have substrate optima of C4, C8, C12, C16, and C16:1 (unsaturated very long chain among others) acyl-CoA esters, respectively, but can utilize other substrates (Ensenauer et al., 2005a; Ikeda et al., 1983; Ikeda et al., 1985a; Ikeda et al., 1985c). The crystal structures of SCAD, MCAD, and VLCAD have been published, (PDB ID: 1JQI, 3MDE, and 43B96, respectively) (Battaile et al., 2002; Kim et al., 1993; McAndrew et al., 2008). The remaining four enzymes in the family are involved in amino acid metabolism and their crystal structures have been published as well, (PDB ID: 1IVH, 1SIR, 1RX0, and 2JIF) revealing relatively restrictive active sites, rendering them highly specific for their bona fide substrates (Battaile et al., 2004; Fu et al., 2004; Tiffany et al., 1997).

It has been observed that patients with MCAD deficiency characteristically accumulate both the glycine and carnitine conjugates of phenylpropionate, a bacterial metabolite from bowel flora that is absorbed into the blood stream (Rinaldo et al., 1988). Mass spectrometry based enzymatic assay of MCAD deficient patient fibroblast cells using phenylpropionyl-CoA as substrate showed lack of conversion to its α,β-unsaturated product (Derks et al., 2008). While the crystal structure of SCAD and VLCAD and homology 3D modeling of ACAD9 show that the active site would not accommodate the phenylbutyryl acyl moiety, the active site of MCAD would. These findings and the structural similarities between phenylpropionate and phenylbutyrate implicate MCAD in the metabolism of phenylbutyryl-CoA. In this study we tested the ability of purified human recombinant ACADs to bind and use phenylbutyryl-CoA as a substrate. We demonstrate that MCAD indeed uniquely utilizes phenylbutyryl-CoA as a substrate. In addition, we show the inability of extracts prepared from MCAD-deficient fibroblast to act upon this substrate.

5.3 MATERIALS AND METHODS

5.3.1 Purification of recombinant human MCAD

Expression and purification of recombinant human MCAD was performed as previously described for isovaleryl-CoA dehydrogenase with minor modifications (Mohsen and Vockley, 1995). *E. coli* JM105 cells (Amersham Biosciences Corp; Piscataway, NJ) containing the human MCAD high expression vector p*Ke*MCAD (Matsubara et al., 1989) and a GroEL/GroES expression plasmid were grown overnight in a 200-ml LB broth pre-culture that was used to inoculate 4 x 2-L cultures in 2-YT broth. The cells were left to grow overnight at 37˚C with shaking and MCAD expression was induced the next morning using IPTG at a final concentration of 0.5 mM for 3 hrs. Cells were harvested by centrifugation and resuspended in 2:1 weight to volume of 100 mM potassium phosphate pH 8.0, 150 mM EDTA. Cells were then lysed by sonication on ice. Including high amounts of EDTA in the cell lysis buffer is for protecting residues with groups, *e.g*., cysteine thiols and methionine sulfide groups, vulnerable to modification by oxygen reactive species generated during sonication cell suspension. This was effective in improving enzyme preparations resulting higher specific activity and consistent kinetic behavior (A-W Mohsen, 1999). Cellular debris was removed by centrifugation at 250,000 x *g* for 60 minutes. The final supernatant was dialyzed for 4 hours with vigorous stirring in 50 mM potassium phosphate pH 8.0, at 4˚C. The sample was then loaded on a 16 x 40 mm DEAE Sepharose FF column preequilibrated in 50 mM potassium phosphate pH 8.0, using an ÄKTA UPC-900 pump FPLC system (Amersham Biosciences Corp; Piscataway, NJ). After washing with 300 ml of 50 mM potassium phosphate pH 8.0, MCAD was eluted with a 300 ml linear gradient from 50 to 500 mM potassium phosphate pH 8.0. Green fractions with a 270/447 nm

ratio <12 containing MCAD were pooled, concentrated, and dialyzed against 25 mM potassium phosphate, pH 8.0. Pooled fractions of essentially pure MCAD (270/447 nm ratio = 5.5), were concentrated and stored at –80˚C. Other recombinant human ACADs were similarly purified except that the protocol was terminated after the DEAE-Sepharose column for LCAD as the enzyme was unstable. LCAD protein purity ~70% at this stage.

5.3.2 The electron transfer flavoprotein (ETF) purification

Porcine ETF was purified as previously published (Vockley et al., 2000), except that the dialysis buffer used after both the 40-60% ammonium sulfate fractionation and DE-52 cellulose anion-exchange chromatography steps consisted of unbuffered 15 mM dibasic potassium phosphate and 5% glycerol.

5.3.3 Fibroblast cell culture and extract preparation

Wild type and MCAD deficient cells (homozygous for the K304E mutation) with the designation GM085401 and GM07844, respectively, were obtained from Coriell Institute for Medical Research, Camden, NJ. Cells were cultured in DMEM medium supplemented with glutamine and ampicillin and streptomycin, and 20% fetal bovine serum. Cells were harvested from a T175 flask by sonication with a buffer consisting of 50 mM Tris buffer and 10 mM EDTA, pH 8.0. The cell debris was removed by centrifugation and the cell free extract was assayed for protein and enzyme activity as described below.

5.3.4 ETF fluorescence reduction assay

The ETF reduction assay was performed using a Jasco FP-6300 spectrofluorometer (Easton, MD) with a cuvette holder heated with circulating water at 32˚C. The assay was otherwise performed as described (Frerman and Goodman, 1985), at the indicated substrate concentrations. The enzyme was diluted 1200-fold into a buffer containing 50 mM Tris, pH 8.0, 5 mM EDTA and 50% glycerol, and 10 µl were used for each assay. The ETF concentration in the reaction mixture was 2 µM. Spectra Manager 2 software (Jasco Inc) was used to collect data and calculate reaction rate and Microsoft Excel was used to calculate the kinetic parameters.

5.3.5 Phenylbutyryl-CoA synthesis

CoASH, octanoyl-CoA, C_{12}-CoA and phenylbutyric acid were obtained from Sigma (St. Louis, MO) 2,6-dimethylheptanoic acid was obtained from Matreya LLC (Pleasant Gap, PA). The phenylbutyryl-CoA and 2,6-dimethylheptanoyl-CoA esters were prepared by the mixed anhydride method as described previously (Schulz, 1974) and was purified by HPLC using a Luna 5 µm C18(2) column (25 cm x 0.46 cm) and a linear gradient (10-60%) of acetonitrile into 50 mM ammonium phosphate, pH 5.5, at a flow rate of 1.5 mL/min over 30 min.

5.3.6 Monitoring the interaction of MCAD with substrates

Formation of the charge transfer ternary complex was monitored by observing the increase in absorbance at the 570 nm area, concomitant with the decrease of absorbance at 447 nm area, of the purified MCAD in 120 mM potassium phosphate spectrum under anaerobic

conditions using a JascoV-650 Spectrophotometer. Phenylbutyryl-CoA solution dissolved in water to 0.53 mM was titrated into the MCAD sample one µL at a time using a 50 µl Hamilton syringe attached to an automatic dispenser. Ten seconds of equilibration time were allowed after mixing before the sample was scanned at 250 to 800 nm. Final substrate concentrations varied as indicated in figure legends. All data were adjusted for the dilution resulting from substrate addition. Substrates were titrated, but with different final concentrations as indicated in the figure legends. The dissociation constant ($K_{D\ app}$) was calculated with the Stockell equation as described previously (McKean et al., 1979):

$$\frac{d}{p} = K_{D\ app}\ \frac{1}{e-p} + n$$

where **d** is the total ligand concentration, **e** is the total molar concentration of enzyme, **p** is the fraction of enzyme sites that bind ligand multiplied by **e**, and **n** is the number of binding sites. The absorbance at 447 nm when all enzyme sites are occupied with ligand was determined separately by adding large excess of octanoyl-CoA and used to calculate the fraction of enzyme with bound ligand at various readings and assuming that at large excess of added substrate would equal to **e**.

5.3.7 Molecular modeling

Computer modeling of MCAD was performed using a Silicon Graphics Fuel workstation (Mountain View, CA) with the *Insight* II 2005 software package and MOE software, from Chemical Computing Group, Montreal, Canada, and the atomic coordinates of pig MCAD (3MDE) in the dimer form as a molecule (Kim et al., 1993). Carbon atoms at positions C5-C8 of

the octanoyl-CoA ligand, which co-crystallized with MCAD, were replaced with a phenyl group. The phenylbutyryl-CoA ligand conformation in the active site was refined using the Discover module. Human LCAD 3D structure was modeled using MCAD atomic coordinates as template and the *Insight* II modeling software.

5.4 RESULTS

5.4.1 Interaction of MCAD with substrates, the reductive half-reaction

Formation of the charge transfer complex, the reductive half-reaction, is evident from the spectral scans of MCAD at various phenylbutyryl-CoA concentrations (Figure 44 and 45).

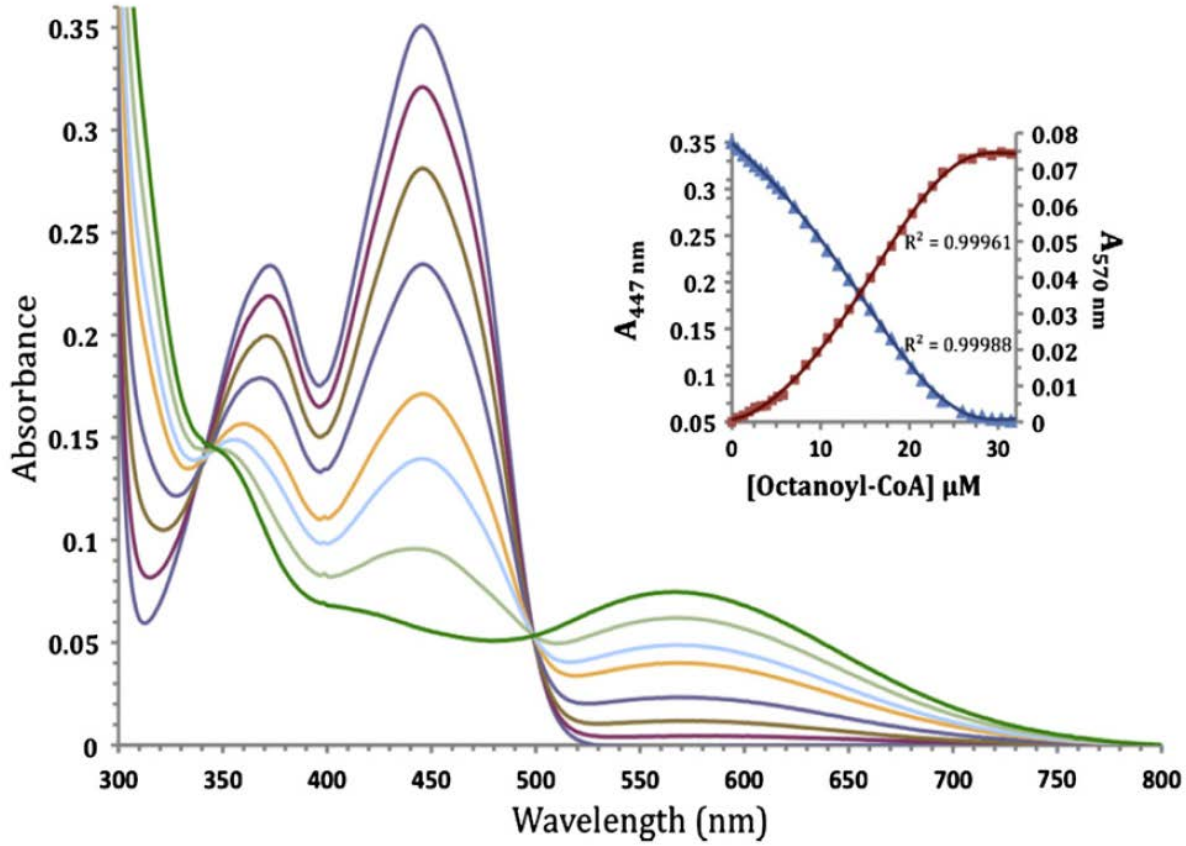

Figure 44. Monitoring the formation of the charge transfer complex with purified MCAD upon addition of increasing amounts of octanoyl-CoA

The absorbance maxima at ~370 nm and ~447 nm are reduced and a new peak centered at 570 nm appears with addition of increasing substrate. Selected scans are shown with octanoyl-CoA concentration at 0, 3.25, 7.1, 10.8, 15.6, 18.0, 21.5, and 28.2 µM. The inset shows the kinetics of these changes. Equation for the decrease at 447 nm is: $y = -1 \times 10^{-9}x^6 + 1 \times 10^{-7}x^5 - 2 \times 10^{-6}x^4 + 2 \times 10^{-5}x^3 - 0.0003x^2 - 0.008x + 0.3489$. Equation for the increase at 570 nm is: $y = 6 \times 10^{-10}\,x^6 - 5 \times 10^{-8}\,x^5 + 1 \times 10^{-6}\,x^4 - 2 \times 10^{-5}\,x^3 + 0.0003x^2 + 0.0003x + 0.0008$. Enzyme concentration was 25.2 µM.

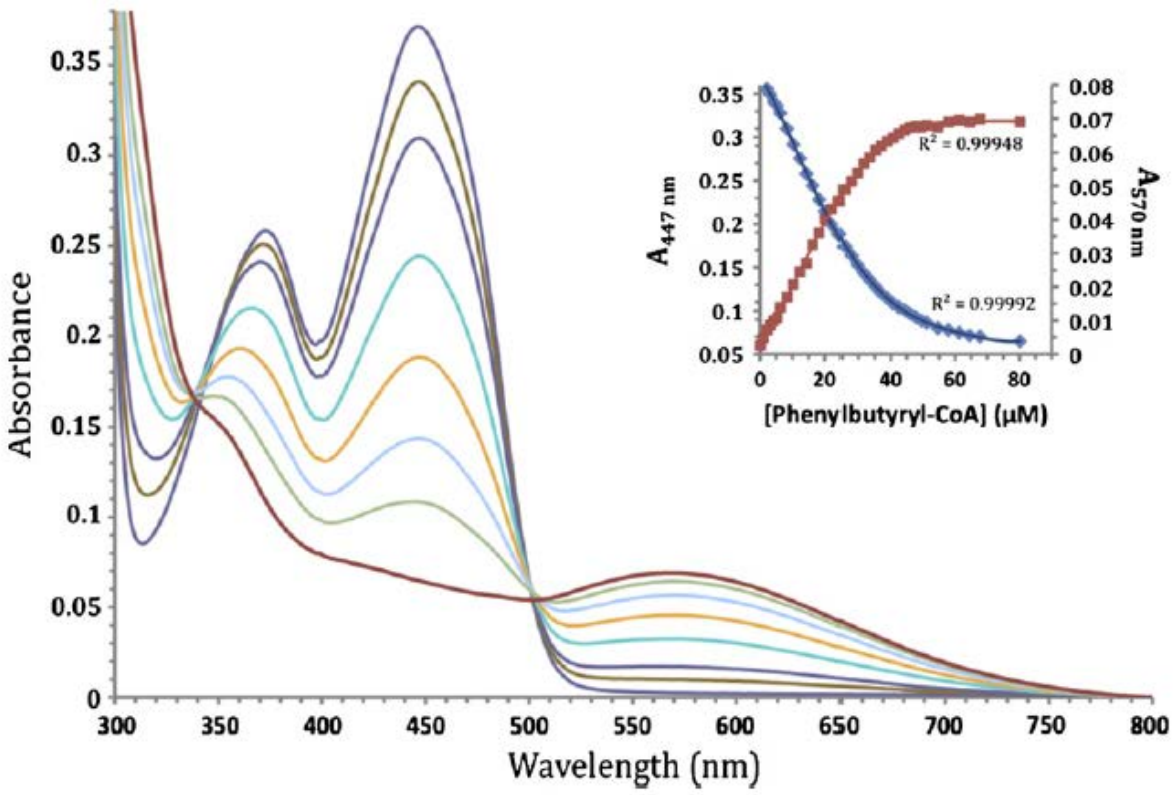

Figure 45. Monitoring the formation of the charge transfer complex with purified MCAD upon addition of increasing amounts of phenylbutyryl-CoA

The absorbance maxima at ~370 nm and ~447 nm are reduced and a new peak centered at ~570 nm appears with addition of increasing substrate. Selected scans are shown with phenylbutyryl-CoA concentration at 0, 4.2, 8.3, 16.3, 24.1, 31.6, 40.7, and 80.2 μM. The inset shows the kinetics of these changes. Equation for the decrease at 447 nm is: $y = 5 \times 10^{-10} x^5 - 1 \times 10^{-7} x^4 + 9 \times 10^{-6} x^3 - 0.0002 x^2 - 0.0061 x + 0.3707$. Equation for the increase at 570 nm is: $y = -1 \times 10^{-10} x^5 + 3 \times 10^{-8} x^4 - 3 \times 10^{-6} x^3 + 7 \times 10^{-5} x^2 + 0.0012 x + 0.0036$. Enzyme concentration was 25.2 μM.

The progressive decrease and increase of absorbance at 447 nm and 570 nm, respectively, are similar to those induced by octanoyl-CoA. The octanoyl-CoA binding curve is sigmoidal in contrast to the phenylbutyryl-CoA binding curve, possibly reflecting differences in enzyme mechanism of interaction. The plot of d/p versus 1/e-p (the Stockell plot) was nonlinear. A line drawn at the straight area of the curve where the substrate:subunit ratio was 1:1 estimates the apparent dissociation constant ($K_{D\ app}$) being 0.12 μM and 2.16 μM for octanoyl-CoA and

phenylbutyryl-CoA, respectively. Other mathematical derivatives of the absorbance data all indicated that the binding sites are non-equivalent.

Table 13. Kinetic Constants of Recombinant Human MCAD Using Octanoyl-CoA and Phenylbutyryl-CoA as Substrates and the ETF Fluorescence Reduction Assay

Substrate	K_m (μM)	V_{max} (μmol•min^{-1})	k_{cat}/K_m Per mol FAD (μM^{-1}•min^{-1})
Octanoyl-CoA	2.8	16.20	2.40 X 10^5
Phenylbutyryl-CoA	5.3	1.35	0.11 X 10^5

5.4.2 Interaction of MCAD: Substrate ternary complex with ETF, the oxidative half reaction

Using ETF as the electron acceptor in the standard enzymatic assay detailed above, transfer of electrons was confirmed as evident from the reduction of ETF fluorescence in the presence of various concentrations of phenylbutyryl-CoA. The catalytic efficiency and K_m for the phenylbutyryl-CoA were 0.2 mM^{-1}· sec^{-1} and 5.3 μM compared to 4.0 mM^{-1}· sec^{-1} and 2.8 μM for octanoyl-CoA, respectively.

Molecular modeling of human LCAD shows possible accommodation of the acyl moiety of the phenylbutyryl-CoA, with the exception of residue L264, which would have one of its side chain methyl hydrogens ~1.3Å away from a phenyl ring hydrogen and so would hinder binding. To test if the LCAD active site has enough plasticity to accommodate this potential substrate, we

measured its activity with LCAD using the ETF fluorescence reduction assay. While the partially purified recombinant human LCAD was active in the presence of various substrates including C_{12}-CoA and 2,6-dimethylheptanoyl-CoA, it was not active in the presence of phenylbutyryl-CoA. Purified SCAD, MCAD, and ACAD9 also showed no activity with phenylbutyryl-CoA as substrate.

5.4.3 The ETF fluorescence reduction assay of cell extract

ETF fluorescence reduction was observed using extracts from wild type fibroblast cells in the presence of 30 μM of phenylbutyryl-CoA, octanoyl-CoA, or palmitoyl-CoA. (The latter substrate was used as internal control and is a substrate of VLCAD.) Enzyme specific activity measured using these substrates was 3.41 (0.53), 4.01 (1.34), 9.10 (2.13) *n*moles ETF reduced· min^{-1}· mg^{-1}, respectively. No activity was observed using similar amounts of extract from fibroblast cells deficient in MCAD with either phenylbutyryl-CoA or octanoyl-CoA. The measured enzyme specific activity of palmitoyl-CoA oxidation in extract from these cells was 3.91 (1.34) *n*moles ETF reduced· min^{-1}· mg^{-1}.

5.5 DISCUSSION

Following the conversion of phenylbutyrate to the CoA ester, one cycle of β-oxidation is expected to result in phenylacetyl-CoA and acetyl-CoA as the final products (Figure 46). Phenylacetyl-CoA is hydrolyzed to phenylacetate, which becomes conjugated with glutamine and is excreted in urine (Figure 43). An analysis of this first step in the β-oxidation of

phenylbutyryl-CoA is important because the first step in the β-oxidation of fatty acids is postulated to be rate-limiting (P Macheroux, 1997), and thus the metabolism of Buphenyl to its active form, phenylacetate, may also be modulated by similar factors that affects energy metabolism at the same step.

The effect of phenylbutyryl-CoA on the MCAD absorbance spectrum at relatively low concentrations is monitored *via* the decrease of absorbance at 447 nm and increase of absorbance at 570 nm. This confirms productive binding of phenylbutyryl-CoA to MCAD in the reductive half reaction with lack of product release. This effect is similar to that induced by octanoyl-CoA binding to MCAD, and indicative of the transfer of a proton and a hydride to the flavin ring and formation of the charge transfer complex, which is comprised of the enzyme, reduced FAD, and enoyl product and detected by the intense absorbance band centered at 570 nm (Ghisla and Thorpe, 2004; Lau and Thorpe, 1988).

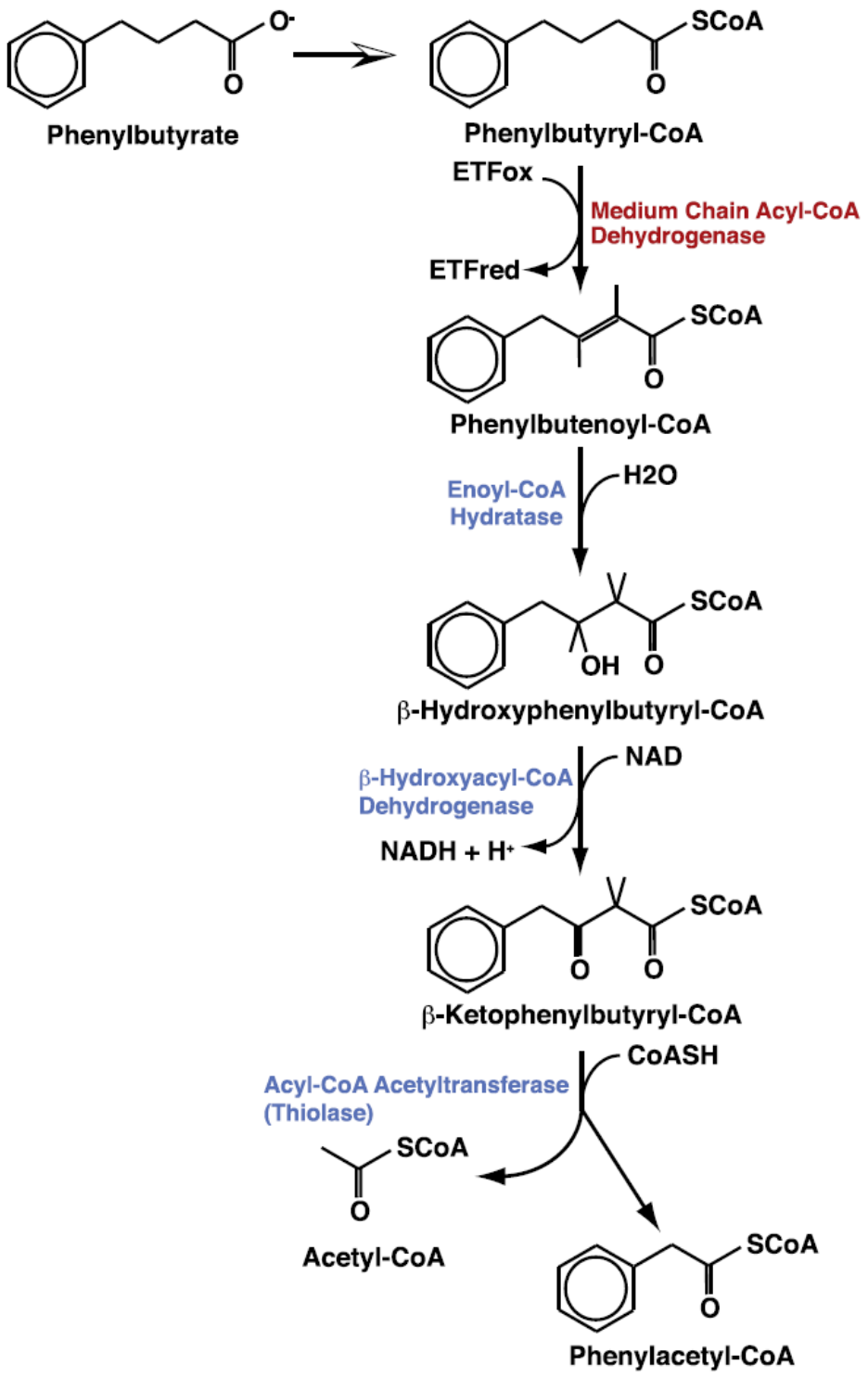

Figure 46. Detailed proposed pathway of metabolism of phenylbutyrate to its active form, phenylacetate

The inset in Figure 44 shows a sigmoidal shaped curve when octanoyl-CoA, but not phenylbutyryl-CoA, was used as substrate. This may imply positive cooperativity between the first and second subunits with octanoyl-CoA binding that does not occur with phenylbutyryl-CoA. Although other interpretations of sigmoidal behavior in this setting are possible, including presence of various MCAD forms or other effector molecules, the argument is weakened by the fact that the only difference between the two reactions is the substrate itself. Impurities in the substrate preparation are also not likely to induce such an effect as such impurities would be present at ineffectively low concentrations at the low substrate concentrations range, between 0.25-1 and 4:1substrate:MCAD tetramer ratio.

Reduction of ETF by the charge transfer complex in the oxidative half-reaction shows that electrons from the bound phenylbutyryl-CoA can be efficiently transferred to ETF and that the product, phenylbutenoyl-CoA, is released to complete the reaction. In contrast, none of the other ACADs are capable of catalyzing this reaction.

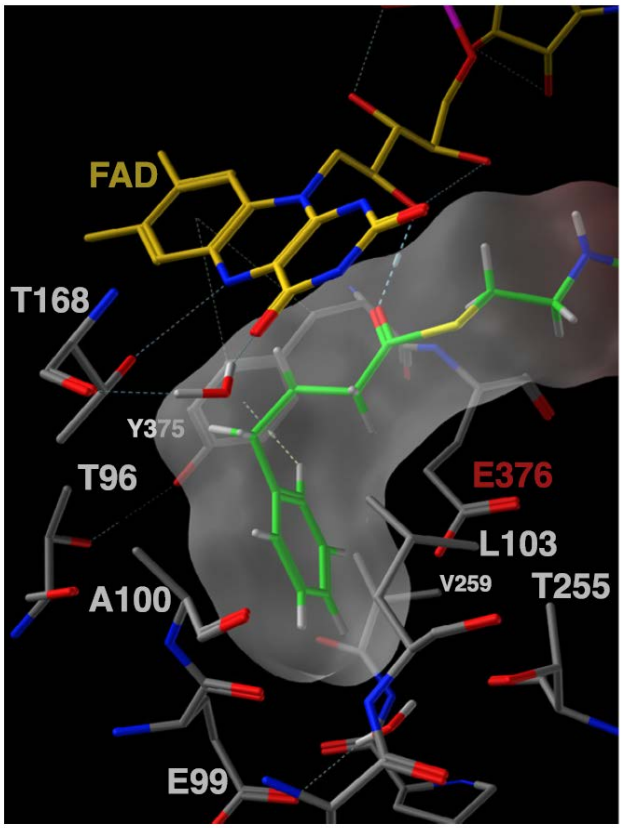

Figure 47. Stick representation of MCAD active site residues and ligands with phenylbutyryl-CoA modeled in place of octanoyl-CoA

The crystal structure of pig MCAD with bound octanoyl-CoA (PDB: 3MDE, [20]) was used to create the model using MOE modeling software. The E376 carboxylate is the active site catalytic base responsible for the substrate C2 proton abstraction to initiate catalysis.

Modeling of a phenylbutyryl moiety in the active site in place of the octanoyl moiety observed in the MCAD crystal structure shows the phenyl moiety accommodated in the acyl moiety binding site pocket with a conformation perpendicular to the aromatic ring of Y375, Figure 47. Other residues involved in binding the phenyl moiety include E99, A100, Leu103, and V259. Furthermore, modeling predicts that the phenyl ring *para* and/or *meta* positions are candidate expansion sites for adding a functional group that may improve binding, while addition at the *ortho* position would prevent the derivative from binding to MCAD.

Based on the kinetic parameters of MCAD with phenylbutyryl-CoA as substrate, individuals with MCAD deficiency are likely to experience a functionally relevant decrease in the ability to metabolize the medication, though indications for use in these patients are likely to be rare. Of note, since octanoyl-CoA has been reported to provide thermal stability to the MCAD K304E mutant (Nasser et al., 2004), it is possible that phenylbutyryl-CoA would behave similarly and may be of benefit *in vivo* in patients carrying at least one copy of this mutation. This requires additional investigation in cellular or whole body systems. It is unknown if carriers for MCAD deficiency, a much more common situation, will display altered metabolism of phenylbutyrate. In other indications where the functional effects of phenylbutyrate are less well characterized, modulation of MCAD activity might be of benefit to alter drug metabolism and/or its half-life and increase its efficacy, depending on the mechanism of action of the medication in each disorder. Detailed biochemical studies to determine the drug's mode of action and its pharmacokinetics for such indications are thus crucial.

5.6 ACKNOWLEDGEMENTS

The project described was supported in part by Award Number R21 HD056004 from the Eunice Kennedy Shriver National Institute of Child Health & Human Development (A-WM) and RO1DK78755 and DK54936 (JV). The content is solely the responsibility of the authors and does not necessarily represent the official views of the Eunice Kennedy Shriver National Institute Of Child Health & Human Development or the National Institutes of Health. The project was also supported in part by an unrestricted research grant from Hyperion Therapeutics, Inc. (JV), and a Missouri State University Faculty Research Award, number F07036 (DC).

BIBLIOGRAPHY

A-W Mohsen, J.V.i.S.G., P. Kroneck, P. Macheroux, and H. Sund, eds.) (1999). Flavins and Flavoproteins 1999, Rudolf Weber, New York 1999. 515-518.

Barral, J.M., Broadley, S.A., Schaffar, G., and Hartl, F.U. (2004). Roles of molecular chaperones in protein misfolding diseases. Seminars in cell & developmental biology *15*, 17-29.

Bartlett, K., and Eaton, S. (2004). Mitochondrial beta-oxidation. Eur J Biochem *271*, 462-469.

Battaile, K.P., Molin-Case, J., Paschke, R., Wang, M., Bennett, D., Vockley, J., and Kim, J.J. (2002). Crystal structure of rat short chain acyl-CoA dehydrogenase complexed with acetoacetyl-CoA: comparison with other acyl-CoA dehydrogenases. The Journal of biological chemistry *277*, 12200-12207.

Battaile, K.P., Nguyen, T.V., Vockley, J., and Kim, J.J. (2004). Structures of isobutyryl-CoA dehydrogenase and enzyme-product complex: comparison with isovaleryl- and short-chain acyl-CoA dehydrogenases. The Journal of biological chemistry *279*, 16526-16534.

Blois, B., Riddell, C., Dooley, K., and Dyack, S. (2005). Newborns with C8-acylcarnitine level over the 90th centile have an increased frequency of the common MCAD 985A>G mutation. Journal of inherited metabolic disease *28*, 551-556.

Bross, P., Andresen, B.S., Winter, V., Krautle, F., Jensen, T.G., Nandy, A., Kolvraa, S., Ghisla, S., Bolund, L., and Gregersen, N. (1993). Co-overexpression of bacterial GroESL chaperonins partly overcomes non-productive folding and tetramer assembly of E. coli-expressed human medium-chain acyl-CoA dehydrogenase (MCAD) carrying the prevalent disease-causing K304E mutation. Biochimica et biophysica acta *1182*, 264-274.

Bross, P., Jespersen, C., Jensen, T.G., Andresen, B.S., Kristensen, M.J., Winter, V., Nandy, A., Krautle, F., Ghisla, S., Bolundi, L., *et al.* (1995). Effects of two mutations detected in medium chain acyl-CoA dehydrogenase (MCAD)-deficient patients on folding, oligomer assembly, and stability of MCAD enzyme. The Journal of biological chemistry *270*, 10284-10290.

Bross, P., Pedersen, P., Winter, V., Nyholm, M., Johansen, B.N., Olsen, R.K., Corydon, M.J., Andresen, B.S., Eiberg, H., Kolvraa, S., *et al.* (1999). A polymorphic variant in the human electron transfer flavoprotein alpha-chain (alpha-T171) displays decreased thermal stability and is overrepresented in very-long-chain acyl-CoA dehydrogenase-deficient patients with mild childhood presentation. Molecular genetics and metabolism *67*, 138-147.

Chohan, K.K., Jones, M., Grossmann, J.G., Frerman, F.E., Scrutton, N.S., and Sutcliffe, M.J. (2001). Protein dynamics enhance electronic coupling in electron transfer complexes. The Journal of biological chemistry *276*, 34142-34147.

Corporation, M.P. (2005-2006). 3Ucyclyd Pharma. BUPHENYL (sodium phenylbutyrate) Tablets andPowder

Corydon, T.J., Hansen, J., Bross, P., and Jensen, T.G. (2005). Down-regulation of Hsp60 expression by RNAi impairs folding of medium-chain acyl-CoA dehydrogenase wild-type and disease-associated proteins. Molecular genetics and metabolism *85*, 260-270.

Derks, T.G., Boer, T.S., van Assen, A., Bos, T., Ruiter, J., Waterham, H.R., Niezen-Koning, K.E., Wanders, R.J., Rondeel, J.M., Loeber, J.G., *et al.* (2008). Neonatal screening for medium-chain acyl-CoA dehydrogenase (MCAD) deficiency in The Netherlands: the importance of enzyme analysis to ascertain true MCAD deficiency. Journal of inherited metabolic disease *31*, 88-96.

Duran, M., Bruinvis, L., Ketting, D., de Klerk, J.B., and Wadman, S.K. (1988). Cis-4-decenoic acid in plasma: a characteristic metabolite in medium-chain acyl-CoA dehydrogenase deficiency. Clinical chemistry *34*, 548-551.

Egger, G., Aparicio, A.M., Escobar, S.G., and Jones, P.A. (2007). Inhibition of histone deacetylation does not block resilencing of p16 after 5-aza-2'-deoxycytidine treatment. Cancer research *67*, 346-353.

Ensenauer, R., He, M., Willard, J.M., Goetzman, E.S., Corydon, T.J., Vandahl, B.B., Mohsen, A.W., Isaya, G., and Vockley, J. (2005a). Human acyl-CoA dehydrogenase-9 plays a novel role in the mitochondrial beta-oxidation of unsaturated fatty acids. The Journal of biological chemistry *280*, 32309-32316.

Ensenauer, R., Winters, J.L., Parton, P.A., Kronn, D.F., Kim, J.W., Matern, D., Rinaldo, P., and Hahn, S.H. (2005b). Genotypic differences of MCAD deficiency in the Asian population: novel genotype and clinical symptoms preceding newborn screening notification. Genetics in medicine : official journal of the American College of Medical Genetics *7*, 339-343.

Foundation, N.U.C.D. (2005).

Frerman, F.E., and Goodman, S.I. (1985). Fluorometric assay of acyl-CoA dehydrogenases in normal and mutant human fibroblasts. Biochemical medicine *33*, 38-44.

Fu, Z., Wang, M., Paschke, R., Rao, K.S., Frerman, F.E., and Kim, J.J. (2004). Crystal structures of human glutaryl-CoA dehydrogenase with and without an alternate substrate: structural bases of dehydrogenation and decarboxylation reactions. Biochemistry *43*, 9674-9684.

Ghisla, S., and Thorpe, C. (2004). Acyl-CoA dehydrogenases. A mechanistic overview. European journal of biochemistry / FEBS *271*, 494-508.

Gore, S.D., Weng, L.J., Zhai, S., Figg, W.D., Donehower, R.C., Dover, G.J., Grever, M., Griffin, C.A., Grochow, L.B., Rowinsky, E.K., *et al.* (2001). Impact of the putative differentiating agent sodium phenylbutyrate on myelodysplastic syndromes and acute myeloid leukemia. Clinical cancer research : an official journal of the American Association for Cancer Research *7*, 2330-2339.

Gregersen, N., Andresen, B.S., Pedersen, C.B., Olsen, R.K., Corydon, T.J., and Bross, P. (2008). Mitochondrial fatty acid oxidation defects--remaining challenges. Journal of inherited metabolic disease *31*, 643-657.

Gregersen, N., Bolund, L., and Bross, P. (2005). Protein misfolding, aggregation, and degradation in disease. Molecular biotechnology *31*, 141-150.

Gregersen, N., Bross, P., Vang, S., and Christensen, J.H. (2006). Protein misfolding and human disease. Annual review of genomics and human genetics *7*, 103-124.

Iafolla, A.K., Thompson, R.J., Jr., and Roe, C.R. (1994). Medium-chain acyl-coenzyme A dehydrogenase deficiency: clinical course in 120 affected children. The Journal of pediatrics *124*, 409-415.

Iannitti, T., and Palmieri, B. (2011). Clinical and experimental applications of sodium phenylbutyrate. Drugs in R&D *11*, 227-249.

Ikeda, Y., Dabrowski, C., and Tanaka, K. (1983). Separation and properties of five distinct acyl-CoA dehydrogenases from rat liver mitochondria. Identification of a new 2-methyl branched chain acyl-CoA dehydrogenase. The Journal of biological chemistry *258*, 1066-1076.

Ikeda, Y., Hine, D.G., Okamura-Ikeda, K., and Tanaka, K. (1985a). Mechanism of action of short-chain, medium-chain, and long-chain acyl-CoA dehydrogenases. Direct evidence for carbanion formation as an intermediate step using enzyme-catalyzed C-2 proton/deuteron exchange in the absence of C-3 exchange. The Journal of biological chemistry *260*, 1326-1337.

Ikeda, Y., Okamura-Ikeda, K., and Tanaka, K. (1985b). Purification and characterization of short-chain, medium-chain, and long-chain acyl-CoA dehydrogenases from rat liver mitochondria. Isolation of the holo- and apoenzymes and conversion of the apoenzyme to the holoenzyme. The Journal of biological chemistry *260*, 1311-1325.

Ikeda, Y., Okamura-Ikeda, K., and Tanaka, K. (1985c). Spectroscopic analysis of the interaction of rat liver short-chain, medium-chain, and long-chain acyl coenzyme A dehydrogenases with acyl coenzyme A substrates. Biochemistry *24*, 7192-7199.

Ikeda, Y., and Tanaka, K. (1983). Purification and characterization of 2-methyl-branched chain acyl coenzyme A dehydrogenase, an enzyme involved in the isoleucine and valine metabolism, from rat liver mitochondria. The Journal of biological chemistry *258*, 9477-9487.

Izai, K., Uchida, Y., Orii, T., Yamamoto, S., and Hashimoto, T. (1992). Novel fatty acid beta-oxidation enzymes in rat liver mitochondria. I. Purification and properties of very-long-chain acyl-coenzyme A dehydrogenase. The Journal of biological chemistry *267*, 1027-1033.

J-J Kim , M.W., R Paschke (1993). Crystal structures of medium-chain acyl-CoA dehydrogenase from pig liver mitochondria with and without substrate. Proc Natl Acad Sci USA, 7523-7527.

Kim, J.J., and Miura, R. (2004). Acyl-CoA dehydrogenases and acyl-CoA oxidases. Structural basis for mechanistic similarities and differences. European journal of biochemistry / FEBS *271*, 483-493.

Kim, J.J., Wang, M., and Paschke, R. (1993). Crystal structures of medium-chain acyl-CoA dehydrogenase from pig liver mitochondria with and without substrate. Proceedings of the National Academy of Sciences of the United States of America *90*, 7523-7527.

Kim, J.J., and Wu, J. (1988). Structure of the medium-chain acyl-CoA dehydrogenase from pig liver mitochondria at 3-A resolution. Proceedings of the National Academy of Sciences of the United States of America *85*, 6677-6681.

Kormanik, K., Kang, H., Cuebas, D., Vockley, J., and Mohsen, A.W. (2012). Evidence for involvement of medium chain acyl-CoA dehydrogenase in the metabolism of phenylbutyrate. Molecular genetics and metabolism *107*, 684-689.

Lau, S.M., and Thorpe, C. (1988). The nature of enzyme-substrate complexes in acyl-coenzyme A dehydrogenases. Archives of biochemistry and biophysics *262*, 293-297.

Leal, J., Ades, A., Wordsworth, S., and Dezateux, C. (2013). Regional differences in the frequency of the c.985A>G ACADM mutation: findings from a meta-regression of genotyping and screening studies. Clinical genetics.

Leandro, P., and Gomes, C.M. (2008). Protein misfolding in conformational disorders: rescue of folding defects and chemical chaperoning. Mini reviews in medicinal chemistry *8*, 901-911.

Lehman, T.C., Hale, D.E., Bhala, A., and Thorpe, C. (1990). An acyl-coenzyme A dehydrogenase assay utilizing the ferricenium ion. Analytical biochemistry *186*, 280-284.

Matern, D., and Rinaldo, P. (1993). Medium-Chain Acyl-Coenzyme A Dehydrogenase Deficiency. In GeneReviews, R.A. Pagon, T.D. Bird, C.R. Dolan, K. Stephens, and M.P. Adam, eds. (Seattle (WA)).

Matsubara, Y., Indo, Y., Naito, E., Ozasa, H., Glassberg, R., Vockley, J., Ikeda, Y., Kraus, J., and Tanaka, K. (1989). Molecular cloning and nucleotide sequence of cDNAs encoding the precursors of rat long chain acyl-coenzyme A, short chain acyl-coenzyme A, and isovaleryl-coenzyme A dehydrogenases. Sequence homology of four enzymes of the acyl-CoA dehydrogenase family. The Journal of biological chemistry *264*, 16321-16331.

Matsubara, Y., Narisawa, K., and Tada, K. (1992). Medium-chain acyl-CoA dehydrogenase deficiency: molecular aspects. European journal of pediatrics *151*, 154-159.

Mayr, L.M., and Bojanic, D. (2009). Novel trends in high-throughput screening. Current opinion in pharmacology *9*, 580-588.

McAndrew, R.P., Wang, Y., Mohsen, A.W., He, M., Vockley, J., and Kim, J.J. (2008). Structural basis for substrate fatty acyl chain specificity: crystal structure of human very-long-chain acyl-CoA dehydrogenase. The Journal of biological chemistry *283*, 9435-9443.

McKean, M.C., Frerman, F.E., and Mielke, D.M. (1979). General acyl-CoA dehydrogenase from pig liver. Kinetic and binding studies. The Journal of biological chemistry *254*, 2730-2735.

Mohsen, A.W., and Vockley, J. (1995). High-level expression of an altered cDNA encoding human isovaleryl-CoA dehydrogenase in Escherichia coli. Gene *160*, 263-267.

Nasser, I., Mohsen, A.W., Jelesarov, I., Vockley, J., Macheroux, P., and Ghisla, S. (2004). Thermal unfolding of medium-chain acyl-CoA dehydrogenase and iso(3)valeryl-CoA dehydrogenase: study of the effect of genetic defects on enzyme stability. Biochimica et biophysica acta *1690*, 22-32.

Neupert, W., and Herrmann, J.M. (2007). Translocation of proteins into mitochondria. Annual review of biochemistry *76*, 723-749.

Nguyen, T.V., Andresen, B.S., Corydon, T.J., Ghisla, S., Abd-El Razik, N., Mohsen, A.W., Cederbaum, S.D., Roe, D.S., Roe, C.R., Lench, N.J., *et al.* (2002). Identification of isobutyryl-CoA dehydrogenase and its deficiency in humans. Molecular genetics and metabolism *77*, 68-79.

P Macheroux, C.S., H Büttner, V Kieweg, H Rüterjans, S Ghisla (1997). Medium-chain acyl CoA dehydrogenase: evidence for phosphorylation. The Journal of biological chemistry, 1381-1385.

Parker, A.R. (2003a). Binding of the human "electron transferring flavoprotein" (ETF) to the medium chain acyl-CoA dehydrogenase (MCAD) involves an arginine and histidine residue. Journal of enzyme inhibition and medicinal chemistry *18*, 453-462.

Parker, A.R. (2003b). A single arginine residue is required for the interaction of the electron transferring flavoprotein (ETF) with three of its dehydrogenase partners. Molecular and cellular biochemistry *254*, 91-100.

Pharmaceutical, M. (2005-2006). BUPHENYL (sodium phenylbutyrate) Tablets and Powder. 3Ucyclyd Pharma.

Qi, X., Hosoi, T., Okuma, Y., Kaneko, M., and Nomura, Y. (2004). Sodium 4-phenylbutyrate protects against cerebral ischemic injury. Molecular pharmacology *66*, 899-908.

Rhead, W.J. (2006). Newborn screening for medium-chain acyl-CoA dehydrogenase deficiency: a global perspective. Journal of inherited metabolic disease *29*, 370-377.

Rinaldo, P., Matern, D., and Bennett, M.J. (2002). Fatty acid oxidation disorders. Annual review of physiology *64*, 477-502.

Rinaldo, P., O'Shea, J.J., Coates, P.M., Hale, D.E., Stanley, C.A., and Tanaka, K. (1988). Medium-chain acyl-CoA dehydrogenase deficiency. Diagnosis by stable-isotope dilution measurement of urinary n-hexanoylglycine and 3-phenylpropionylglycine. The New England journal of medicine *319*, 1308-1313.

Roberts, D.L., Frerman, F.E., and Kim, J.J. (1996). Three-dimensional structure of human electron transfer flavoprotein to 2.1-A resolution. Proceedings of the National Academy of Sciences of the United States of America *93*, 14355-14360.

Rozen, R., Vockley, J., Zhou, L., Milos, R., Willard, J., Fu, K., Vicanek, C., Low-Nang, L., Torban, E., and Fournier, B. (1994). Isolation and expression of a cDNA encoding the precursor for a novel member (ACADSB) of the acyl-CoA dehydrogenase gene family. Genomics *24*, 280-287.

Saito, Y., Suzuki, H., Tsugawa, H., Nakagawa, I., Matsuzaki, J., Kanai, Y., and Hibi, T. (2009). Chromatin remodeling at Alu repeats by epigenetic treatment activates silenced microRNA-512-5p with downregulation of Mcl-1 in human gastric cancer cells. Oncogene *28*, 2738-2744.

Schulz, H. (1974). Long chain enoyl coenzyme A hydratase from pig heart. The Journal of biological chemistry *249*, 2704-2709.

Shekhawat, P.S., Matern, D., and Strauss, A.W. (2005). Fetal fatty acid oxidation disorders, their effect on maternal health and neonatal outcome: impact of expanded newborn screening on their diagnosis and management. Pediatric research *57*, 78R-86R.

Smith, E.H., Thomas, C., McHugh, D., Gavrilov, D., Raymond, K., Rinaldo, P., Tortorelli, S., Matern, D., Highsmith, W.E., and Oglesbee, D. (2010). Allelic diversity in MCAD deficiency: the biochemical classification of 54 variants identified during 5 years of ACADM sequencing. Molecular genetics and metabolism *100*, 241-250.

Swigonova, Z., Mohsen, A.W., and Vockley, J. (2009). Acyl-CoA dehydrogenases: Dynamic history of protein family evolution. Journal of molecular evolution *69*, 176-193.

Tiffany, K.A., Roberts, D.L., Wang, M., Paschke, R., Mohsen, A.W., Vockley, J., and Kim, J.J. (1997). Structure of human isovaleryl-CoA dehydrogenase at 2.6 A resolution: structural basis for substrate specificity. Biochemistry *36*, 8455-8464.

Toogood, H.S., van Thiel, A., Basran, J., Sutcliffe, M.J., Scrutton, N.S., and Leys, D. (2004). Extensive domain motion and electron transfer in the human electron transferring flavoprotein.medium chain Acyl-CoA dehydrogenase complex. The Journal of biological chemistry *279*, 32904-32912.

Toogood, H.S., van Thiel, A., Scrutton, N.S., and Leys, D. (2005). Stabilization of non-productive conformations underpins rapid electron transfer to electron-transferring flavoprotein. The Journal of biological chemistry *280*, 30361-30366.

Vilatoba, M., Eckstein, C., Bilbao, G., Smyth, C.A., Jenkins, S., Thompson, J.A., Eckhoff, D.E., and Contreras, J.L. (2005). Sodium 4-phenylbutyrate protects against liver ischemia reperfusion injury by inhibition of endoplasmic reticulum-stress mediated apoptosis. Surgery *138*, 342-351.

Vockley, J., Mohsen al, W.A., Binzak, B., Willard, J., and Fauq, A. (2000). Mammalian branched-chain acyl-CoA dehydrogenases: molecular cloning and characterization of recombinant enzymes. Methods in enzymology *324*, 241-258.

Vockley, J., and Whiteman, D.A. (2002). Defects of mitochondrial beta-oxidation: a growing group of disorders. Neuromuscular disorders : NMD *12*, 235-246.

Vogtle, F.N., Wortelkamp, S., Zahedi, R.P., Becker, D., Leidhold, C., Gevaert, K., Kellermann, J., Voos, W., Sickmann, A., Pfanner, N., *et al.* (2009). Global analysis of the mitochondrial N-proteome identifies a processing peptidase critical for protein stability. Cell *139*, 428-439.

Wanders, R.J., Vreken, P., den Boer, M.E., Wijburg, F.A., van Gennip, A.H., and L, I.J. (1999). Disorders of mitochondrial fatty acyl-CoA beta-oxidation. Journal of inherited metabolic disease *22*, 442-487.

Willard, J., Vicanek, C., Battaile, K.P., Van Veldhoven, P.P., Fauq, A.H., Rozen, R., and Vockley, J. (1996). Cloning of a cDNA for short/branched chain acyl-Coenzyme A dehydrogenase from rat and characterization of its tissue expression and substrate specificity. Archives of biochemistry and biophysics *331*, 127-133.

Yokota, I., Saijo, T., Vockley, J., and Tanaka, K. (1992). Impaired tetramer assembly of variant medium-chain acyl-coenzyme A dehydrogenase with a glutamate or aspartate substitution for lysine 304 causing instability of the protein. The Journal of biological chemistry *267*, 26004-26010.

Zhang, J., Zhang, W., Zou, D., Chen, G., Wan, T., Zhang, M., and Cao, X. (2002). Cloning and functional characterization of ACAD-9, a novel member of human acyl-CoA dehydrogenase family. Biochemical and biophysical research communications *297*, 1033-1042.

Zhang, R., Chen, L., Jiralerspong, S., Snowden, A., Steinberg, S., and Braverman, N. (2010). Recovery of PEX1-Gly843Asp peroxisome dysfunction by small-molecule compounds. Proceedings of the National Academy of Sciences of the United States of America *107*, 5569-5574.

Zhang, Z.F., Kelly, D.P., Kim, J.J., Zhou, Y.Q., Ogden, M.L., Whelan, A.J., and Strauss, A.W. (1992). Structural organization and regulatory regions of the human medium-chain acyl-CoA dehydrogenase gene. Biochemistry *31*, 81-89.

Zhu, Z., and Cuozzo, J. (2009). Review article: high-throughput affinity-based technologies for small-molecule drug discovery. Journal of biomolecular screening *14*, 1157-1164.